

Spring 2003

Nanoscale platinum and iron -cobalt catalysts deposited in microchannel microreactors for use in hydrogenation and dehydrogenation of cyclohexene, selective oxidation of carbon monoxide and Fischer -Tropsch process to higher alkanes

Shihuai Zhao

Follow this and additional works at: <https://digitalcommons.latech.edu/dissertations>

Recommended Citation

Zhao, Shihuai, "" (2003). *Dissertation*. 654.
<https://digitalcommons.latech.edu/dissertations/654>

This Dissertation is brought to you for free and open access by the Graduate School at Louisiana Tech Digital Commons. It has been accepted for inclusion in Doctoral Dissertations by an authorized administrator of Louisiana Tech Digital Commons. For more information, please contact digitalcommons@latech.edu.

INFORMATION TO USERS

This manuscript has been reproduced from the microfilm master. UMI films the text directly from the original or copy submitted. Thus, some thesis and dissertation copies are in typewriter face, while others may be from any type of computer printer.

The quality of this reproduction is dependent upon the quality of the copy submitted. Broken or indistinct print, colored or poor quality illustrations and photographs, print bleedthrough, substandard margins, and improper alignment can adversely affect reproduction.

In the unlikely event that the author did not send UMI a complete manuscript and there are missing pages, these will be noted. Also, if unauthorized copyright material had to be removed, a note will indicate the deletion.

Oversize materials (e.g., maps, drawings, charts) are reproduced by sectioning the original, beginning at the upper left-hand corner and continuing from left to right in equal sections with small overlaps.

ProQuest Information and Learning
300 North Zeeb Road, Ann Arbor, MI 48106-1346 USA
800-521-0600

UMI[®]

**NANO-SCALE PLATINUM AND IRON-COBALT CATALYSTS
DEPOSITED IN MICROCHANNEL MICROREACTORS FOR
USE IN HYDROGENATION AND DEHYDROGENATION
OF CYCLOHEXENE, SELECTIVE OXIDATION OF
CARBON MONOXIDE AND FISCHER-TROPSCH
PROCESS TO HIGHER ALKANES**

by

Shihuai Zhao, B.S.

**A Dissertation Presented in Partial Fulfillment
of the Requirements for the Degree
Doctorate of Philosophy in Engineering**

**COLLEGE OF ENGINEERING AND SCIENCE
LOUISIANA TECH UNIVERSITY**

May 2003

UMI Number: 3084550

UMI[®]

UMI Microform 3084550

Copyright 2003 by ProQuest Information and Learning Company.
All rights reserved. This microform edition is protected against
unauthorized copying under Title 17, United States Code.

ProQuest Information and Learning Company
300 North Zeeb Road
P.O. Box 1346
Ann Arbor, MI 48106-1346

LOUISIANA TECH UNIVERSITY

THE GRADUATE SCHOOL

May 8, 2003

Date

We hereby recommend that the thesis/dissertation prepared under our supervision
by SHIHUAI ZHAO

entitled NANO-SCALE PLATINUM AND IRON-COBALT CATALYSTS DEPOSITED IN MICRO-
CHANNEL MICROREACTORS FOR USE IN HYDROGENATION AND DEHYDROGENATION OF
CYCLOHEXENE, SELECTIVE OXIDATION OF CARBON MONOXIDE AND FISCHER-TROPSCH
PROCESS TO HIGHER ALKANES

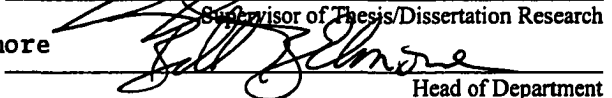
be accepted in partial fulfillment of the requirements for the Degree of
Doctorate of Philosophy in Engineering

James Palmer Debasish Kuila

 Debasish Kuila

Supervisor of Thesis/Dissertation Research

Bill B. Elmore

 Bill B. Elmore

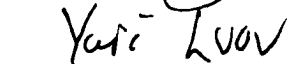
Head of Department

Chemical Engineering

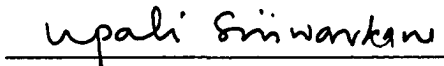
Department

Recommendation concurred in:

 Bill B. Elmore

 Yuri Lvov

Advisory Committee

 Upali Siriwardne

 Raja Nassar

Approved:

 Bob Pundarik
Director of Graduate Studies

Approved:

 Terry McElroy
Dean of the Graduate School

 Stan Nappa
Dean of the College

ABSTRACT

Chemical Process Miniaturization (CPM) has predominant advantages in heat and mass transfer limited unit operations, synthesis of hazardous materials, and as a process development tool. For years, engineers have been seeking ways to apply CPM to practical applications. Studies of catalysts and catalyst supports that can be applied to microreactors are important for a number of commercially desirable gas phase reactions. Parameters such as surface-to-volume ratio and the pore structure of catalyst supports influence the activity and selectivity of the catalysts.

In this study, platinum, iron and cobalt catalysts were fabricated by sputtering deposition and compared with catalysts deposited by chemical procedures. The chemical methods to fabricate silica-supported or alumina-supported Pt and alumina-supported Fe/Co catalysts were investigated using the sol-gel and ion impregnation techniques. A substantial increase in the reaction surface area was observed for the sol-gel supports; however, the sol-gel could not be uniformly applied in the smaller microchannels tested. The characterization of the catalysts and supports was performed using SEM, XPS, BET surface area measurement, EDX, and VSM. The support particles are approximately 80 nm in diameter, which results in a specific surface area of 400 m²/g and dramatically increases the surface area of the catalysts in a microreactor from 0.03 m² to 7 m².

The activity and efficiency of catalysts were evaluated in microreactors with 100 micron and 5 micron wide channels. Process optimization of the Inductive Coupled

Plasma (ICP) etching was necessary to achieve the desired microchannel dimensions and uniformity. The ICP parameters' studies included cycle time of SF₆ gas flow, bias power, and chamber pressure. The conversion of cyclohexene to cyclohexane and benzene is the model reaction for comparison of the various deposition methods of the catalysts and the supports.

In addition, screening studies were performed on two reactions of enormous commercial potential: Fischer-Tropsch (F-T) synthesis, and preferential oxidation of CO in fuel cell. An over 50% conversion of CO and 78% selectivity to propane in F-T synthesis has been achieved. Meanwhile, a 70% conversion of CO and 80% selectivity to CO₂ in preferential oxidation is reached in the fuel cell feed gas reaction. Statistical modeling studies were done using a Central Composite Design (CCD) to achieve the optimal condition (temperature 158 °C, CO: O₂ ratio 1.77 and total flow rate 0.207 sccm) for preferential oxidation of CO in fuel cells.

APPROVAL FOR SCHOLARLY DISSEMINATION

The author grants to the Prescott Memorial Library of Louisiana Tech University the right to reproduce, by appropriate methods, upon request, any or all portions of this Thesis/Dissertation. It is understood that "proper request" consists of the agreement, on the part of the requesting party, that said reproduction is for his personal use and that subsequent reproduction will not occur without written approval of the author of this Thesis/Dissertation. Further, any portions of the Thesis/Dissertation used in books, papers, and other works must be appropriately referenced to this Thesis/Dissertation.

Finally, the author of this Thesis/Dissertation reserves the right to publish freely, in the literature, at any time, any or all portions of this Thesis/Dissertation.

Author  _____

Date 05/12/03

**This work is dedicated to my parents, my brother and Shi, who accompany me
with the emergence of this dissertation.**

TABLE OF CONTEXTS

ABSTRACT	iii
LIST OF TABLES.....	x
LIST OF FIGURES.....	xii
ACKNOWLEDGMENTS.....	xvi
CHAPTER I INTRODUCTION.....	1
Research Need	2
Research Objectives.....	3
CHAPTER II BACKGROUND.....	5
Chemical Microreactor	5
Catalyst Study for Microreaction	6
Application of Microreaction Technology.....	10
Conversion Reaction of Cyclohexene to Cyclohexane and Benzene.....	10
Preferential Oxidation for CO Amelioration in Hydrogen Fuel Cell Feeds	12
Fischer-Tropsch Synthesis.....	14
CHAPTER III THEORY.....	18
Microfluidics	18
Surface Catalyst Kinetics	20
Microfabrication	22
Photolithography	22
Inductively Coupled Plasma (ICP) Etching	23
Sputtering Deposition.....	24
Sol-gel Method and Ion Impregnation	26
Anodic Bonding	28
Analysis theory	29
Gas Sorption Theory	29
Scanning Electron Microscopy	31
X-ray Photoelectron Spectroscopy	32
Energy Dispersive X-Ray	33
Vibrating Sample Magnetometer.....	34
Response Surface Methodology.....	35
CHAPTER IV MATERIALS AND MEHTODS.....	39

Microfabrication	39
Photolithography	39
Inductively Coupled Plasma (ICP) etching	40
Sputtering Deposition	41
Chemicals for Sol-Gel and Ion Impregnation Coating of Catalysts.....	43
Analytical Methods for Characterization of Catalysts	44
Amray 1830 SEM	44
The Physical Electronics 5800 MultiTechnique System	45
Quantachrome NOVA 2000.....	46
KeveX LPX1 Super Dry Quantum Detector EDX system.....	47
880A Digital Measurement Systems (DMS) Vibrating Sample Magnetometer (VSM).....	48
Methods for Microreaction Analysis	49
CHAPTER V MICROREACTOR DESIGN, FABRICATION, CATALYST PREPARATION AND MICROREACTION SETUP.....	50
Microreactor Design, Fabrication	50
Catalyst Preparation	58
Sputtering Deposition of Pt, Iron and Cobalt	58
Sol-gel Method and Ion Impregnation	60
Microreactor Packaging.....	68
Microreaction Setup	70
CHAPTER VI CHARACTERIZATION OF MICROREACTORS AND CATALYSTS	73
Characteristics of Microreactors.....	73
Catalyst Characteristics on Microreactor	79
Scanning Electron Microscopy (SEM) Analysis.....	80
X-ray Photoelectron Spectrometer (XPS) Analysis.....	82
BET Surface Area Measurement.....	87
Mixed Catalyst Analysis with EDX and VSM.....	90
CHAPTER VII CATALYST PERFORMANCE AND APPLICATIONS IN MICROREACTORS.....	93
Catalyst Performance in Cyclohexene Reaction.....	93
Application of Catalyst Study.....	104
Fischer-Tropsch Synthesis	105
Preferential Oxidation for CO Amelioration in Hydrogen Fuel Cell Feeds	112
CHAPTER VIII STATISTICAL ANALYSIS.....	119
CHAPTER VIII CONCLUSIONS.....	125

APPENDIX NOMENCLATURE.....128
REFERENCES.....130

LIST OF TABLES

Table 3.1 Classification of the type of gas flow by Knudsen number.....	19
Table 4.1 Chemicals for sol-gel coating and ion impregnation of catalysts	44
Table 5.1 Sputtering deposition parameters for Pt, Fe and Co.....	60
Table 6.1 Etching characteristics with different ICP parameters.....	78
Table 6.2 Atomic concentration table for different processes.....	82
Table 6.3 Standard binding energy peaks of the elements in alumina.....	83
Table 6.4 Different sol-gel coated Pt conditions.....	85
Table 6.5 Specific surface area for alumina coated by different procedures.....	88
Table 6.6 The surface area results of silica prepared by different coating techniques.....	89
Table 6.7 EDX composition analysis result.....	91
Table 7.1 Four different kinds of catalyst conditions.....	93
Table 7.2 Experimental design for comparison of impregnated Pt with sputtered Pt.....	97
Table 7.3 Reaction design for studying the deactivation of impregnated Pt.....	100
Table 8.1 Central Composite Design for Fuel Cell Experiment.....	120
Table 8.2 SAS output of the 2 nd -order fuel cell model on CO conversion with parameter estimates for the uncoded factor levels.....	120
Table 8.3 SAS output of the 2 nd -order fuel cell model on CO ₂ selectivity with parameter estimates for the uncoded factor levels.....	121
Table 8.4 SAS output of the Estimated Ridge of Maximum Response for the conversion of CO.....	121

Table 8.5 SAS output of the Estimated Ridge of Maximum Response for the selectivity of CO.....	122
Table 8.6 SAS output of the correlation between CO conversion and CO₂ selectivity.....	122

LIST OF FIGURES

Figure 3.1 Hypothetical response surface for two factors.....	36
Figure 3.2 Central composite designs for $p = 2$ and $p = 3$ factors.....	38
Figure 4.1 Inductively Coupled Plasma (ICP) Etcher (Alcatel System A 601E) at IFM, Louisiana Tech University.....	41
Figure 4.2 PVD-300 system for sputtering deposition at IfM , Louisiana Tech University.....	42
Figure 4.3 Amray 1830 SEM at IfM, Louisiana Tech University.....	45
Figure 4.4 The Physical Electronics 5800 MultiTechnique System at IfM, Louisiana Tech University.....	46
Figure 4.5 Quantachrome apparatus Model: NOVA 2000 for surface area measurement of catalysts.....	47
Figure 5.1 Two types of microreactors.....	51
Figure 5.2 Microreactor fabrication process. (Cross section of reactor).....	57
Figure 5.3 Schematic view of Alcatel A 601E process module.....	57
Figure 5.4 Microreactors on one wafer (left: 1 cm \times 3 cm in size, right: 1.6 cm \times 3.1 cm in size).....	57
Figure 5.5 The fixture for microreactor sputtering deposition.....	59
Figure 5.6 Microreactor held by fixture in sputtering chamber.....	60
Figure 5.7 Three sol-gel deposition methods.....	61
Figure 5.8 The microreactor bonded with wafer.....	64
Figure 5.9 Selective deposition of sol-gel on the microreactor.....	65
Figure 5.10 Setup for platinum reduction.....	67

Figure 5.11 Anodic bonding profile.....	69
Figure 5.12 Anodic bonding setup at IfM , Louisiana Tech University.....	69
Figure 5.13 Microreaction setup at IfM, Louisiana Tech University.....	70
Figure 6.1 Two types microreactors (left: 1×3 cm in size, right: 1.6×3.1 cm in size).....	73
Figure 6.2 SEM pictures for two type microreactors.....	74
Figure 6.3 SEM photos with different SF ₆ gas flow time.....	75
Figure 6.4 SEM photos with different bias power.....	76
Figure 6.5 Etching profile with different SF ₆ cycle time and bias power settings.....	77
Figure 6.6 Silica inside 5 μm wide and 100 μm wide channels.....	80
Figure 6.7 Top view of silica on 5 μm channels.....	81
Figure 6.8 Alumina on 100 μm channels.....	81
Figure 6.9 SEM picture of Alumina particles.....	82
Figure 6.10 XPS peak shape of alumina during sputter depth profiling	83
Figure 6.11 XPS plot of different samples of impregnated platinum on sol gel support.....	85
Figure 6.12 Binding energy shift in Pt [110].....	86
Figure 6.13 Comparison between the Pt ⁰ standard plot [110] and the experimental result (before and after reduction of Pt).....	86
Figure 6.14 Sputtered XPS profile of Pt.....	87
Figure 6.15 X-ray spectrum from EDX spectrometer for a sol-gel deposited micro-reactor.....	90
Figure 6.16 Magnetization of as-deposited sol-gel coated Fe/Co micro-reactor.....	91

Figure 6.17: Magnetization of hydrogenated (pre-catalytic reaction) sol-gel coated Fe/Co micro-reactor.....	92
Figure 6.18 Magnetization of sol-gel coated micro-reactor after catalytic reaction is conducted.....	92
Figure 7.1 Conversion vs. residence time on sputtered Pt.....	94
Figure 7.2 Conversion vs. residence time using sputtered Pt on silica support	95
Figure 7.3 Comparison of conversion vs. H_2/C_6H_{10} partial pressure ratio.....	95
Figure 7.4 Comparison of conversion of cyclohexene vs. temperature.....	96
Figure 7.5 Comparison of selectivity vs. temperature.....	97
Figure 7.6 Conversion comparison for impregnated Pt and sputtered Pt.....	98
Figure 7.7 Temperature effect on conversion of cyclohexene impregnated Pt.....	99
Figure 7.8 Deactivation study on impregnated Pt.....	102
Figure 7.9 Cyclohexene conversion using impregnated Pt on alumina support.....	103
Figure 7.10 F-T synthesis study with sputtered Fe and Co (Conversion vs. temperature).....	106
Figure 7.11 F-T synthesis study with sputtered Fe and H_2/CO ratio.....	107
Figure 7.12 F-T study with sol-gel coated Fe/Co catalyst at 240 °C (Conversion vs. H_2/CO ratio).....	108
Figure 7.13 F-T synthesis study with alumina sol-gel coated Fe/Co catalyst (Conversion vs. temperature).....	109
Figure 7.14 F-T synthesis study with alumina sol-gel coated Fe/Co catalyst (conversion vs. temperature with different flow rate).....	109
Figure 7.15 F-T synthesis study with alumina sol-gel coated Fe/Co catalyst (selectivity vs. temperature).....	110

Figure 7.16 F-T synthesis study with alumina sol-gel coated Fe/Co (selectivity vs. temperature with different ratio of H ₂ /CO).....	110
Figure 7.17 Preferential oxidation for CO (Conversion vs. ratio of O ₂ /CO).....	113
Figure 7.18 Preferential oxidation for CO (Selectivity vs. ratio of O ₂ /CO).....	113
Figure 7.19 Preferential oxidation for CO (Conversion vs. temperature with different O ₂ /CO ratio) (Air as oxidizer).....	114
Figure 7.20 Preferential oxidation for CO (Selectivity vs. temperature with O ₂ /CO ratio of 0.75) (Air as oxidizer).....	115
Figure 7.21 Preferential oxidation for CO (Conversion of CO or Selectivity vs. temperature with O ₂ /CO ratio of 0.5).....	116
Figure 7.22 Preferential oxidation for CO (Conversion of CO or Selectivity vs. Residence time with O ₂ /CO ratio of 0.5).....	116
Figure 7.23 Preferential oxidation for CO (Conversion of CO or Selectivity vs. time with O ₂ /CO ratio of 0.5).....	117

ACKNOWLEDGEMENTS

I would like to thank the chairmen of my advisory committee, Dr. James Palmer and Dr. Debasish Kuila, for their help for my graduation. Special thanks go to my previous advisor, Dr. Ronald Besser, who gave me a lot of ideas. I would also like to thank the other members of my committee – Dr. Bill Elmore, Dr. Yuri Lvov, Dr. Raja Nassar and Dr. Upali Siriwardane – for their advice and help.

I want to express my thanks to the director of IfM, Dr. Kody Varahramyan, for financial support (NSF-EPSCoR). I would also like to thank the IfM staff, Dr. Karen Xu, Mr. Scott Williams, Mr. John McDonald, Dr. Alfred Gunasekaran, and others who helped me in my projects.

I thank all the students in microreactor group, especially Jing Hu, for her statistical analysis, and Satish Nagineni, for his cooperation on Fe-Co catalyst preparation.

Last but not least, deep in my heart, I want to present my special thanks to my grandmother, grandfather, uncle, and aunt, who gave me love and encouragement all the time.

CHAPTER I

INTRODUCTION

The Chinese are capable of engraving poems on a single hair. To read them, one must use a microscope. Imagine how small a single word is. This technique could be called micro-art. What parallel exists in the mechanical world? In November 1960, the first functioning microelectric motor, measuring $1/64^{\text{th}}$ of an inch, came to the world [1]. Process miniaturization started with microelectrical mechanical systems (MEMS), which have created an amazing new world. The change of computer size from several rooms down to a laptop brings us to a micro-scale world.

Chemical engineers are striving to bring micro-technology to chemical labs and chemical plants. Traditionally, the chemical industry operates reactors in a few large facilities to achieve economies of scale. Today, a small group of research institutes and companies in the chemical process industries are working in the opposite direction, developing micrometer-scaled reactors and integrating microstructured heat exchangers, pumps, valves, and other devices. This is called Chemical Process Miniaturization (CPM). The idea of chemical processing on a chip can be fully utilized step by step by employing the microelectronic and micromachining technology.

Chemical Process Miniaturization (CPM) technologies may apply to a variety of areas, including environmental sensing and control, improved operation of chemical processes, stronger economic performance through reduced costs, and increased safety

for processing hazardous materials. The ultimate goal in the CPM is to integrate an entire process plant or lab on a single chip. According to recent developments in the fields of silicon bulk and surface micromachining, the fabrication of devices with characteristic dimensions of the order of a few microns has become possible. Microreactors can be advantageous in analytical and synthesis applications due to high surface area to volume ratios, resulting in better heat and mass transfer properties, and easy integration with peripheral devices [2].

Research Need

A large number of applications within the last decade have demonstrated advantages for miniaturized analysis systems compared to lab-scale equipment. Smaller devices need less space, materials, and energy and often have faster response times. In particular, more information per space and time is gained. Process miniaturization and microreaction technology provide opportunities for improving process capability and control in chemical synthesis and can allow safer and more efficient chemical kinetics investigations.

A catalyst is a material used to increase the rate of a chemical reaction. Many reactions need catalysts. Catalysts are of crucial importance for the chemical industry; the number of catalysts applied in industry is very large and catalysts come in many different forms, from heterogeneous catalysts in the form of porous solids, or homogeneous catalysts dissolved in the liquid reaction mixture to biological catalysts in the form of enzymes. Catalyst studies can be applied to a broad range of petroleum refining, automotive, aerospace, and environmental problems. Since catalysts are very important to

chemical reactions and chemical analysis, the utility of miniaturization of reaction and analysis cannot be realized without the microfabrication of catalysts.

The surface-to-volume ratio of microreactor scales with the interface area between reactant and catalyst. The structure of catalysts on the wall of a microreactor greatly impacts the activity of catalysts. The pore structure of catalysts can be manipulated to increase reaction surface. Therefore, the study of catalyst microstructure and microfabrication methods is important to chemical process miniaturization.

Catalyst deactivation is a phenomenon that must be understood to effectively employ a catalyst in commercial applications. This problem can be reduced by the use of combined catalysts. Catalyst development has traditionally been an empirical and time-consuming process. There are strong business demands for speeding up the development of active substances and new catalysts. Worldwide, several groups are attracted by the fields of combinatorial methods for chemistry and catalysis [3-6].

Research Objectives

The Institute for Micromanufacturing (IfM) at Louisiana Tech University is one of the major groups investigating the fundamentals of microreaction technology in the world. In this research, based on previous success and the need of present micro-chemical process development, I will apply advanced microfabrication and micromasurement technology to realize the following objectives:

1. Establish an effective deposition process of catalysts. Adapt or alter the reviewed methods of catalyst deposition to apply catalyst films in the microchannels of reactors. The methods include sputtering deposition, sol-gel process, anodic

oxidation, immobilized nanoparticles (e.g. impregnation or precipitation), and combination of these methods.

2. Based on the surface catalyst kinetics and microfluidics, Design and fabricate microreactors for testing catalysts using photolithography and dry etching technology.
3. Characterize both the microreactors and catalysts using a variety of analytical tools: SEM (scanning electron microscopy), XPS (X-ray photoelectron spectroscopy), and BET surface area measurement, EDX (Energy Dispersive X-Ray), and VSM (Vibrating Sample Magnetometer).
4. Utilize the hydrogenation and dehydrogenation of cyclohexene as a model reaction to compare the catalytic activity of catalysts of various deposition techniques.
5. Conduct two commercially viable reactions in the microreactor: preferential oxidation for CO amelioration in hydrogen fuel cell feeds and Fischer-Tropsch synthesis to higher alkanes.

The final objective will demonstrate the suitability of using microreactors as a process development tool. Potential benefits include: faster transfer of research results into production, easier scale-up of production capacity, earlier start of production at lower costs for transportation, and more flexible response to market demands.

CHAPTER II

BACKGROUND

Chemical Microreactor

Microreactors consist of channels etched on metal, glass, silicon, or other substrates *via* photolithography or other techniques. The channels have lateral dimensions in the order of micrometers. Silicon is often chosen due to well developed photolithography and etching techniques developed in the microelectronic industry. In addition to the environmental and safety benefits of dealing with smaller quantities of material, microreactors offer a number of performance benefits. Most of these advantages stem from the high surface-to-volume ratio inherent at the micro-scale. Microreactors' narrow channels and thin walls make them desirable candidates for studying potentially explosive reactions. The small channels and the large surface-to-volume ratios serve to inhibit gas-phase free-radical reactions as well as improve heat transfer for exothermic reactions.

Microreactors exhibit different fluid dynamics than conventional reactors due to their inherent small scale. Microchannels have a large length-to-depth ratio, which is proportional to the number of molecular collisions with the channel wall in Knudsen flow [7]. Hence, the reaction efficiency is improved with the enhanced collision frequency.

Microreactors are able to promote the performance of some reactions by narrowing the residence time. Improved heat transfer can allow one to reduce reaction

time needed for highly exothermic reactions. They can also provide relatively simple and quick means for commercializing a process. Conventional scale-up involves a transition from laboratory scale to a single large reactor unit through a series of costly laboratory experiments, pilot plant studies, and simulations. In contrast, a microreactor can be “scaled-out” through the combination of large numbers of reactors in parallel, allowing for a quick and simple construction and maintenance with less cost [8].

Catalyst Study for Microreaction

A catalyst is a substance that affects the rate of a reaction but emerges from the process unchanged. Catalysts have been used by humankind for over 2000 years [9]. The first observed uses of catalysts were in the making of wine, cheese, and bread. A catalyst usually changes a reaction rate by promoting a different molecular path (“mechanism”) for the reaction. Catalysis is the occurrence, study of catalysts and catalytic process. Commercial chemical catalysts are immensely important. Approximately one-third of the material gross national product of the United States involves a catalytic process somewhere between raw material and finished product. Catalysis is of crucial importance for the chemical industry; the number of catalysts applied in industry is very large. Catalysts come in many different forms, from heterogeneous catalysts in the form of porous solids, and homogeneous catalysts dissolved in the liquid reaction mixture, to biological catalysts in the form of enzymes. Catalyst studies address a broad range of petroleum refining, automotive, aerospace, and environmental problems. The structure of catalysts on the wall of a microreactor impacts the activity of the catalyst, which affects the rate of reaction. The surface-to-volume ratio of microreactor scales with the interface

area between reactant and catalyst. The pore structure of catalysts can also increase the reaction surface area. Both of them impact the efficiency of catalysts. Therefore, the study of catalyst microstructure and microfabrication methods is critical to chemical process miniaturization.

A Pt-catalyzed NH_3 oxidation as a model reaction was investigated by the researchers of Massachusetts Institute of Technology in a novel reactor having micrometer flow channels with integrated heaters and flow and temperature sensors [10]. The reactor behavior as a function of operating conditions shows that conversion and selectivity behaviors of conventional reactors can be reproduced and demonstrates the feasibility of conducting chemical reactions in microfabricated systems. Another example of using Pt as catalyst is an experimental system to test the effectiveness of a microreactor design for the catalyst and to test the behavior of the catalyst itself [11].

The mixture of platinum and other materials as catalysts is new and a challenging technology. A reactor system designed for low mass flows of reactant gas, for evaluation of the activity of electron beam lithography-nanofabricated model catalysts with a small total active area, is described by Stefan [12].

Reliable and reproducible results can be obtained in such microreactor studies, under flow conditions, on Pt/CeO_x catalysts. James demonstrated aqueous phase heterogeneous catalytic oxidation of trichloroethylene over 5% ruthenium and 20% platinum (w/w) catalyst supported on activated carbon [13]. The metals were impregnated into the carbon support using ruthenium chloride dissolved in 15% HCl, and platinum was dissolved in aqueous hexachloroplatinic acid. This catalyst was also used in

development of a catalytic fuel processing system, which is integrated with a solid oxide fuel cell power source. This catalytic device also can utilize a novel three-way catalytic system consisting of an *in-situ* pre-reformer catalyst, the fuel cell anode catalyst, and a platinum-based combustion catalyst. The three individual catalytic stages have been tested in a model catalytic microreactor by Finnerty [14]. The third example is direct formation of isobutene from n-butane over zeolite and Al₂O₃ supported platinum and platinum-copper catalysts. Hamid showed that the addition of Cu decreases Pt dispersion, irrespective of preparation methods and the nature of catalyst supports. The presence of potassium was found to reduce acidity and Pt dispersion [6].

Catalytic properties of supported platinum can be modified by using promoters known as dehydrogenation catalysts: tin, zinc aluminate spine, and transition metal pyrophosphates. Sadykov V.A. designed a tubular microreactor with independent control of feed preheat as well as catalyst temperatures that allowed rapid quenching of the reaction products for testing performance of supported Pt-based monolithic catalysts in the oxidative dehydrogenation of propane at short contact times [16]. Platinum was supported onto monolithic supports *via* incipient wetness impregnation with aqueous solutions of H₂PtCl₆. The phase composition of catalysts was studied by X-ray diffraction (XRD).

Non-Pt catalysts that have been applied to microreactors include zeolites, sulfated titania solid acid, and alloys. The application of catalysts based on zeolites and related materials is one of the latest developments in the field of heterogeneous catalysis, which started with the use of amorphous silica-alumina. These crystalline materials are

thermally and hydrothermally stable, and the number and strength of their acid sites can be controlled. They have a high adsorption capacity, and contain channels of molecular dimensions - properties of interest for a number of applications [17].

Sulfated titania catalysts were prepared by the precipitation of titanic acid from titanium tetrachloride using aqueous ammonia, followed by impregnation with sulfuric acid. The sulfate concentrations in the catalysts were in the range of 5-15 wt %. These sulfated catalysts were calcined at temperatures in the range of 450-650 °C. The characteristics of these sulfated titania catalysts were examined using the BET method, powder X-ray diffraction (XRD), Auger Electron Spectroscopy (AES) elemental analysis, and ¹H MAS solid state NMR measurements [18]. Three kinds of Fe₇₈Si₁₂B₁₀ alloys have been tested as catalysts for the hydrogenation of CO in a flow microreactor. Their catalytic activity, selectivity and deactivation mechanisms were studied. It was found that the activity depends mainly on Fe grain size and partially amorphous Fe₇₈Si₁₂B₁₀ alloy that shows an activity six times higher than the crystalline one. It has also been found that the selectivity and deactivation of the FeSiB catalysts are affected mainly by the segregation of silicon and boron on the surface [19].

In this study, we adapted or altered published methods for catalysts deposition in microchannels. The sputtering deposition, sol-gel washcoating, and impregnation were selected in this research. By testing the activity and selectivity of catalysts we provide the first known published comparison of physical and chemical deposition techniques of catalysts applied to microreactors with two different widths.

Application of Microreaction Technology

Process miniaturization and microreaction technology provide opportunities for improving process capability and control in chemical synthesis and can allow safer and more efficient chemical kinetic investigations. Compared to normal scale reactors, microreactors have the following advantages: decrease of linear dimensions, increase of surface to volume ratio, decrease of volume, fast and efficient process development, decreased potential of environmental impact, and increased safety.

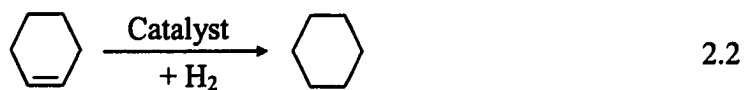
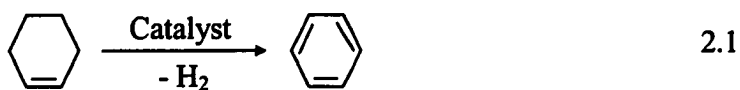
In this project, the conversion of cyclohexene has been chosen as a model reaction for microfabricated catalysts inside microreactors due to its use for characterization of microreactors in the literature [45-47]. In addition, two reactions of industrial significance have been demonstrated in the microreactor: preferential oxidation for CO amelioration in hydrogen fuel cell feeds and Fischer-Tropsch synthesis to high alkanes.

Conversion of Cyclohexene to Cyclohexane and Benzene

The reaction of cyclohexene (C_6H_{10}) and hydrogen has been explored in recent years by a number of investigators [20-24]. This reaction system is a popular model for many similar systems ubiquitous in the chemical process and petroleum refining industries, including (a) hydrotreating [25] for aromatics reduction, desulfurization, and denitrogenation, (b) reforming for aromatics reduction and dehydrocyclization, [26,27], and (c) fuel processing of liquid hydrocarbons for the generation of hydrogen feed for fuel cells [28].

There are numerous metals, such as tungsten, platinum, silver, cobalt, carbon, etc, catalyze cyclohexene to cyclohexane or benzene. The dehydrogenation of cyclohexene

on Pt-modified C/W (111) surfaces was studied by Liu [43]. Temperature Programmed Desorption (TPD), Auger Electron Spectroscopy (AES), and high-resolution EELS (HREELS) were used to characterize the surface reactivity of tungsten carbide modified by the presence of submonolayer Pt and the properties of O-modified C/W (111) surfaces [43,44]. The reacting system permitted the study of effects influencing reaction selectivity towards cyclohexane (C_6H_{12}) versus benzene (C_6H_6) through the reactions in Equations 2.1 and 2.2.



Dehydrogenation or hydrogenation of cyclohexene depends on the type of catalyst used and operating conditions. The use of silver favors the dehydrogenation of cyclohexene. The benzene formed from cyclohexene remains chemisorbed on the silver surface until 275 K [45]. Different catalysts have different mechanisms of dehydrogenation. For example, benzene produced from cyclohexene forms on the surface of Pd(111) at 150 K with no stable intermediate, which is different from that found on the Pt(111) [46]. In addition, the catalyst supports also affect the selectivity to cyclohexane or benzene. Cobalt phthalocyanine (CoPc) supported on Al_2O_3 , SiO_2 and $SiO_2-Al_2O_3$ of varying SiO_2 mole ratios have been investigated by Hassanto and exhibit good selectivity in the oxidative dehydrogenation of cyclohexene toward benzene [47].

In this study, dehydrogenation and hydrogenation of cyclohexene have been investigated. The activity and efficiency of sputtered and sol-gel coated Pt have been tested using this reaction. The conversion of cyclohexene selectivity towards benzene or cyclohexane will be discussed in detail.

Preferential Oxidation for CO Amelioration in Hydrogen Fuel Cell Feeds

Fuel cells hold substantial promise in reducing the environmental impact of transportation. A fuel cell is a battery in which a fuel - normally hydrogen or methanol - reacts at the anode and oxygen reacts at the cathode. However, unlike in a normal battery, fuel cell electrodes are not consumed - only the fuel is consumed [29]. In most cases, hydrogen is the preferred fuel for use in the present generation of fuel cells being developed for commercial applications [30]. When generating hydrogen from natural gas, methane, or methanol, one of the by-products is carbon monoxide. The presence of carbon monoxide in the hydrogen rich feed gas to fuel cells can poison the platinum anode electrode and dramatically reduce the power output [31]. Therefore, carbon monoxide clean-up and amelioration is very important for fuel cell technology development.

The hydrogen generation reactions are classified into 1) decomposition, 2) steam reforming, 3) partial oxidation, and 4) auto-thermal reforming. Various reactors have been developed: 1) external heating steam reformer, 2) recuperated plate stacked reformer, 3) adiabatic auto-thermal reformer. Various CO-removal technologies have been developed: 1) water-gas shift, 2) preferential oxidation, 3) methanation, 4) hydrogen separation, and 5) CO-adsorption [32].

Loughborough developed a compact CO selective oxidation unit based on two coated aluminum heat exchangers. Experimental results show that the selective oxidation unit can reduce the CO from 2% to less than 15 ppm and is suitable for a vehicle fuel cell power plant of 20 kW_e [33]. In 2001, the same group reported a metal based catalytic CO oxidation reactor which makes CO concentrations from a typical steam reformer output of 7000 ppm input to less than or equal 15 ppm in the presence of approximately 75% hydrogen [34,35]. The reactor design was based upon the catalyst coating of high surface area heat transfer technology. Catalyst screening studies have revealed a mixed transition metal oxide promoted platinum-ruthenium formulation to be suitable for the particular reactor application, *i.e.* acceptable CO oxidation activity and selectivity within a temperature range of 130-200 °C.

Removal of CO contained in hydrogen has been attempted by using different catalysts. Oxidative removal of a small quantity of CO from hydrogen atmosphere has been examined using catalysts containing 3d transition metal oxides. The oxidation of CO takes place in preference to that of H₂ on catalysts containing Co or Mn in a temperature range from 323-423 K. Currently, the most popular catalyst is platinum, due to its good performance in reactors. In Italy, the oxidation kinetics of H₂ and H₂ + 100 ppm CO were investigated on Pt, Ru and Pt-Ru electrocatalysts supported on a high-surface area carbon powder. Best performances, both in H₂ and H₂ + CO, were achieved by the catalyst with the ratio of Pt/Ru = 1 [35]. In the U.S., Denis presented the results of selective CO oxidation, in macro-scale, in simulated reformat gas over single-step sol-gel prepared Pt/alumina catalysts [36]. The effects of water vapor, carbon dioxide, CO

and oxygen concentrations, temperature, and Pt loading on the activity and selectivity were presented. Their results showed that a 2% Pt/alumina sol-gel catalyst can selectively oxidize CO down to a few ppm with constant selectivity and high space velocity. Water vapor in the feed increases the activity of the catalysts dramatically and in the absence of water vapor, CO₂ in the feed stream decreases the activity of the catalysts significantly [36].

In our current study, we have focused on preferential oxidation of CO using a microreactor. The reaction are shown below:



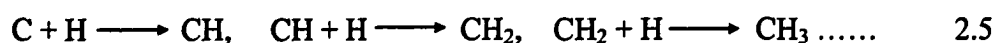
High conversion is required to reduce the CO concentration to a level that is not detrimental to a Proton Exchange Membrane (PEM)-based fuel cell. High selectivity to CO₂ is necessary because hydrogen is used to generate electricity in the fuel cell. Oxidation of hydrogen to water reduces energy available in the fuel.

Fischer-Tropsch Synthesis

As the global reserves of oil are being consumed, Fischer-Tropsch (F-T) synthesis becomes an important route for the production of fuels and chemicals. F-T synthesis involves the conversion of carbon monoxide and hydrogen to higher molecular weight hydrocarbons. The first conversion of CO and H₂ to methane was reported by Sabatier and Senderens in 1902 [43]. More than two decades later, Fischer and Tropsch described

their catalyst development efforts, which included the synthesis of higher hydrocarbons over nickel- and cobalt-based catalysts [43].

Despite tremendous efforts devoted to this process in the last 70 years, the reaction mechanism of F-T synthesis remains uncertain. With extensive Density Functional Theory (DFT) studies on F-T reactions, Liu [44] obtained relative stabilities of many key intermediates and compared quantitatively several C/C coupling mechanisms that are likely to be involved [44]. The first step of the F-T synthesis is the CO and H₂ dissociations, followed by hydrogenation process. Then the CH_x species (x = 0, 1, 2) couple with each other (C/C coupling) to form higher-weight hydrocarbons.



During the last two decades, F-T synthesis, being the technology for conversion of natural gas to liquid and an attractive alternative for bringing static gas resources to market, has been re-visited by several corporations. Active research is pursued by Exxon-Mobil, Rentech, and Syntroleum, and commercialized processes have been offered by Shell and Sasol. Among these companies and other research groups, extensive interest has been focused on finding a better catalyst to increase productivity, control hydrocarbon product distribution, and lengthen the catalyst life [45, 46]. Exxon's AGC-21 process is the result of a \$300 million R&D program that began in 1981 [47]. The centerpiece of this technology is a proprietary high-productivity process for hydrocarbon synthesis (HCS) in which Fischer-Tropsch technology has been used to convert H₂ – CO syn-gas to heavy hydrocarbons using a cobalt-based slurry. Exxon has spent more than a decade developing cobalt catalysts and slurry reactors. A 2:1 H₂-CO synthesis gas feed

for HCS is prepared by contacting methane with limited amounts of steam and oxygen in a catalyzed fluid-bed reactor. Another catalyst for F-T synthesis is iron. Iron-based catalysts presented by Linda. have demonstrated higher activity than other known iron F-T catalysts developed for maximizing production of high molecular weight hydrocarbons [48]. Their objectives were to demonstrate a repeatability of performance and preparation procedure of two high activity, high alpha iron F-T catalysts (100 Fe/5 Cu/6 K/24 SiO₂ and 100 Fe/3 Cu/4 K/16 SiO₂) and to improve the catalyst performance through variations in process conditions, pretreatment procedures and/or modification in catalyst preparation steps. Catalyst calcination temperature is shown to be insignificant for both catalysts, and it was learned that catalyst activity and selectivity could be controlled to some extent through variations in the pretreatment conditions. The Texas A&M University (TAMU) group investigated the performance of catalysts in a small-scale reactor and explored the feasibility of producing catalysts on a large scale with catalyst manufacturers.

Water-gas shift activity is undesirable in Fischer-Tropsch (F-T) synthesis with hydrogen-rich synthesis gas, such as that derived from natural gas, purely on the basis of optimizing carbon efficiency [48]. The high carbon efficiency is of increasing environmental importance in minimizing the production of greenhouse gases. Production of synthesis gas is by far the most expensive step in FT fuel production, representing about twice the cost of its conversion to synthetic crude, and four times the cost of subsequent refining. It is well known that cobalt-based catalysts show lower water-gas shift activity than iron-based ones [48]. Barrault *et al.* have reported a Fischer-Tropsch

catalyst comprising 9.4 wt.% Co on commercial CeO₂, prepared by impregnation of cobalt nitrate.

In this dissertation, combined catalysts of iron/cobalt supported by aluminum oxide for syn-gas reactions have been considered. The effect of different concentrations of iron and cobalt are presented.

CHAPTER III

THEORY

Microfluidics

When one studies a microreactor, it is important to understand fluid transport in microchannels. The study of fluid flows in micro-scaled channels has been an interesting research topic for nearly a century. However, most of the microflow studies were conducted using capillary tubes (Knudsen, 1909). The measurements were limited to global quantities, since no instrument with fine spatial resolution was available.

Progress in micromachining techniques has revived interest in studying microflows. Bulk micromachining technology can make channels with precise dimensions and implement measurement sensors along the channel.

The distinction among the various flow regimes can be obtained with the introduction of the Knudsen number Kn , defined as $Kn = (\lambda/d)$, where λ is the mean free path of the molecules and d is a characteristic flow dimension (across flow). In microchannels, depth is chosen as the characteristic flow dimension. Mean free path is defined as the average distance traveled by gas molecules between intermolecular collisions and can be calculated as

$$\lambda = \frac{kT}{\sqrt{2}\pi(di)^2 P} \quad 3.1$$

Where k = Boltzmann's constant, 1.381×10^{-23} J/K;

T = Gas temperature, Kelvin;

d_i = Gas molecule diameter, meters;

P = Gas partial pressure, Pa;

A typical value of mean free path for air in ambient conditions is $\lambda \approx 10^{-7}$ m. The classification of type of gas flow by Schaaf and Chambre [49] is listed in Table 3.1.

Table 3.1 Classification of the type of gas flow by Knudsen number

Knudsen Number Range	Flow Type
$Kn \leq 0.01$	Continuum flow
$0.01 < Kn \leq 0.1$	Slip flow
$0.1 < Kn < 3$	Transitional flow
$Kn \geq 3$	Free molecular flow

In channels with large dimensions, the Knudsen number (the ratio of molecular mean free path to channel height) is small, and the continuum assumption holds. It is well established that the pressure distribution is linear and velocity at the wall is zero. Liu and Tai studied pressure distribution in microchannels with a height of 1.2 μm , length of 3000 μm , and width of 40 μm [50]. These microchannels were fabricated and integrated with pressure sensors using combined surface micromachining and bulk micromachining. Pressure distribution measurements have been carried out using both nitrogen and helium as the working fluids. It is found that the pressure distribution is nonlinear inside a microchannel that has a uniform cross-sectional area. For the microchannel specified above with nitrogen as a working gas, the Knudsen number is about 0.01. The Knudsen number was increased by one order of magnitude when helium was used. The non-linearity of pressure is much more pronounced for the case for helium than is the case for

nitrogen. Hence, it is concluded that the non-linear pressure drop distribution is due to the transition from the continuum region to slip flow region.

Arkilic and Breuer studied the flow and pressure distribution of gases in microchannels in 1994 [51]. The channel was fabricated on a silicon wafer using standard photolithography techniques, resulting in 1.33 μm depth, 52 μm width and 7500 μm length. The helium mass flow rate through microchannels was measured for inlet pressures ranging from 1.2 to 2.5 atmospheres with outlet pressures at atmosphere. The Knudsen number at the channel outlet condition in their experiment is 0.165. They compared experimental results with the prediction from the Navier-Stokes equations and found the non-slip solution of Navier-Stokes equation failed to model the mass flow-pressure relationship. Arkilic and Breuer developed an accurate model by including a slip-flow boundary condition at the wall. The model predicts an increase in the mass flow, and they suggested that the mass increase is caused by the friction decrease. Their experiments also presented a non-linear pressure distribution along the length of the channel.

Surface Catalyst Kinetics

Catalysis is a kinetic phenomenon, and the efficiency of catalyst is determined by various factors, such as fabrication method, preparation condition, materials used, etc. The catalytic reaction turnover frequency, f , is defined as the number of product molecules formed per second. Its inverse, $1/f$, yields the turnover time, the time necessary to form a product molecule. By dividing the turnover frequency by the catalyst surface area, a , the specific turnover rate is obtained,

$$R_s = (f / a) \quad 3.2$$

The specific turnover rate gives us the number of molecules produced per site per unit time (molecules/cm²/sec). This type of analysis assumes that every surface site is active. Although the number of catalytically active sites could be much smaller (usually uncertain) than the total number of available surface sites, the specific rate defined by this way result in a conservative lower limit of the catalytic turnover rate. If R is multiplied by the total reaction time t , the turnover number, the number of product molecules formed per surface site, can be gained. A turnover number of one corresponds to a stoichiometric reaction. Because of the experimental uncertainties, the turnover number must be on the order of 10^2 or larger for the reaction to qualify as catalytic.

While the turnover number provides a figure of merit for the activity of the catalyst sites, the reaction probability RP reveals the overall efficiency of the catalytic process under the reaction conditions. The reaction probability is defined as

$$RP = \frac{\text{rate of formation of product molecules}}{\text{rate of incidence of reactant molecules}} \quad 3.3$$

RP can be readily obtained by dividing R by the rate of molecular incidence F. From kinetic theory of gases [52], the flux F of molecules striking the surface of unit area at a given ambient pressure P is

$$F \text{ (mole/cm}^2\text{/sec)} = P/(2\pi MRT)^{1/2} \quad 3.4$$

where M is the average molar weight of the gaseous pieces. T is the temperature, and R is the gas constant. For air, at $P = 4 \times 10^{-4}$ Pa and $M = 28$ g/gmole and $T = 300$ K, we obtain $F \approx 10^{15}$ molecules/cm²/sec. Thus, at this condition, 10^{15} molecules are striking one unit catalyst surface area per second [52].

Microfabrication

Advances in micro fabrication technology offer researchers new options in design and fabrication. The technology uses standard integrated-circuits manufacturing steps such as thin-film deposition, ion implantation, lithography, and etching to machine miniature mechanical devices with feature sizes in the micrometer scale or even less. It offers the ability to design reactors for other purposes such as chemical production [53].

Photolithography

Both micromachining and microelectronic fabrication start with lithography, the technique used to transfer copies of a master pattern onto the surface of a solid material, such as a silicon wafer [54]. The sources can be optical, electron, x-ray, or ion radiation [55]. The most widely used form of lithography is photolithography. It comprises the formation of images with visible or ultraviolet radiation in a photoresist using contact, proximity, or projection printing.

Photoresists are of two types. A negative resist on exposure to light becomes less soluble in a developer solution, while a positive resist becomes more soluble. Commercial negative resists consist of two parts: a chemically inert polyisoprene rubber, which is the film-forming component, and a photoactive agent, which on exposure to light reacts with the rubber to form crosslinks between rubber molecules and make the rubber less soluble in an organic developer solvent. Positive resists have two components: a resin, which becomes more soluble in an aqueous developer solution after exposure to light, and a photoactive compound. In this study, we have used both positive and negative photoresists for different purposes.

The stencil used to generate a desired pattern in resist-coated wafers is called a mask. A photomask, a nearly optically flat glass or quartz plate with a metal absorber pattern, is placed into direct contact with or very close to the photoresist coated surface, and the wafer is exposed to the ultraviolet radiation. The absorber pattern on the photomask is opaque to ultraviolet light, whereas glass or quartz is transparent. A light field or dark field image is then transferred to the semiconductor surface. This is the basic principle of photolithography.

Inductively Coupled Plasma (ICP) Etching

Dry plasma etching, compared with wet etching, can offer many advantages in the fabrication of MEMS because of its anisotropic etching behavior, high etch rate, and its compatibility with traditional IC processing [56]. The basis of plasma-assisted etching is to use a glow discharge to produce chemically reactive and ionic species and which react with the wafer to form volatile products.

Inductively Coupled Plasma (ICP) is widely used for etching materials for integrated circuit fabrication and micromachining applications [57-59]. The basic process of ICP etching can be classified into two major steps. The first step is ion-assisted etching of silicon substrate by etching gas (SF_6) and the second is a sidewall passivation step to achieve a straight sidewall feature with polymeric gas (C_4F_8). After a few seconds, SF_6 is pumped out of the chamber and C_4F_8 is pumped in. A thin Teflon-like passivation layer is deposited on the wafer, including the base and sidewalls of the previously etched hole. Then SF_6 is pumped in again and the cycle is repeated. To obtain more anisotropic processes, it is necessary to etch at pressures lower than those currently used in

corresponding Reactive Ion Etching. In order to obtain reasonable etch rates, the plasma densities at these pressures have to be increased.

A patented high density inductively coupled RFIC plasma source with independent source power and substrate bias control has been developed by Alcatel for deep etching of silicon. With the optimization of hardware and process parameters in a Fluorine based chemistry, processes with silicon etch rate up to 6 $\mu\text{m}/\text{min}$, Si:Photoresist selectivity of more than 100:1, etch depths of greater than 500 μm have been demonstrated. The periodic change of different gases for etching (SF_6) and passivation (C_4F_8) can lead to very high aspect ratios and very high etch rates [60].

Sputtering Deposition

Sputtering is preferred over evaporation in many applications due to a wider choice of materials to work with, better step coverage, and better adhesion to the substrate. Actually, sputtering is employed in laboratories and production settings, whereas evaporation mainly remains a laboratory technique.

Plasmas are generated by supplying energy to a neutral gas, causing the formation of charge carriers [61-63]. Electrons and ions are produced in the gas phase when electrons or photons with sufficient energy collide with the neutral atoms and molecules in the feed gas. The most widely used method for plasma generation utilizes the electrical breakdown of a neutral gas in the presence of an external electric field. Charge carriers accelerated in the electric field couple their energy into the plasma via collisions with other particles. Electrons retain most of their energy in elastic collisions with atoms and molecules because of their small mass and transfer their energy primarily in inelastic

collisions. Discharges are classified as dc discharges, ac discharges, or pulsed discharges on the basis of the temporal behavior of the sustaining electric field. The spatial and temporal characteristics of plasma depend to a large degree on the particular application for which the plasma will be used.

During sputtering, the target at a high negative potential is bombarded with positive argon ions. The target material is sputtered away mainly as neutral atoms by momentum transfer and ejected surface atoms are deposited onto the substrate placed on the anode. During ion bombardment, the source is not heated to high temperature and the vapor pressure of the source is not a consideration as in the case of vacuum-evaporation. The amount of material, W , sputtered from the cathode, is inversely proportional to the gas pressure, P_t , and the anode-cathode distance, D :

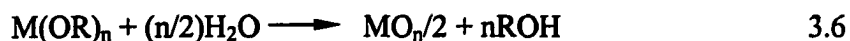
$$W = \frac{kVi}{PtD} \quad 3.5$$

with V being the working voltage, i the discharge current, and k a proportionality constant. Other energetic particles such as secondary electrons, secondary ions and photons, and X-rays are created at the target and can be incorporated in the growing film and/or influence its properties through heating, radiation, or chemical reactions. The sputter yield, S , stands for the number of atoms removed per incident ion and is a function of the bombarding species, the ion energy of the bombarding species, the target materials, the incident angle of the bombarding species, and its electronic charge. Deposition rate is roughly proportional to yield for a given plasma energy [54].

Sol-gel Method and Ion Impregnation

The sol-gel technique is a widespread method of synthesizing materials and depositing them in the form of thin, homogeneous films. Accordingly, it has gained importance with respect to scientific and application purposes. Based on the chemistry of the synthesis, a large variety of materials, e.g. oxide semiconductors, glasses and even superconducting films can be obtained [64-67].

In this process, an inorganic or organic molecular precursor $M(OR)_n$, a sol, is used as starting material, where M is a metal and (OR) an organic compound, respectively. A macromolecular oxide network is then obtained in a moist environment through hydrolysis and polycondensation, which transforms the precursor into a highly viscous (gel-like) hydrated metal oxide (MO_x). In a final heat treatment at typically 100-300 °C the coating is then dried in an oven to complete hydrolysis and condensation. In principle the sol-gel reaction can be written as



The hydrolysis of metal oxides is accelerated by the presence of an acid or base catalyst. The parameters that affect the sol preparation are either the relative amount of acid or base, water and alkoxide, and temperature. During the aging of the sol, the polycondensation process proceeds by leading to cross-linking and the formation of polymers.

In regard to silicon alkoxide precursors (such as the tetraethoxysilane $Si(OEt)_4$ or TEOS), the chemical conditions are generally chosen in such a way that nearly complete hydrolysis occurs in a few minutes. This allows one to realize separately the condensation

with the formation of siloxane bridges [=Si-O-Si=] between the hydrolyzed species [=Si-OH] [64, 68, 69].

For aluminum oxide, the same principle holds. But it is more difficult to apply on the surface of microreactor because the adhesion between aluminum oxide and silicon is lower than that between silicon oxide and silicon.

The basic advantage of the sol-gel process is its ability to form inorganic structures (semiconductors, ceramics and glasses) at relatively low temperatures. Furthermore, the process being very similar to conventional coating techniques such as dip-, spin- or spray coating does not require any vacuum steps, and is therefore a cost-effective way to produce thin homogeneous inorganic films on large scales [70].

Sol-gel method can be used to deposit catalyst support (SiO_2 and Al_2O_3) in the microreactor because the pore structure of catalyst support can increase surface area of microreactor, making more interfaces between reactants to produce more products each unit time.

For catalyst coating, we have used two methods: physical method, which includes sputtering deposition, and chemical method, which includes sol-gel method and ion impregnation. Metal oxide organics can be dissolved in an organic solvent. Then the solution can be impregnated into microreactor channels. A reduction of metal is the following step to yield a pure metal catalyst. In this study, platinum, iron and cobalt were used as catalysts.

Anodic Bonding

The bonding technique of two wafers is a very important technology in the packaging and design of microstructures [71,72]. Protection of the device from the atmosphere is one of the greatest problems for durability and performance [72,73]. In particular, the anodic bonding method has attracted interest in microsensors and microdevices with many advantages, such as solid-state bonding, a bonding process without the requirement of either a post-heat-treatment at high temperature [74] or hydrophilic cleaning [75] which can bring degradation of device lifetime [76]. The method was invented by Wallis and Pomerantz in 1969 [77]. It has been concentrated on silicon-to-silicon bonding since the anodic bonding method using a sputtered Pyrex glass layer was invented later by Brooks and Donovan in 1972 [78, 79]. Anodic bonding can provide a strongly bonded, hermetic seal, which protects the devices from the atmosphere, in spite of the simple process involved.

Anodic bonding is typically performed between a sodium-bearing glass wafer and a silicon wafer. At elevated temperatures, the mobility of the positive sodium ions present in the glass is fairly high and the presence of an electric field causes them to migrate to the negatively charged cathode at the back of the glass wafer. As the Na^+ ions migrate towards the cathode, they leave behind a fixed charge in the glass, which creates a high electrostatic field with positive charge in the silicon. As a consequence, the surfaces of the contacted wafers are pulled together by the electrostatic force and the atomic bonds Si-O-Si are presumed to occur [80].

The anodic bonding process can be carried out by 1) placing a glass (e.g., Pyrex 7740) sheet on a bare or oxidized silicon wafer, 2) heating the assembly to 400 °C, and 3) holding the silicon at positive (anodic) potential relative to the glass (a power supply on the order of 1.2 kV is typically used).

To help minimize thermal stresses, one should use glasses with thermal expansion coefficients close to that of silicon, such as Corning 7740 (Pyrex™) and 7070; Schott 8330 and 8329; and Iwaki 7570. A key point for anodic bonding is that while several references in the literature state that anodic bonding must be done in vacuum, this is not the case that we have observed (atmospheric bonding works well) [81].

Analysis Theory

Gas Sorption Theory

The tendency of all solid surfaces to attract surrounding gas molecules gives rise to a process called gas sorption. Monitoring the gas sorption process provides a wealth of useful information about the characteristics of solids. Before performing gas sorption experiments, solid surfaces must be freed from contaminants such as water and oils. Surface cleaning (degassing) is most often carried out by placing a sample of the solid in a glass cell and heating it under a vacuum. Once clean, the sample is brought to a constant temperature by means of an external bath. Then, small amounts of a gas (the adsorbate) are admitted in steps into the evacuated sample chamber. Adsorbate molecules quickly find their way to the surface of every pore in the solid (the adsorbent). These molecules can either bounce off or stick to the surface. Gas molecules that stick to the surface are said to be adsorbed. The strength with which adsorbed molecules interact with

the surface determines if the adsorption process is considered physical (weak) or chemical (strong) in nature [89].

The Brunauer-Emmett-Teller method [1] is the most widely used procedure for the determination of the surface area of solid materials and involves the BET equation 3.7 [91].

$$\frac{1}{W((P_0/P)-1)} = \frac{1}{W_m C} + \frac{C-1}{W_m C} \left(\frac{P}{P_0}\right) \quad 3.7$$

W is the weight of gas adsorbed at a relative pressure P/P₀ and W_m is the weight of adsorbate constituting a monolayer of surface coverage. The term C, the BET constant, is related to the energy of adsorption in the first adsorbed layer and consequently, its value is an indication of the magnitude of the adsorbent/adsorbate interactions [91].

Multipoint BET Method. The BET equation 3.7 requires a linear plot of 1/[W(P₀/P)-1] vs P/P₀ which for most solids, using nitrogen as the adsorbate, is restricted to a limited region of the adsorption isotherm, usually in the P/P₀ range of 0.05 to 0.35. This linear region is shifted to lower relative pressures for microporous materials. The standard multipoint BET procedure requires a minimum of three points in the appropriate relative pressure range. The weight of a monolayer of adsorbate W_m can then be obtained from the slope s and intercept I of the BET plot. From equation 3.7:

$$s = \frac{C-1}{W_m C} \quad 3.8$$

$$i = \frac{1}{W_m C} \quad 3.9$$

Thus, the weight of a monolayer W_m can be obtained by combining equations 3.8 and 3.9.

$$W_m = \frac{1}{s+i} \quad 3.10$$

According to knowledge of the molecular cross-sectional area A_{cs} of the adsorbate molecule, the total surface area S_t of the sample can be expressed as:

$$S_t = \frac{W_m N A_{cs}}{M} \quad 3.11$$

The specific surface area S of the solid can be calculated from the total surface area S_t and the sample weight w .

$$S = S_t / w \quad 3.12$$

Single Point BET Method. For nitrogen, the C value is usually sufficiently large to warrant the assumption that the intercept in the BET equation is zero. Thus, the BET equation 3.7 reduces to

$$W_m = W(1-P/P_0) \quad 3.13$$

By measuring the amount of nitrogen adsorbed at one relative pressure (preferably near $P/P_0=0.3$) the total surface area can be calculated using equation 3.11, 3.13 and the ideal gas equation.

$$S_t = \frac{PVNA_{cs}(1-P/P_0)}{RT} \quad 3.14$$

Scanning Electron Microscopy

The Scanning Electron Microscope (SEM) is a metrology tool used to visually inspect devices [82]. In contrast to optical microscopy, a SEM employs an electron beam,

while the optical microscope uses natural light. Though the SEM is restricted in operation and application due to its illuminating beam (electron beam) and its operating medium (vacuum), it is still widely used for conductive materials or semiconductors because of its ease of operation and its ability to give high-resolution images of small objects [83]. A SEM can produce clear images of specimens ranging from objects visible to the naked eye to structures as small as several nanometers. Furthermore, since image contrast is varied according to the shape or composition of the specimen and there are fewer restrictions on specimen size and type, and specimen preparation is simple.

X-ray Photoelectron Spectroscopy

The surface of a solid in contact with a liquid or gaseous phase usually differs substantially from the interior of the solid both in chemical composition and physical properties. Characterization of the surface of a catalyst is often of vital importance in the heterogeneous catalysis.

One of the popular methods for characterizing surfaces is X-ray Photoelectron Spectroscopy. XPS operates on the principle of introducing monoenergetic soft x-rays or photons to a substrate [86]. When the energy is introduced, some electrons are released [84, 52]. These electrons have an energy, when released, that is the difference between the kinetic energy and the energy of the incident beam, referred to as the binding energy. The chemical environment of an atom being excited in this way changes the electron's characteristic energy by causing the valence electrons to redistribute. The generated equation that relates the photon energy to the binding energy is shown in Equation 3.15,

where KE is the kinetic energy of the emitted electron, $h\nu$ is the energy of the photon, BE is the binding energy, and ϕ_s is the work function of the spectrometer.

$$KE = h\nu - BE - \phi_s \quad 3.15$$

The XPS yields the material's composition as well as an approximate thickness of the catalyst deposited [87] to observe the depth profiles of catalysts. The sensitivity of the XPS to the surface increases as the angle is increased by tilting the substrate with respect to the electron collector. The Equation used for determining the analysis depth, d , is

$$d = \lambda \sin \theta \quad 3.16$$

where λ is the inelastic mean free path, and θ is the take-off angle of the analyzed electrons [88]. This λ is read from the universal inelastic mean free path curve at the point corresponding to the kinetic energy of the catalyst.

Energy Dispersive X-Ray

Energy Dispersive X-Ray (EDX) is reliable, tolerant of high count rates, and can perform a qualitative analysis of a sample. The basic principle of Energy Dispersive X-Ray (EDX) is that, when x-ray photons are captured by the detection crystal, they create electron-hole pairs. These electron-hole pairs are formed as charge pulses by the applied bias and further converted to voltage pulses by a charge-to-voltage converter (preamplifier). The signals are further amplified and shaped by a linear amplifier and finally passed to a computer x-ray analyzer (CXA), where the data are displayed as a histogram of intensity by voltage. The key to understanding an energy-dispersive spectrometer (EDS) is to recognize that each voltage pulse is proportional to the energy of the incoming x-ray photon. The EDX analysis, in general, is nondestructive with

regard to the specimen so that the same sample can be used for other studies. EDX uses low probe currents as its detectors are quite efficient under these conditions. Thus, EDX is useful for studies of thin films on surface and for studies of rough surfaces and powders.

Vibrating Sample Magnetometer (VSM)

A vibrating sample magnetometer (VSM) operates on Faraday's Law of Induction, with a changing magnetic field that produces an electric field. This electric field can be measured and can provide information about the change in magnetic field. The VSM is used to measure the magnetic behavior of magnetic materials. A VSM can be operated by first placing the sample in a constant magnetic field. If the sample is magnetic, this constant magnetic field will magnetize the sample by aligning the magnetic domains, or the individual magnetic spins, with the field. The stronger the constant field, the larger will be the magnetization. The magnetic dipole moment of the sample will create a magnetic field around the sample, sometimes called the magnetic stray field. As the sample moves up and down, this magnetic stray field changes as a function of time and can be sensed by a set of pick-up coils. The alternating magnetic field will cause an electric field in the pick-up coils according to Faraday's Law of Induction. This current will be proportional to the magnetization of the sample. The greater the magnetization, the greater is the induced current. The induction current is amplified by a transimpedance amplifier and a lock-in amplifier. The various components are connected to a computer interface. Using controlling and monitoring

software, the system can determine how much the sample is magnetized and how its magnetization depends on the strength of the constant magnetic field [92].

Response Surface Methodology

Response surface methodology developed by Box and Wilson in 1951 is to aid the improvement of manufacturing processes in the chemical industry. The main purpose is to optimize chemical reactions to obtain, for example, high yield and purity at low cost. This is accomplished through the use of sequential experimentation involving factors such as temperature, pressure, duration of reaction, and proportion of reactants. The same methodology can be used to model or optimize any response that is affected by the levels of one or more quantitative factors.

The general idea is as follows. The response is a quantitative continuous variable (e.g., yield, purity, cost), and the mean response is a smooth but unknown function of the treatment combinations, which is a surface in $p + 1$ dimensions, and called the response surface. For example, Figure 3.1 shows a response surface for two factors A and B. The levels at which the observations were taken are marked on the plot.

The levels of A are denoted by values of x_1 or x_A and the levels of B by values of x_2 or x_B . A treatment combination is denoted by $\mathbf{x} = (x_1 \ x_2 \dots \ x_p)$ or by $\mathbf{x} = (x_A \ x_B \dots \ x_p)$ and the mean response at \mathbf{x} by $\eta_{\mathbf{x}} = E[Y_{\mathbf{x}}]$. The general response surface model is of the form

$$Y_{\mathbf{x}} = \eta_{\mathbf{x}} + \epsilon_{\mathbf{x}} \quad 3.17$$

Where $\epsilon_{\mathbf{x}}$ is a random error variable.

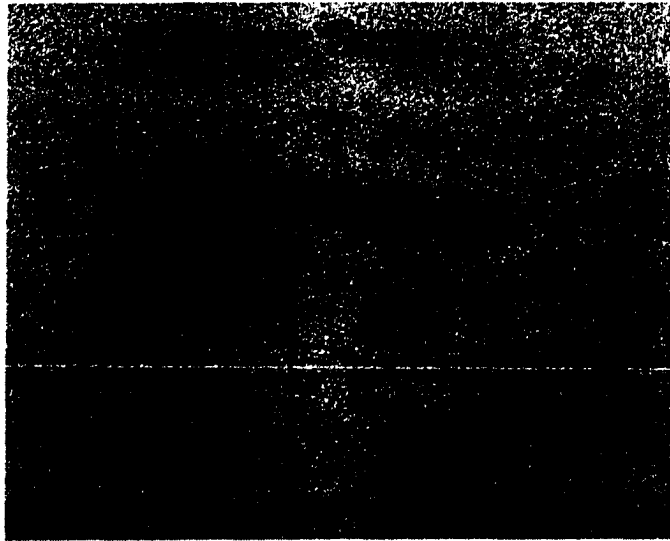


Figure 3.1 Hypothetical response surface for two factors [93]

The objective of obtaining a response surface is twofold:

- (i) to locate a feasible treatment combination \mathbf{x} for which the mean response is maximized (or minimized, or equal to a specific target value); and
- (ii) to estimate the response surface in the vicinity of this good location or region, in order to better understand the “local” effects of the factors on the mean response.

Before the peak of the response surface is reached, a small local experiment is conducted to assess the local terrain. If the local experiment is not in the vicinity of the peak, then a first-order regression model often provides an adequate approximation to the local response surface. For p factors, the standard *first-order model* is a first-order polynomial regression model:

$$Y_{\mathbf{x},t} = \beta_0 + \beta_1 x_1 + \dots + \beta_p x_p + \epsilon_{\mathbf{x},t}, \quad 3.18$$

Where $Y_{x, t}$ denotes the t th observation at treatment combination $\mathbf{x} = (x_1 \dots x_p)$, and the error variables $\epsilon_{x, t}$ are assumed to be independent with $N(0, \sigma^2)$ distributions. The parameter β_i is a measure of the local *linear effect* of the i th factor ($i = 1, \dots, p$).

The standard first-order designs consist of n_f “factorial points” and n_0 “center points.” The factorial points consist of the treatment combinations of a 2^p factorial experiment as a completely randomized design, or a 2^{p-s} fractional factorial design of Resolution III or higher. The center points are observations collected at the center of the local region under study, that is, at $z_0 = (0 \ 0 \ \dots \ 0)$. These are needed to provide error degrees of freedom and to provide adequate power for a test of the model with lack of fit.

Second-order designs and analysis are used when the test for lack of fit of the first-order model indicates that the vicinity of the maximum (or minimum) of the response surface has been reached and a second-order model should be fitted.

Central Composite Designs (CCD) were first described by Box and Wilson in 1951, and they are now the most popular second-order designs. Each design consists of a standard first-order design with n_f orthogonal factorial points and n_0 center points, augmented by n_a “axial points.”

Following the convention of coding the factor levels, the factorial points have coded levels ± 1 for each factor. However, it should be noted that some software packages will recode the levels in a central composite design before doing the analysis. Under this convention, *axial points* are points located at a specified distance α from the design center in each direction on each axis defined by the coded factor levels. On the z_i -axis, for example, two axial points are obtained by setting $z_i = \pm \alpha$, with $z_j = 0$ for all $j \neq i$.

Thus, if there are p factors, there are $2p$ distinct axial points. Axial points are also commonly referred to as *star points*. Figure 3.2 shows central composite designs for $p = 2$ and $p = 3$ factors.



Figure 3.2 Central composite designs for $p = 2$ and $p = 3$ factors [93]

A CCD is easily built up from a standard first-order design by the addition of axial points, and possibly some extra factorial and center points. If the factorial portion of the design is a complete factorial or a fractional factorial of resolution V or more, all model parameters can be estimated. Otherwise, some aliasing will occur, and some terms will need to be omitted from the second-order model. A design should include enough replication, often at the center points, to allow for a test for model lack of fit. The axial points are located at a distance α from the center of the design, where the choice of α depends on the properties required of the design. A popular choice is $\alpha = (n_f)^{1/4}$ [93].

CHAPTER IV

MATERIALS AND METHODS

Microfabrication

Photolithography

In this study, lithography technology was used for microreactor microfabrication and catalyst selective deposition. The photoresists were the materials used to transfer the reactor patterns from the mask to the substrate. Two types of photoresists were used: positive photo resist and negative photoresist. Positive photoresist, MICROPOSIT S-1813 photoresist from Shipley Company, was for fabrication of the microreactor front-side. It is a combination of 1-methoxy-2-propyl acetate [108-65-5], mixed cresol novolak resin, fluoroaliphatic polymer esters, and diazo photoactive compound. The exposure of this type of photoresist is g-line, the resolution is $< 65\mu\text{m}$, and the sensitivity is $150\text{mJ}/\text{cm}^2$. The developer Miroposit MF 319 can be used to generate the pattern on the photoresist S-1813. MP Primer HMDS can improve the adhesion between the MICROPOSIT Shipley S-1813 and the silicon wafer [94].

For etching backside of the microreactor, AZ[®] EXP P4903 photoresist and AZ[®] 9260 from Clariant were the materials used to transfer the microreactor's pattern. The maximum thickness of AZ[®] EXP P4903 was around $10\mu\text{m}$. It consists of 1-methoxy-2-propanol acetate [108-65-6], cresol-novolak resin [117520-84-0], and diazonaphthoquinonesulfonic esters [5610-94-6] [95]. The developer for this photoresist

was AZ 400K 1:3 DI water. AZ[®] 9260 thick film photoresist is designed for the more demanding, higher-resolution thick resist requirements. It provides high-resolution with superior aspect ratios, as well as wide focus and exposure latitude and good sidewall profiles. AZ[®] 9260 photoresist is available for a film thickness up to 24 μm . Critical dimension resolutions range from $< 1 \mu\text{m}$ lines and spaces at a film thickness of 4.6 μm , to 3.5 μm lines and spaces at a film thickness of 24 μm on silicon using today's standard broadband exposure tools. Aspect ratios of 5 - 7 can be achieved. The preferred developer is AZ[®] 400K Developer 1:4, a buffered developer designed to maximize bath life and process stability. Another negative photoresist, NR9-1500P from the Futurrex Company, was used for catalyst selective deposition in the microchannels of the reactor. It consists of cyclohexanone [108-94-1], resins, and sensitizers [95]. The developer RD6 from Futurrex Inc. can open channel areas for catalyst coating.

Inductively Coupled Plasma (ICP) Etching

Inductively Coupled Plasma (ICP) etching was the dry etching method for micromachining the reactor channels into the silicon wafer. At the Institute for Micromanufacturing (IfM) of Louisiana Tech University, an Alcatel 601E ICP etcher is used. (Figure 4.1) The process technology underlying this machine is the so-called Bosch process. This process is currently widely used on inductively-coupled plasma equipment for the deep reactive ion etching (RIE) technology in silicon micromachining. Alcatel's deep plasma etch technology is designed to deliver superior process performance and maximum process and was flexible to meet the needs of a broad range of deep silicon etch applications. Applications in MEMS and microsystems fabrication include: high

aspect ratios, etch depths of as great as 500 μm , etching through-the-wafer, etching into a buried cavity in the wafer, or etching onto buried oxide. The deep etch process uses a patented high-density inductively-coupled plasma (ICP) source and a fluorine based non-corrosive etch chemistry. The process chamber is fitted with permanent magnets on the chamber walls, giving excellent etch uniformity across a wafer ($< \pm 5\%$). Wafer sizes can be 100 mm, 125 mm, 150 mm, or 200mm. Si etch rates of up to 10 $\mu\text{m}/\text{min}$ can be achieved. Selectivity of Si to SiO_2 of up to 1000:1 and Si to resist of up to 100:1 can be achieved. High-precision vertical profiles can be controlled by sidewall passivation.



Figure 4.1 Inductively Coupled Plasma ICP Etcher (Alcatel System A 601E) at IfM, Louisiana Tech University

Sputtering Deposition

Deposition of conducting and insulating thin-films can be realized by using DC or RF plasma. For this research, sputtering deposition was the method for uniform catalyst

coating inside the microchannels of the microreactors. IfM in Louisiana Tech University owns a PVD-300 system. (Figure 4.2)

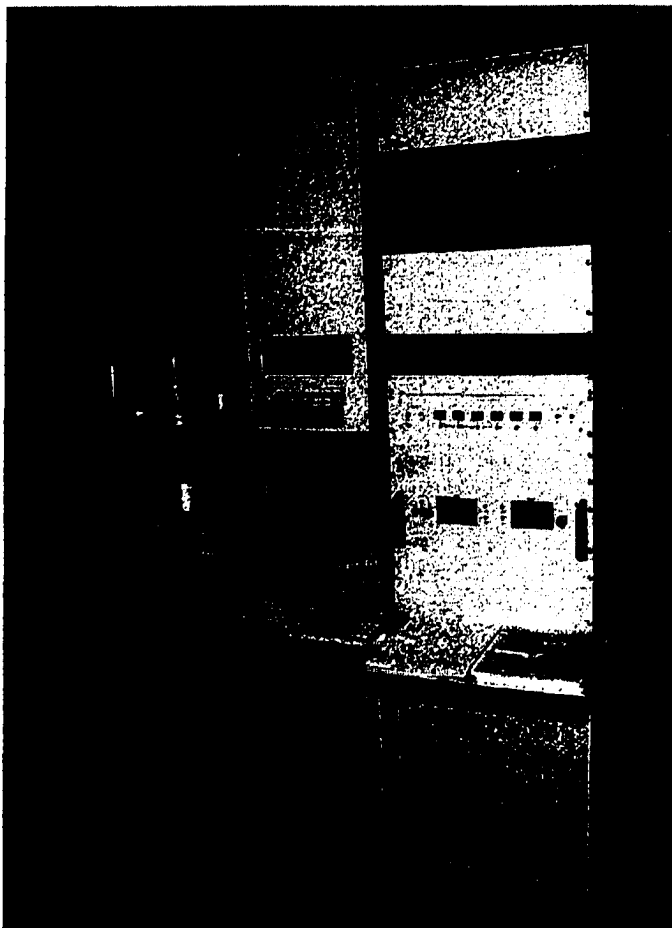


Figure 4.2 PVD-300 system for sputtering deposition at IfM , Louisiana Tech University.

The system currently has three DC power supplies and a single RF power supply. The amount of time required to perform a deposition is not a linear function of the film's deposition rate. For example, it takes much longer than 10 minutes to deposit a 1 μm film if the deposition rate is 100 nm/min. The maximum film thickness, which should be deposited via sputtering, is material- and process-dependent. However, maximum

thickness should not exceed 1 μm for precious metals (Au, Pt, & Pd), or 5 μm for other materials. It is not possible to use a single power supply to simultaneously power both a magnetron and the substrate. The PVD-300 system incorporates a new approach to thin film deposition that results in an unprecedented combination of efficiency, versatility, and high-performance. The approach is based on the premise that if one has complete knowledge of the amplitude and shape of a source distribution, as well as full control of a mobile substrate fixture capable of placing any point on the substrate at any position in the Source Distribution for any prescribed period of time, then it is possible to predict and implement source-substrate motion scenarios that produce extremely uniform deposition onto substrates of any specified size, irrespective of the size of the source. In particular, the PVD-300 is capable of routinely and reproducibly depositing extremely uniform (>99%) and homogeneous single- or multi- layer films of metal, alloys, and insulators onto substrates up to 8 inches in diameter, using a variety of small, high-performance sources. Resistive substrate can be heated over the range of 300–700 $^{\circ}\text{C}$ during deposition. The sputtering etching for cleaning the substrate prior deposition is available in this PVD-300 system [96].

Chemicals for Sol-Gel Coating and Ion Impregnation of Catalysts

In this study, platinum, iron, and cobalt were the catalysts fabricated by the sol-gel method and ion impregnation. Silica and alumina were the catalyst supports for increasing the surface area of the catalysts. Platinum was used for dehydrogenation/hydrogenation of cyclohexene and preferential oxidation for CO in fuel cell. Silica and alumina were the supports for Pt. Iron and cobalt were for Fischer-

Tropsch (F-T) synthesis. Alumina was the support for Fe and Co. Table 4.1 shows the chemicals of sol-gel precursors and ion impregnation precursors.

Table 4.1 Chemicals for sol-gel and ion impregnation of catalysts

		Precursors
Catalysts	Platinum	Platinum (II) 2,4 Pentanedionate (Pt (C ₅ H ₇ O ₂) ₂)
	Iron	Ferric nitrate
	Cobalt	Cobalt nitrate
Supports	Silica	tetraethoxysilane (Si(OC ₂ H ₅) ₄) (TEOS)
	Alumina	Aluminum Iso-propoxide (Al(OC ₃ H ₇) ₃), Aluminum tri-sec-butoxide ([C ₂ H ₅ CH(CH ₃)O] ₃ Al)

Analytical Methods for Characterization of Catalysts

Amray 1830 SEM

The SEM is a metrology tool used to visually inspect devices, and was chosen for studying microreactor and catalyst structures because of its ease in operation and its ability to give high-resolution images of small objects [82]. The instrument 1830 SEM, acquired from Amray, is an electron gun type SEM with a tungsten filament (Figure 4.3).

The filament emits electrons that excite the surface atoms. These atoms are collected by the detector, and finally a video amplifier turns the signal into an image [98]. The 1800 Series SEMs were among the first automatic imaging SEMs which included digital image storage and processing system as standard equipment. This new development incorporates image storage, integration, and signal-to-noise ratio processing, as well as real time presentation of the image on a TV rate monitor. In addition, microcomputers control several automated functions designed to relieve the casual user from acquiring high technical skills. These automated functions, such as

focusing, stigmating, video contrast and brightness control, electron gun filament, and heat and emission control, may also be operated in the traditional manual modes [99].

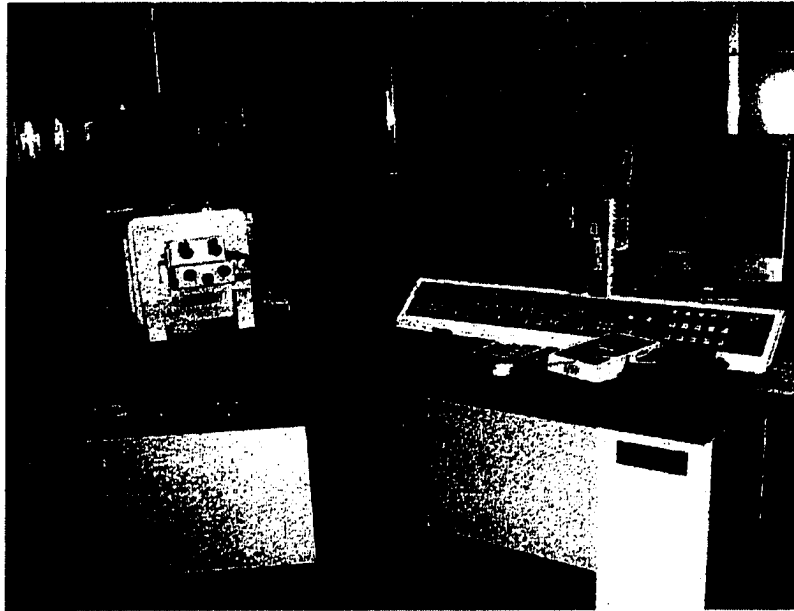


Figure 4.3 Amray 1830 SEM at IfM, Louisiana Tech University

The Physical Electronics 5800 Multi-Technique System

XPS was employed to chemically analyze the material deposited by the sol-gel method and ion impregnation. The Physical Electronics 5800 MultiTechnique System was used at IfM of Louisiana Tech University. These automated surface analysis instruments can be easily operated (Figure 4.4). MultiTechnique Systems allow for the combination of any of these surface analysis techniques: X-ray Photoelectron Spectroscopy (XPS) [also known as Electron Spectrometry for Chemical Analysis (ESCA)], Ion Scattering Spectroscopy (ISS), Auger Electron Spectroscopy (AES), Scanning Auger Microscopy (SAM), and Secondary Ion Mass Spectrometry (SIMS). A

monochromatic source can also be added to enhance the energy resolution of the system. The 5800 has a new vacuum chamber layout to accommodate a new ion gun and electron neutralizer. The new Model 06-350 ion gun was optimized for sputter depth profiling and provided a capability of showering samples with low energy (5eV) ions to facilitate charge neutralization.

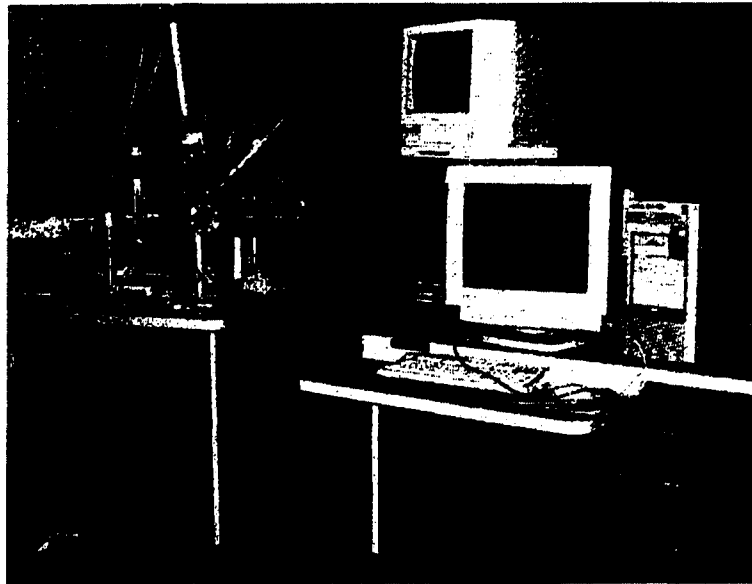


Figure 4.4 The Physical Electronics 5800 MultiTechnique System at IfM, Louisiana Tech University

Quantachrome NOVA 2000

One of the differences between sputtered catalysts and sol-gel coated catalysts is the increased surface area in sol-gel coated catalysts. In this study, a Quantachrome NOVA 2000 instrument was utilized for measuring the surface area of the catalyst (Figure 4.5). NOVA 2000 has an automated, high speed surface area and pore size analyzers, and can be used to examine two samples simultaneously. It also has two

degassing stations. The degassing temperature reaches ambient – 450 °C, in 1 °C intervals with an accuracy of ± 5 °C. Either nitrogen flow or vacuum can be used for degassing. Analysis data can be printed out by connecting a printer with a built-in printer port or can be transferred to available Windows PC software. The surface area range that NOVA 2000 can measure is 0.01 – >2,000 m²/g. The adsorption and desorption isotherm can be studied for pore diameter in the range of 3.5 – 2,000Å, with minimum pore volume $> 2.2 \times 10^{-6}$ cc [100].

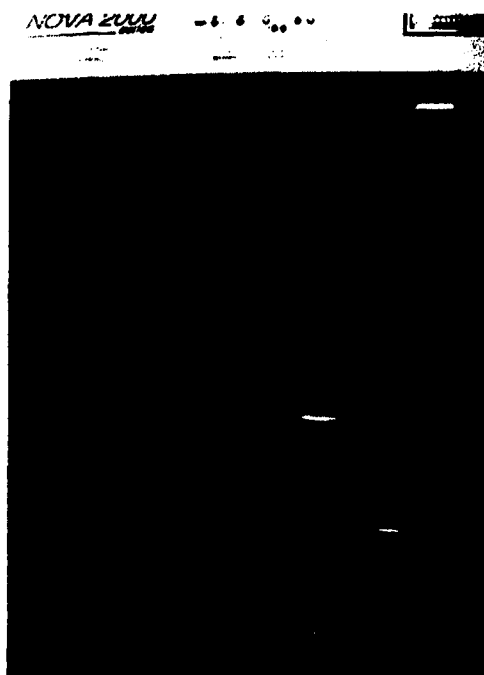


Figure 4.5 Quantachrome apparatus Model: NOVA 2000 for surface area measurement of catalysts

Kevex LPX1 Super Dry Quantum Detector
EDX system

To study the uniformity and elemental composition of sol-gel deposited micro-channel reactors, the Carl Zeiss DSM 942 SEM, equipped with the Kevex LPX1 Super

Dry Quantum Detector EDX system was used at Grambling State University. An EDX system analyzes the x-rays emitted from a sample after it has been bombarded by an electron beam from the scanning electron microscope. Depending upon the material being analyzed, characteristic spectral peaks are observed which allow the identification of elements within the top 1% of the sample surface. This technique is essentially non-destructive in nature and requires little preparation of the sample under examination.

880A Digital Measurement Systems (DMS)
Vibrating Sample Magnetometer (VSM)

In this study, iron and cobalt were employed as catalysts for Fischer-Tropsch (F-T) synthesis. Both Fe and Co have magnetic properties. An 880A Digital Measurement Systems Vibrating Sample Magnetometer (VSM) at Grambling State University was used to determine the magnetization characteristics of the Fe/Co encapsulated Al_2O_3 sol-gel micro-reactors. The DMS Vibrating Sample Magnetometer (VSM) is a computer-controlled measurement system capable of characterizing a wide variety of magnetic samples. Its reliability, user friendliness, and ability to measure both high and low coercivity materials make it the de-facto standard measurement system used by almost all hard disk manufacturers and magnetic recording research facilities. The high precision stepped field control used in conjunction with Digital Signal Averaging leads to increased accuracy of the measured graphs and measurement parameters. The DMS Vibrating Sample Magnetometer (VSM) benefits include proven reliability in the field, digital field control for high accuracy, new comprehensive control and analysis software (Easy VSM), rapid sample loading, automated complex test routines and data extraction, and no hardware change between heating and cooling.

DMS offers a unique combination system including Torque and/or Magneto-Resistance (MR) options, which can be added to the VSM without increasing the system footprint and are less expensive than buying separate systems [101].

Methods for Microreaction Analysis

For quantitative analysis of the effluent of reactants and products in the outlet of the reaction system, a QMS 100 Series Gas Analyzer from Stanford Research Systems was employed to record continuous partial pressure data during the course of experiments while temperature and reactant flow rates were varied.

The QMS 100 series instruments are modern mass spectrometers designed for the analysis of light gases. The spectrometer operates at high vacuum, 10mbar. Not only the data are acquired continuously, the response is also fast. A change in composition at the inlet can be detected in less than 0.5 second. The system allows data to be collected quickly; a complete spectrum can be acquired in less than one minute and individual masses can be measured at rates up to 25 ms per point. The QMS consists of two subsystems: gas handling and the analyzer. The analyzer specializes in large dynamic range measurements of light gases. For users with specialized needs, the QMS can be controlled from user programs. This modern system allows many new applications in contrast to the traditional mass spectrometer that is too large and heavy [102].

CHAPTER V

MICROREACTOR DESIGN, FABRICATION, CATALYST PREPARATION AND MICROREACTION SETUP

Microreactor Design and Fabrication

The microreactor used in this project was made from a four-inch in diameter, 500 μm thick, double side polished, [110] silicon orientation wafer. The microreactor consists of a *via* (the holes through the wafer) to allow gas to flow into the reactor, inlets, outlets, and microchannels. The reactant gas flows through the *via* into the microreactor and into the inlet area. After entering the inlet, the species will mix in the manifold area and then flow into the microchannel, or reaction zone. Once the reaction is complete, the effluent of the microreactor will leave the reactor through another *via*. The effluent is sent to a mass spectrometer for analysis. Two types of microreactors have been used in this study: straight-line channel and wave channel. (Figure 5.1) For straight-line channel reactors, the dimension was 3 cm long and 1 cm wide, and for zigzag channel reactors, it was 3.1 cm long and 1.6 cm wide. 5 μm and 100 μm wide microchannels were produced for straight wall reactors. The wave channel microreactor was only produced in 5 μm width. The depth of all microreactors was 100 μm .

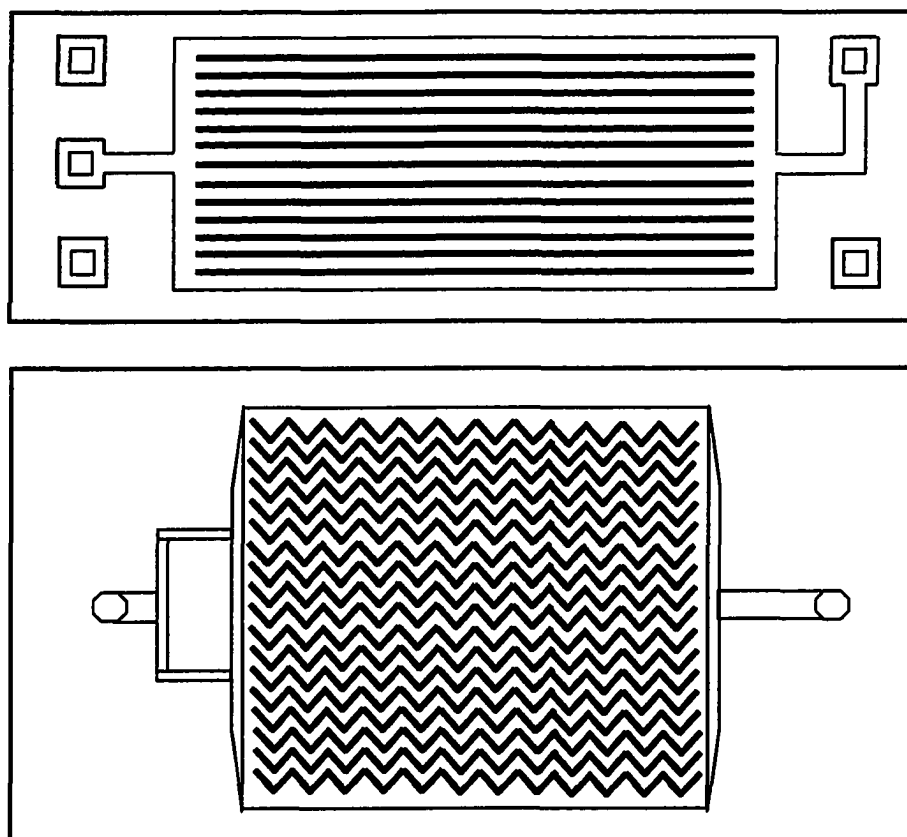


Figure 5.1 Two types of microreactors

The microreactor was fabricated using a lithography-based process and dry etching method. The lithography process used to make the microreactor is much like the one used in the integrated circuit (IC) industry [103]. Before fabrication, the microreactor mask layout was designed. The masks were designed with flexibility as a major issue. The major reactor parts were implemented on separate masks to allow the flexibility of creating different types of microreactors. As a result, separate sets of masks were designed: one set for the vias, one set for the inlets and outlets, and one set for the reaction zone or channels itself. With this flexibility, many different reactor combinations could be made with the same masks. For example, a reactor with 5 μm channel width and

two or three inlets could be made just by using a different inlet/outlet mask. AutoCAD 2000 software was used to draw the masks. The masks were produced on a glass plate covered with chromium. In addition, future masks can be easily integrated within this process, upgrading the reactor to meet new reaction needs.

The fabrication process for the reactor used in this project starts with a double-side polished silicon wafer. It is shown in Figure 5.2.

1. The wafer was cleaned in baths of trichloroethane, acetone, and isopropyl alcohol for 10 minutes in each bath.
2. The wafer was prebaked at 165 °C for 90 seconds in a nitrogen environment while being clamped to the hotplate by means of a vacuum. The wafer was allowed to cool down for 5 minutes in a petri dish to prevent dust contamination.
3. After the wafer cooled down, hexamethydisiloxane (HMDS) was spun on to dehydrate the surface at 1500 rpm with 150 rpm/s for 40 seconds to improve the adhesion of the photoresist.
4. Then Microposit 1813 positive photoresist was spun at 3000 rpm with 500 rpm/s, for 50 seconds, which creates a photoresist film with a thickness of 1-2 μm on the wafer.
5. The wafer was soft baked at 115 °C for 35 seconds. Shorter times and lower temperatures lead to a soft, wet photoresist film, which is not suitable for producing small patterns. Longer times and higher temperatures over-dry the film, causing non-uniformities in the film. Then, the inlet/outlet of the front side was

aligned and exposed for 5, 8, or 15 seconds at proximity of 20 μm . 8 seconds was found to be the best time for a large feature size. After exposure, the wafer was developed in Microposit MF 319 developer for 70 seconds and rinsed in DI water for 2 minutes. Times shorter than 70 seconds did not developed completely, while times longer than 70 seconds over-etched the photoresist.

6. The *vias* of the front side were aligned and exposed for 8 seconds at a proximity of 20 μm . Again, after the exposure, the wafer was developed in Microposit MF 319 developer for 70 seconds and rinsed in DI water for 2 minutes.
7. As in the above two steps, the channel zone was aligned and exposed for 6 seconds at a proximity of zero, and developed in Microposit MF 319 developer for 60 seconds and rinsed in DI water for 2 minutes. Here, proximity of zero means that the wafer and mask contacted each other to increase alignment resolution because of smaller feature size (5 μm or 100 μm channels). Shorter exposure time and development time avoided the over-exposure and over-development.
8. After patterning the front side of the wafer, the wafer was etched by Inductively coupled plasma etching (ICP etching). The equipment used for this study was an Alcatel 601E ICP etcher, as mentioned in the previous chapter. (Figure 5.3) First, the vacuum level of the reaction chamber has to be checked, which should remain below 2.6×10^{-3} mTorr. Then the flow rate and cycle time of SF_6 and C_4F_8 , plasma source power and processing duration were set. After that, the wafer was loaded

in the reaction chamber and the run was started. This process transferred the pattern from the photoresist to the silicon wafer. At the etching rate of 5-7 μm per minutes for 20 min, the depth of the microreactor was around 100 μm . The periodic change of different gases for etching (SF_6) and passivation (C_4F_8) can lead to very high aspect ratios and very high etch rates.

9. The etched wafer was cleaned by three steps: removing the photoresist residuals, rinsing with acetone and isopropyl alcohol and drying with room nitrogen.
10. One silicon wafer was used to bond with the ICP-etched wafer on the front side by AZ[®] EXP P4903 for backside patterning. This is because a vacuum held the wafer during the photoresist spin coating and ICP etching. Thicker photoresist was required for backside etching because the wafer should be etched through around 400 μm from the backside for microreaction flow into the microreactor, and ICP etching selectivity of Si to the photoresist was 100:1. The thickness of photoresist AZ[®] EXP P4903 is up to 10 μm , which is enough for backside etching of the microreactor. Thus, AZ[®] EXP P4903 was spread on the wafer for 20 sec at 600 rpm, spun for 3 min at 3k rpm and soft baked 60 min at 90 °C.
11. Backside vias were aligned and exposed for 20 seconds at a proximity of 20 μm . Again, after the exposure, the wafer was post baked 60 min at 120 °C, developed in Microposit AZ 400K 1:3 DI water for 90 seconds, and rinsed in DI water for 2 minutes.
12. ICP etching transferred via patterns from the photoresist to the backside of the

wafer. During etching, AZ[®] EXP P4903 was buried and peeled off, which led to a bad pattern on the silicon wafer, especially in the feature size. Thus, the thicker photoresist, AZ[®] 9260 was selected.

13. For photoresist AZ[®] 9260, a 300 rpm dispense and a 2400 rpm spin for 60 seconds was needed for a 10 μm thickness. Then the wafer needed to soft bake at 110 °C for 165 seconds. After exposure, AZ 400K 1:4 developer was used to generate the pattern within 180 seconds.

14. ICP etched through the wafer to 400 μm . After that, the patterned wafer was separated from the support wafer in an acetone solution. Figure 5.4 shows the finished wafer.

15. Finally, the patterned wafer was sent to MPE Inc. for dicing. The microreactors were then ready for catalyst coating and microreaction testing.

Note, the aligner was an Electronic Visions Inc. EV420 and the spinner was from the Coat Effective Equipment Company. A microscope (OLYMPUS VANOX AHMT 3) was used to check the quality of the pattern, and surface profiler (TENCOR Alpha-step 500) was used for depth checking of channels.



a. Clean bare silicon wafer.



b. Coat photoresist on the wafer.



c. Expose and develop to make Inlet/outlet pattern on the photoresist.



d. Expose and develop to make vias pattern on the photoresist.



e. Expose and develop to make channel pattern on the photoresist.



f. ICP etching to transfer pattern from photoresist to silicon wafer.



g. Remove photoresist and clean the wafer.



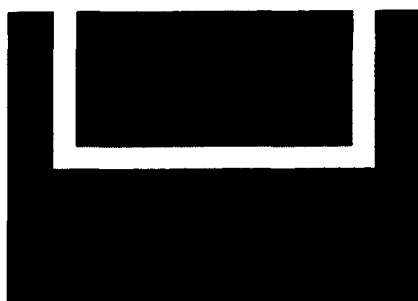
h. Bond the patterned wafer with other silicon wafer for backside etching.



i. Coat photoresist on the backside of the patterned wafer.



j. Expose and develop to make backside via on photoresist.



k. ICP etching through the patterned wafer



l. Separate patterned wafer from bare silicon wafer.

Figure 5.2 Microreactor fabrication process. (Cross section of reactor)

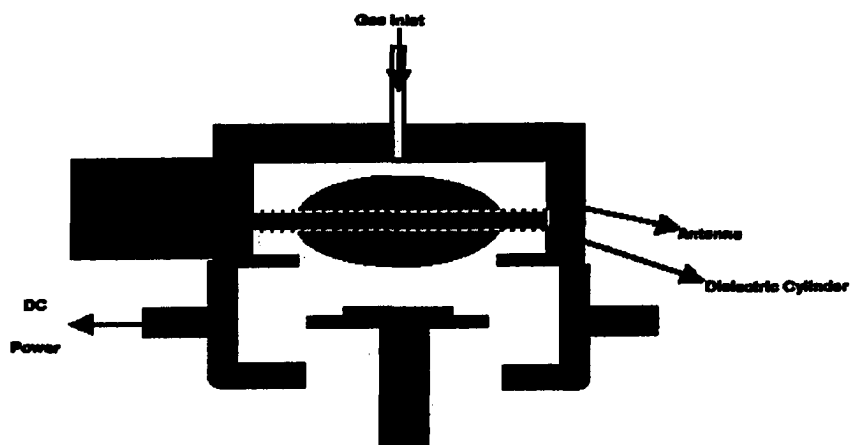


Figure 5.3 Schematic view of Alcatel A 601E process module.

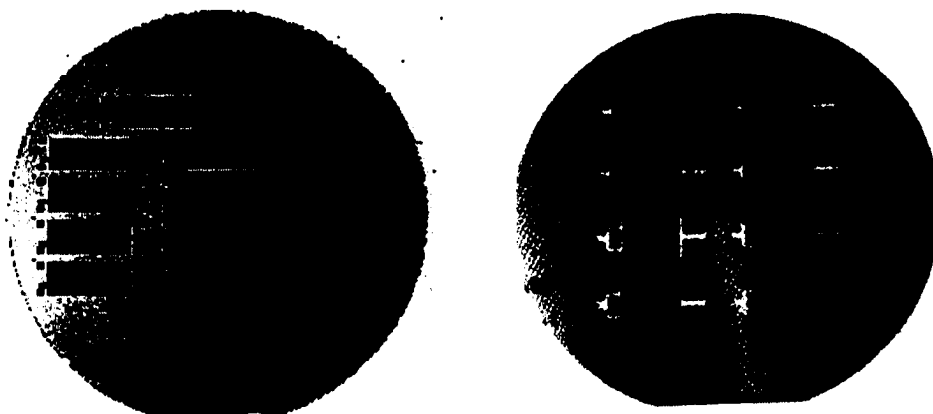


Figure 5.4 Microreactors on one wafer (left: 1 cm x 3 cm in size, right: 1.6 cm x 3.1 cm in size)

Catalyst Preparation

The higher the active surface area of the catalyst, the greater the number of product molecules produced per unit of time. Therefore, much of the art and science of catalyst preparation deals with high-surface-area materials. As mentioned before, there are two types of catalyst preparation: physical methods and chemical methods. Catalysts were fabricated using both techniques to perform a comparison. For the physical method, sputtering deposition was used to coat platinum, cobalt, or iron into microreactor channels, which included channel top, sidewall, and bottom. For the chemical method, the sol-gel method, ion impregnation, or a combined method of both was used. The reasons for choosing the chemical method is to increase the surface area of the catalyst and to lower cost, compared to the sputtering deposition. Both SiO_2 and Al_2O_3 were prepared in such a way that they were crystalline with well-defined microstructures and behaved as active components of the catalyst system in spite of their accepted name, “supports”. Then, platinum was deposited on them, either by sputtering deposition or by impregnation. Solutions of iron and cobalt were mixed with the solution of Al_2O_3 , and then applied them on the channels of the microreactor.

Sputtering deposition of Platinum, Iron and Cobalt

For sputtering deposition, a fixture had to be made for holding the microreactor stable on the substrate holder inside the chamber because the size and weight of the microreactor was too small. During the sputtering process, for a uniform thin film, the holder moves around the metal target and also rotates. Without the holder, the reactor would slide around, resulting in non-uniform film deposition. Figure 5.5 shows the

fixture. It consists of two aluminum plates and one transparent mask. The bottom plate has a bed for microreactor. There is a window on the mask for selective deposition of the catalyst. The channel region is coated with the catalysts because the edge side of the microreactor should be bare silicon for subsequent anodic bonding. The hole at the top plate provides alignment with the holes at the mask and the columns of the bottom plate.

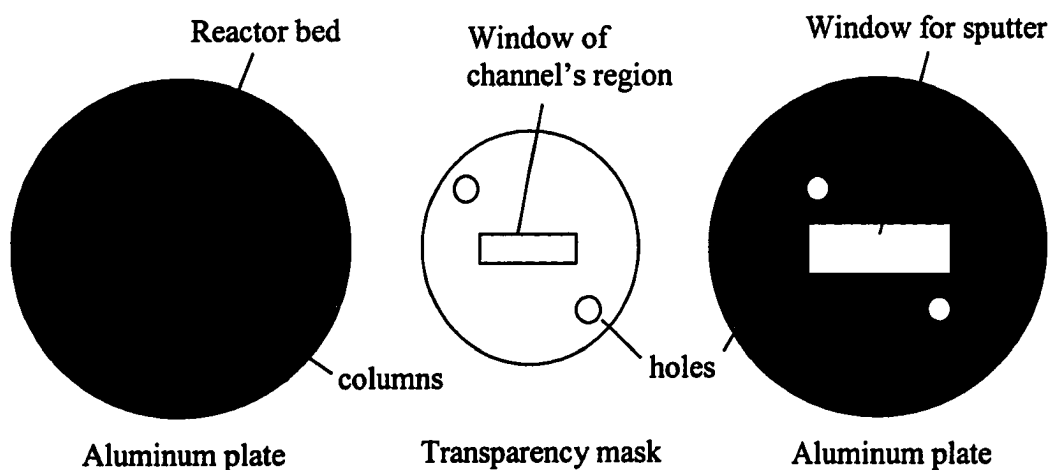


Figure 5.5 The fixture for microreactor sputtering deposition.

The sputtering deposition equipment, Uniform Technology-PVD-300 of IfM, was used. Figure 5.6 shows the microreactor held by the fixture in the sputtering chamber. The sputtering parameters for platinum, iron, and cobalt are listed in table 5.1. Thicknesses from 10 nm to 800 nm were studied for each catalyst. Thicker catalyst film was found to be not necessary for better microreaction results because only the surface of the catalyst was involved in the reaction. To minimize cost, platinum thicknesses of 50 nm, iron thicknesses of 30 nm and cobalt thicknesses of 10 nm were used for different reactions studied. The deposition rate, power voltage, etc., were determined by calibration for each target material.

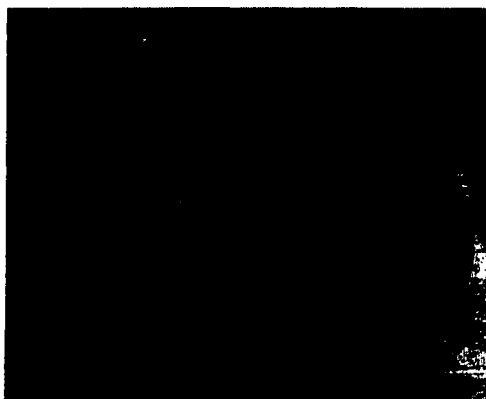


Figure 5.6 Microreactor held by fixture in sputtering chamber.

Table 5.1 Sputtering deposition parameters for Pt, Fe and Co

Target materials	Platinum	Iron	Cobalt
Power supply	DC	RF	RF
Thickness of catalyst (nm)	50	30	10
Deposition rate (nm/min)	50	10	10
Deposition time (min)	5	34	8
Current/ Power	0.032 Amp	484 watts	48 watts
Voltage (volt)	134	878	132

Sol-gel Method and Ion Impregnation

In order to obtain high surface areas, a sol-gel method was used. The catalytic properties of metal-supported catalysts may be strongly affected by the surface properties of the carrier. These properties can be modified by changing the experimental conditions during the preparation of the catalyst and/or the support. Three sol-gel methods were used for the catalyst and support coating inside microreactor channels, dip coating, spin coating, and drop coating. (Figure 5.7)

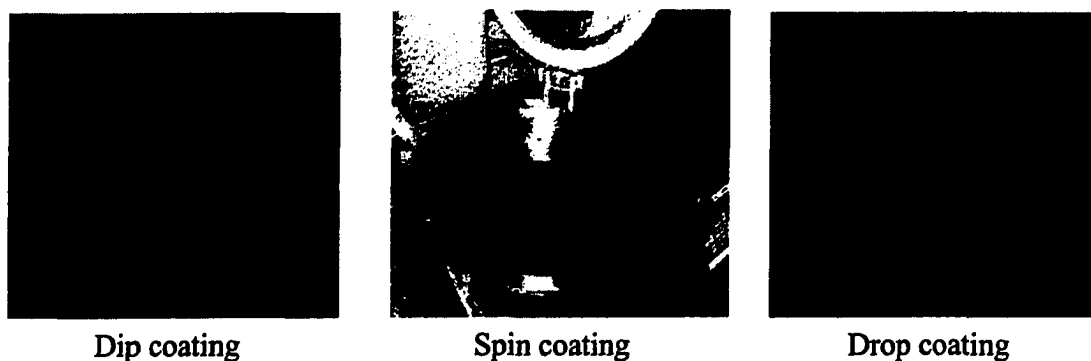


Figure 5.7 Three sol-gel deposition methods

Two preparation methods for the catalyst/support were used. For the platinum catalyst, we deposited the support and catalyst separately in a conventional way. The supports are silicon dioxide and aluminum oxide because both are common catalyst supports and have high surface areas. For iron and cobalt catalysts, the sol-gel solution was mixed the catalyst solution to apply inside the microreactor. The support was aluminum oxide.

Platinum/Support Coating. Most silica can be prepared from either tetraethoxysilane ($\text{Si}(\text{OC}_2\text{H}_5)_4$) or tetramethoxysilane ($\text{Si}(\text{OCH}_3)_4$). tetraethoxysilane ($\text{Si}(\text{OC}_2\text{H}_5)_4$) was chosen as the precursor of silica because of its ease of preparation and compatibility to microfabrication. The silica sol-gel was prepared by mixing tetraethoxysilane ($\text{Si}(\text{OC}_2\text{H}_5)_4$), water, ethanol ($\text{C}_2\text{H}_5\text{OH}$), and nitric acid in the molar ratio of 1:12:45:0.26 [103]. Water was added to the ethanol, then silica precursor was added, and subsequently, nitric acid was added. The resultant solution was then stirred at 40 °C, with vigorous stirring for 30 min. The other recipe for preparing SiO_2 included tetraethoxysilane, water, ethanol, and HCl in the molar ratio of 1:10:7:0.1 [109]. An

acidic environment was used instead of a basic environment because the surface area was expected to be approximately ten times higher with the former [104].

The basic principles involved in all of the methods for the synthesis of the alumina coating solution are the hydrolysis of aluminum alkoxide to form its hydroxide, and the peptization and polymerization of an aluminum hydroxide to form an alumina. An alumina sol-gel was prepared using the molar ratio of aluminum iso-propoxide ($\text{Al}(\text{OC}_3\text{H}_7)_3$), water, and acetic acid as 1:100:0.2. [105,106]. This recipe was from Yoldas' paper, which discussed alumina synthesis using aluminum iso-propoxide, water, and an acid. It also discussed the effect of acid concentration on the formation of the sol. In order to allow for a good three-dimensional network to be formed, the previous method was modified by refluxing the resultant solution obtained after acid addition for 13 hours and then cooling the sol-gel after reflux before coating the channels of the microreactor. The other way to prepare alumina was to synthesize copper oxide coated meso porous alumina granular particles by the sol-gel process [107]. So, the initial step in producing the Boehmite solution was modified to prepare the alumina sol-gel. The molar ratio of aluminum tri-sec-butoxide ($[\text{C}_2\text{H}_5\text{CH}(\text{CH}_3)\text{O}]_3\text{Al}$), water, and nitric acid was chosen as 1:100:4, which was determined based on a trial and error basis. Initially, water was heated to 80 °C. Then, aluminum tri-sec-butoxide was added through a syringe very slowly while stirring the water. Nitric acid was then added at this point. The solution was then briskly stirred for 45 minutes, maintaining a temperature of 80 °C. The temperature was then increased to 90 °C and the resultant solution was refluxed for 12-14 hours. At the end of the reflux, the resultant sol-gel was cooled and then used for coating.

Lithography technology was used to coat the desired regions of the microreactor with the sol-gel. It is also called selective deposition.

The microreactor was bonded to a support wafer using negative photoresist, which was also used in the selective coating of the catalyst supports. (Figure 5.8) Following that, a bake of 115 °C for 3 minutes was required for good adhesion. Negative photoresist (NR1500-P) was chosen as the mask for the selective deposition because the unexposed channel part of negative photoresist can be completely removed by the developer, which minimizes residual photoresist. The photoresist was first spin-coated on the silicon wafer, and then it was exposed in a conventional UV photomask aligner (Electronic Visions, Inc.) for 120 second. After baking at 100 °C for 1 min. on a hotplate, the film was developed in RD6 developer for 20 second and dried with nitrogen gas. A window was thus opened on channel region of microreactor. The coating was applied by dispensing droplets of sol into the microchannels and allowing the sol to permeate by capillary action, thus forming the silica and the alumina films on the microreactors. A 200 °C, 20-minute baking step in air was required to dry the sol-gel coating for good adhesion. Acetone was used to separate the microreactor from the support wafer before drop coating and after spin coating, as the wafer was still needed to hold the reactor on the spinner. (Figure 5.9)

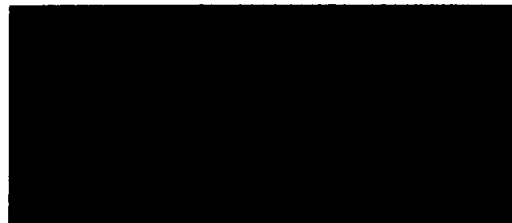


Figure 5.8 The microreactor bonded with wafer.

The aging of a catalyst is very important for a catalyst's properties. Different aging times will affect the surface area of catalysts and microstructures. Aging times from two weeks to ten weeks were considered for silicon oxide and aluminum oxide. The sol-gel solution was converted to a gel when the aging time was longer than ten weeks.



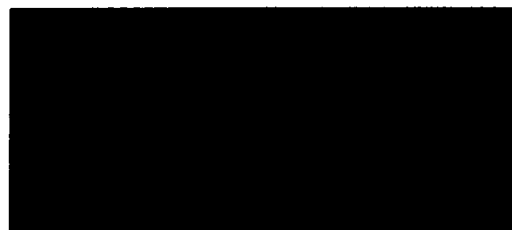
Step 1: Cleaning the reactor.



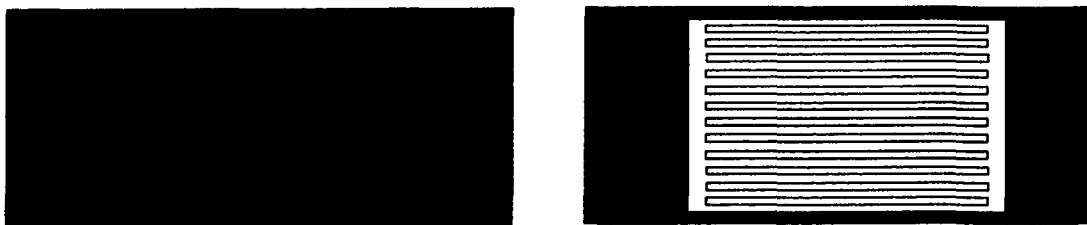
Step 2: Coating the photoresist.



Step 3: Exposing the photoresist.



Step 4: Coating silica sol-gel.



Step 5: Striping PR with acetone.

Step 6: coating Platinum.

Figure 5.9 Selective deposition of sol-gel on the microreactor.

The effect of temperature during calcination is to promote dehydration by creating more active sites by the loss of water and hydroxyl groups or overcoming activation barriers. Calcination was performed on the silicon wafers that were coated with the alumina and silica support. In this study, calcination was carried out in a furnace with a continuous flow of air from the atmosphere. The coated wafers were placed in small ceramic crucibles in a long quartz tube in the furnace. The temperature was increased slowly from 150 °C to 450 °C for 4 hours. Temperatures lower than 150 °C had no effect on calcination.

After catalyst support coating by the sol-gel method, platinum was deposited on the catalyst support in the form of Pt^{+2} by chemical deposition, known as ion impregnation. Platinum (II) 2,4 Pentanedionate ($\text{Pt}(\text{C}_5\text{H}_7\text{O}_2)_2$) was dissolved completely in a toluene solution with different concentrations. The solution was dropped into the channel area of the microreactor on a hotplate at 70 °C, using a required amount to get a metal loading of 100wt% or 50wt% ($\text{Pt}/(\text{catalyst support})$) and continued baking at the same temperature for 12 hours. In order to convert the deposited Pt^{+2} to metallic Pt^0 , the reactor was subjected to reducing conditions (40% H_2 in N_2 , 0.2L/min) at 400 °C for 4.5 hours in the furnace [108].

Figure 10 shows the design of the Pt reduction setup. One important issue is that, before the 40% H₂ could be used, nitrogen or inert gas is needed to replace the air in the furnace and tubes to separate oxygen from hydrogen because of the high temperature of operation. The process for the reduction of platinum is listed below.

1. Calculate the volume of the furnace (15.67 L) and the volume of all tubes (2.695 L). The total volume is 55 L. Close V1, V2, and V6, open V3, V4, V5, and V8. Flow N₂ at 4 SLPM for 14 min to remove air from the furnace and tubes.
2. Close V7, open V6, and fill in H₂ into the furnace at 4 SLPM for 14 min.
3. Heat the furnace to 450-600 °C at the same time. Then, change the flow rate to 150 mL/min. Keep this flow rate and temperature around 4.5 hours for platinum reduction. These parameters were from the literature's recipe [108]. But we observed that the Pt⁺² was not completely reduced even after increasing the temperature from 450 °C to 600 °C. So we took a longer reduction time of up to 6 hours, until the Pt⁺² was finally reduced.
4. Stop heating after 6 hours and allow the system to cool down.
5. Close V6, open V7, and fill in N₂ in the furnace at 4 SLPM for 14min when the temperature reaches to 100 °C.
6. Close V7, unload the samples.

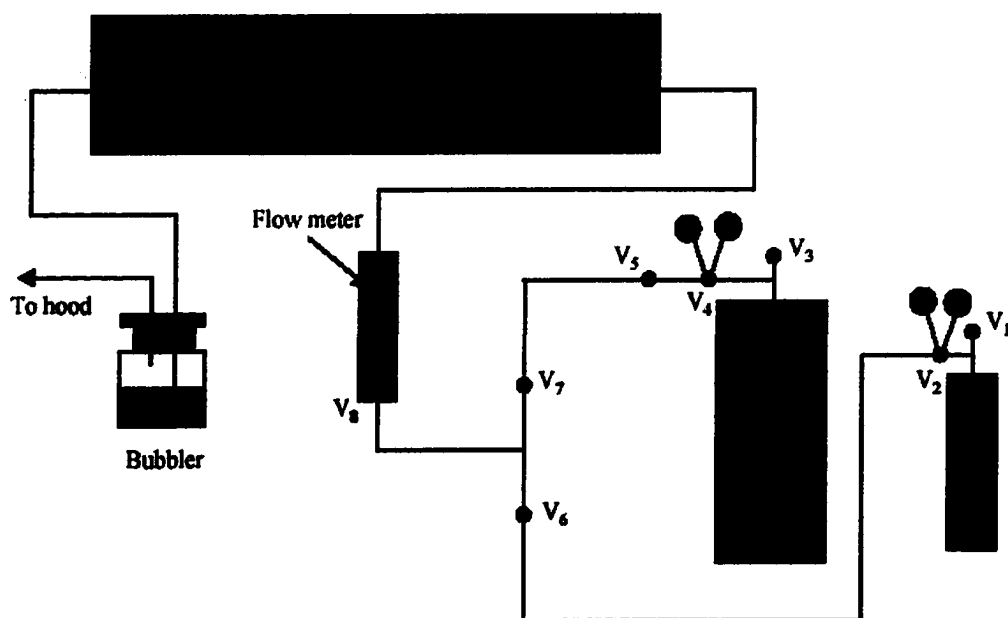


Figure 5.10 Setup for platinum reduction

Iron/Cobalt/Aluminum Oxide Coating. For iron and cobalt coating, the support solution was mixed with the catalyst solution before applying it into the microchannels. This technique is known as wash-coating. Recipes from literatures were modified to make the catalyst/aluminum more flexible for microreactor coating [107]. Here, the aluminum precursor was Al tri-sec-butoxide, which was as the same as that used for platinum support. But for a mixed catalyst with support, we modified the process for different catalyst coatings. A typical procedure is given below:

1. Take 25 ml of water in a beaker and heat it to 80 °C.
2. Slowly add 13 ml of Al tri-sec-butoxide into the beaker using a syringe, while stirring continuously with a magnetic stirrer.
3. Add 3.75 ml 1M HNO₃ into the solution slowly.
4. Heat the mixture for 30 min, until the temperature rises to about 90 °C.

5. Reflux the contents of the beaker for 12-16 hrs
6. After refluxing, decrease the temperature to 60-70 °C.
7. Take 0.75 gm (6% wt. loading of catalyst) or 1.5 gm (12%) cobalt nitrate salt and 1.1 gm (6%) or 2.2 gm (12%) ferric nitrate salt into a small beaker and dissolve them separately.
8. Slowly add the Fe/Co salt into the aluminum sol-gel while stirring continuously.
9. Apply the sol-gel catalyst into the microchannels of the reactor and dry it in hot air for a few minutes.
10. Wash the sample with 10% NH₄OH solution for 15-20 minutes, followed by washing in hot water.
11. Dry the sample in a vacuum oven for 30 minutes at 60 °C.
12. Take out the sample and calcinate it in an oven at 400-450 °C for 2 hours.
13. Hydrogenate the sample in H₂ flow for 4 hours at 350 °C.

Microreactor Packaging

After microreactor fabrication and catalyst coating, the reactor should be packed with a cover on the top for testing catalyst activity and efficiency. To complete this, the Pyrex glass 7740, which was the same size as the microreactor and 500 μm in thickness, was assembled with the microreactor by anodic bonding. (Figure 5.11) The process of anodic bonding is

1. Clean the microreactor and the Pyrex glass with acetone, distilled water, and isopropyl alcohol.

2. Place the microreactor into the bed of the bottom plate. Cover the microreactor with the glass. Put the top plate on the glass.
3. Hold them together and put into the furnace (Figure 5.12). Connect to the high power supply.
4. Heat the furnace to 450 °C and maintain for 45 minutes.
5. Apply the voltage to 750 volts and keep close to 0 amps for 45 minutes.
6. Turn off the power of the furnace and power supply. Cool down the furnace to room temperature. Then take out the microreactor for pressure testing.



Figure 5.11 Anodic bonding profile

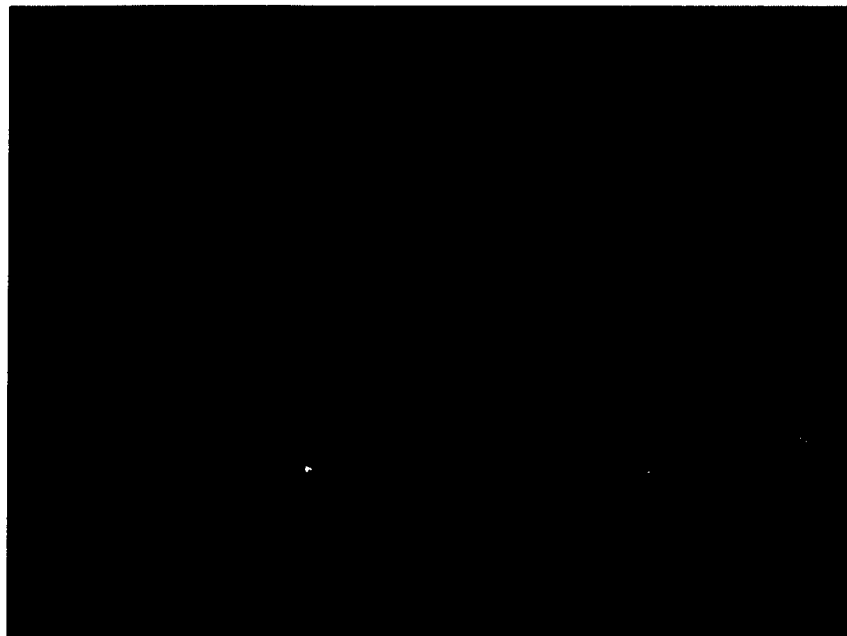


Figure 5.12 Anodic bonding setup at IfM, Louisiana Tech University.

Figure 5.12 shows the anodic bonding setup for microreactor assembling. The left side is the furnace with a temperature controller for heating the microreactor and the Pyrex. The right side is a high power supply used to generate the electric field between the reactor and the glass for bonding.

Microreaction Setup

While the reaction was conducted in the microreactor, additional peripheral equipment was needed for control of flow, temperature, and pressure, and for the acquisition of the product distribution of the effluent stream. (Figure 5.13) The reactor chip interfaces to a steel holding block fitted with o-ring sealed gas connections to the inlet and outlet openings on the bottom side of the chip. The block also has resistive heating elements and a thermocouple for temperature control. Gases are fed to the block



Figure 5.13 Microreaction setup at IfM, Louisiana Tech University.

by mass flow controllers, and digital pressure sensors are situated in the inlet and outlet streams to monitor pressure drops. The experiments for a liquid reactant, such as cyclohexene, were carried out by bubbling a carrier gas, such as argon. The flow and reactor temperature settings were monitored and controlled by a PC running NI LabView software.

The outlet stream for the experiments was exhausted at atmospheric pressure. Reactor effluent was monitored for composition using a Stanford Research Systems mass spectrometer with PC data acquisition and control. The effluent stream, which in these experiments varied between approximately 0.2 sccm and 2 sccm, was diluted with helium prior to the mass spectrometer sampling point in order to prevent the spectrometer's pumping system from affecting the reactor operating pressure while also supplying an adequate sampling flow. Gas lines downstream of the bubbler were heated to a few degrees above room temperature to prevent condensation of reactants or products.

The procedure for quantitative analysis of the effluent began by calibrating the mass spectrometer with ambient air as a standard for establishing the sensitivity to nitrogen.

Pure reactant and products were fed in the reactor in combination with nitrogen in order to determine their respective sensitivity factors. The calibrated mass spectrometer was then used to record continuous partial pressure data during the course of experiments where conditions of temperature and reactant flow rates were varied.

For cyclohexene conversion reactions, a carrier gas (argon) equilibrated the cyclohexene and was fed to the microreactor because of liquid cyclohexene. Pure H₂ was

the other gas used for this reaction to dehydrogenate/hydrogenate cyclohexene.

For Fischer-Tropsch reactions, pure hydrogen (from Nexair) and carbon monoxide (from Aldrich) were the reactants mixed together before being fed into the microreactor. The reaction was conducted with sputtered Fe and sol-gel coated Fe to compare the two catalyst deposition methods. A high conversion of carbon monoxide and high alkane was obtained.

For preferential oxidation of carbon monoxide, mixed gas was obtained from Nextair. The concentration of mixed gas was 70% hydrogen, 2% carbon monoxide, with the remaining concentration argon. The composition of carbon monoxide and hydrogen is representative of a commercial fuel cell feed gas. Pure oxygen or air (from Nextair) was used to oxidize carbon monoxide.

CHAPTER VI

CHARACTERIZATION OF MICRO- REACTORS AND CATALYSTS

Characteristics of Microreactors

Fabrication of the chemical microreactor was achieved by employing standard microfabrication technology normally applied in the IC industry, as mentioned in the fabrication section. Two kinds of microreactors with different dimension and channel structures were fabricated (See Figure 6.1 and Figure 6.2). The first design is 1 cm × 3 cm in size with 0.8 cm × 1.9 cm for the straight-line catalyst channel area. There are two widths of the microchannels: 5 μm and 100 μm with 799 and 39 channels respectively. The second design is 1.6 cm × 3.1 cm in size, with 1.2 cm × 1.4 cm for the wave-line channel area for increasing the contact of the reactants with the microchannel walls. 599 5 μm-wide channels were fabricated in this design. The inlet flow of the second design was split into two regions to enhance flow distribution throughout the reactor.

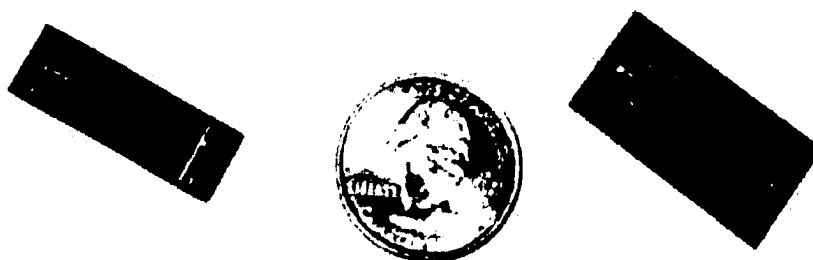


Figure 6.1 Two type microreactors (left: 1×3 cm in size, right: 1.6×3.1 cm in size)

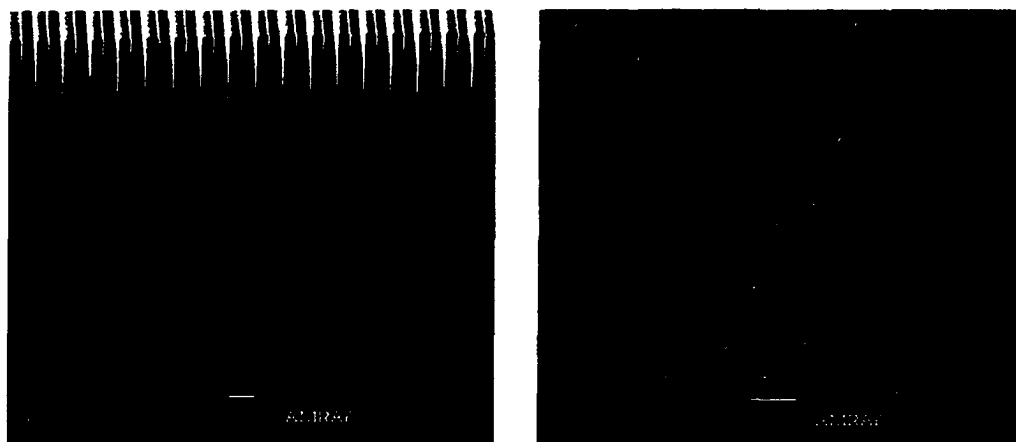
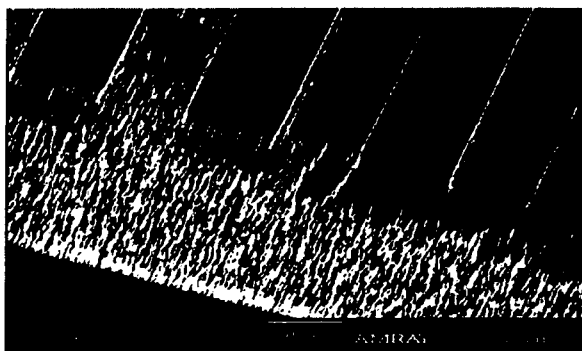


Figure 6.2 SEM pictures for two type microreactors.

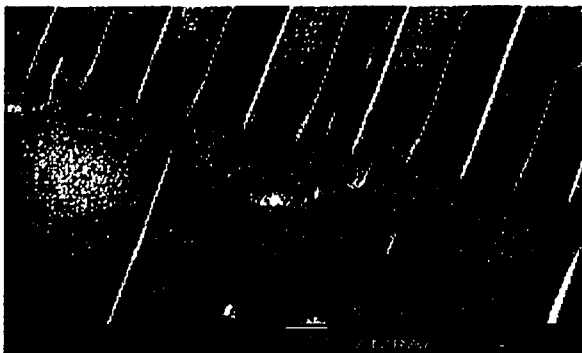
The microreactors were etched by inductively coupled plasma (ICP), allowing high aspect ratios to be achieved. Feature scale pattern dependencies and wafer level loading affects the use of deep silicon etching. ICP has been widely embraced for MEMS processing due to its high etching selectivity, its ability to precisely transfer photoresist patterns into silicon substrates, and its cleanliness and compatibility with vacuum processing technologies. However, ICP etching has its own specific problems, which include “grass” formation, etching uniformity, mask selectivity, etc. Etching gas cycle time, bias power, and chamber pressure were the parameters adjusted to solve these unfavorable phenomena. The etched wafers were investigated by SEM (scanning electron microscope) and TENCOR profilometer to characterize the surface morphology and etching depth profile. The periodic change of different gases for etching (SF_6) and passivation (C_4F_8) can lead to very high aspect ratios and very high etch rates. The cycle time of SF_6 gas flow was increased from 4 seconds to 8 seconds. Figure 6.3 shows the effects of changing gas flow time in the ICP etcher. The surface morphologies of the

wafer with respect to the increasing of SF_6 gas flow time changed dramatically. A major problem during etching silicon was the forming of “grass” on the surface, a result of particulate material inadvertently deposited on the silicon surface. This material can

SF_6 : C_4F_8 = 4sec:2sec



SF_6 : C_4F_8 = 6sec : 2sec



SF_6 : C_4F_8 = 8sec : 2sec



Figure 6.3 SEM photos with different SF_6 gas flow time.
(W. Shin , J. McDonald, S. Zhao, R. Besser)

locally mask the silicon during etching and can be formed due to redeposition and growing of polymer material from the sidewall passivation step. By increasing the cycle time of SF_6 , the “grass” formation was markably decreased.

Bias power = 30 Watts



Bias power = 40 Watts



Bias power = 50 Watts



Figure 6.4 SEM photos with different bias power. (W. Shin, J. McDonald, S.Zhao, R. Besser)

As the SF_6 gas flow time increased, the sidewall at the base of the reactor channel assumed a slight retrograde profile. This was caused by thin sidewall polymer layers at

the bottom part of channel. When the cycle time of SF₆ gas was increased, lateral ion bombardment to the sidewall also increased. The passivated polymer layer was thinner at the base of channels than at the top of the channels. Thus, the etching profile of trenches could be broadened at the bottom. It is useful to achieve high etch rates, but this is often at the expense of sidewall broadening problems. Figure 6.4 shows the results of changing bias power in the ICP etcher. By increasing bias power, the grass formation was reduced and the overall etching rate was increased, but the etching uniformity over the wafer was not improved (Figure 6.5). Thus, increasing the bias power in an attempt to reduce the grass formation on the surface of the silicon wafer may have unfavorable side effects. In Table 1, the standard deviations of etching rate in the bias power of 40 Watts and 50 Watts were 8.7% and 8.3%. These values are excessive, relative to the deviations of the best wafers.

Figure 6.5 shows the results of the etching profile with different SF₆ cycle time and bias power settings. In the long SF₆ gas cycle time region, the overall etching rate and

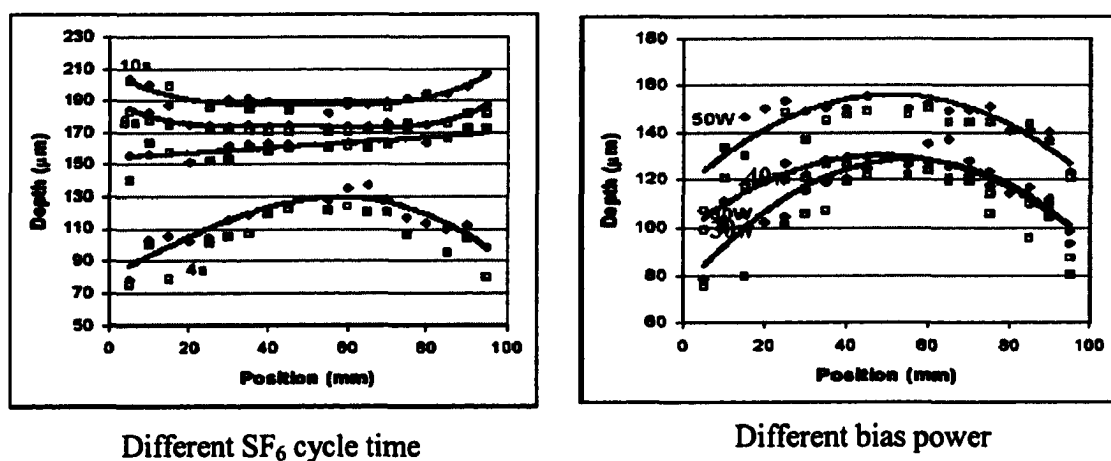
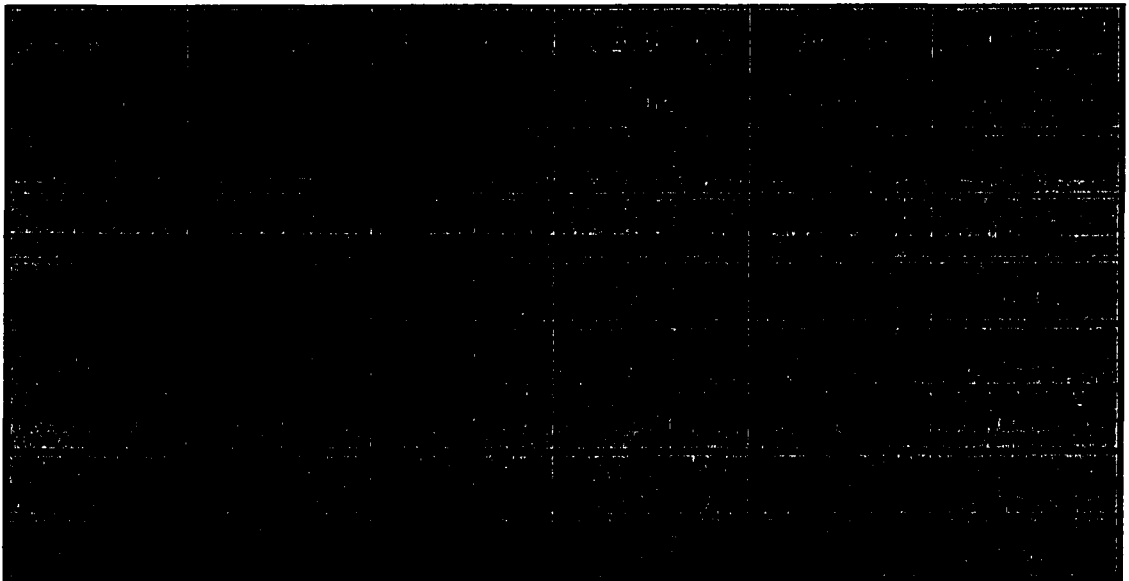


Figure 6.5 Etching profile with different SF₆ cycle time and bias power settings. ◆ = via (1500 × 1500 μm²) □ = manifold (500 × 8000 μm²) (W. Shin, S. Zhao, R. Besser)

etching uniformity are improved and also the etching rate is nearly independent of the feature size. Increasing bias power causes high average etching rate but does not contribute to improving etching uniformity to acceptable levels.

In Table 6.1, the etching characteristics in low chamber pressure show that the average etching rate is decreased but the etching uniformity over the wafer is improved. However, grass formation was not reduced at the low chamber pressure. Etching uniformity over the wafer was 2.4% at the SF₆ cycle time of 8 seconds and the average etching rate was up to 5.9 μm/min at the SF₆ cycle time of 8 seconds. By increasing the SF₆ cycle time to 10 seconds, the overall etching rate reached to 6.4 μm/min, but the etching uniformity dropped to 3.5 %. The highest etching selectivity between the silicon and the photoresist was determined to be 167:1 and the aspect ratio was as high as 40:1.

Table 6.1 Etching characteristics with different ICP parameters.
(W. Shin, S. Zhao, R. Besser)



By increasing SF₆ gas flow time in the ICP etcher, the etching uniformity over the wafer improved from 11.6% to 4.2% and the average etching rate increased from 4.13 μm to 5.90 μm. Increased bias power enhanced overall etching rate but the etching uniformity was not improved. The surface morphology of the silicon substrate was strongly affected by etching gas species and the gas flow sequence time. The formation of micro grass on the silicon surface could result from several factors. Etching gas sequence time, bias power, and chamber pressure can all greatly change the surface morphology of silicon surface. Grass formation was dramatically reduced by increasing SF₆ gas flow time. As optimum conditions of the ICP etching for fabricating silicon micro-channel reactors, longer cycle time of SF₆ gas flow, high bias power, and low chamber pressure are all recommended.

Characterization of Catalyst Deposited on the Channels of Microreactor

Catalysts are very important in the chemical process. The number of catalysts applied in industry is very large and catalysts come in many different forms, from heterogeneous catalysts in the form of porous solids, and homogeneous catalysts dissolved in the liquid reaction mixture, to biological catalysts in the form of enzymes. Because a heterogeneous catalytic reaction occurs at the fluid-solid interface, a large interfacial area can be helpful or even essential in attaining a significant reaction rate. Therefore, the properties of a catalyst surface are the critical issues for catalyst activity and efficiency during any specific reaction. For the reactions in microreactors, the catalyst should be compatible with the coating in the microchannels. In this study, Scanning Electron Microscopy (SEM), X-ray Photoelectron Spectroscopy (XPS), Atomic

Force Microscopy (AFM), and the BET surface area method have been employed to characterize catalysts inside the microreactors. The catalysts include sputtered platinum, sputtered iron, sputtered cobalt, sputtered platinum on sol-gel coated SiO_2 , impregnated platinum on sol-gel coated SiO_2 , or Al_2O_3 , and a mixture of iron/cobalt encapsulated Al_2O_3 in sol-gel.

Scanning Electron Microscopy (SEM) Analysis

SEM analysis was performed on the coated channels to examine the catalyst support and to verify the thickness of the film. The following pictures show the SEM image of the coated catalyst support on 5 μm and 100 μm channels. Figure 6.6 depicts SiO_2 in 5 μm channels and 100 μm channels. In 5 μm wide channels, SiO_2 is present only



5 μm wide channel

100 μm wide channel

Figure 6.6 Silica inside 5 μm wide and 100 μm wide channels.

(S. Zhao and R. Besser)

to a small extent inside of the channels. But, in 100 μm channels, SiO_2 uniformly cover the channel walls. This suggests that the smaller channel is less compatible with sol-gel coating. Thus, the 100 μm channel microreactors were used for many of our reactions.

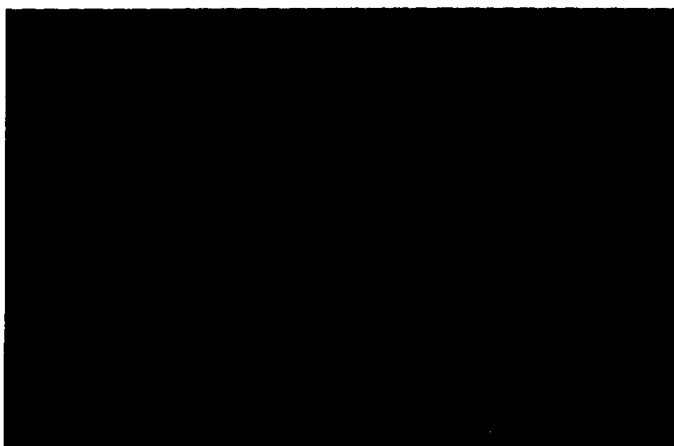


Figure 6.7 Top view of silica on 5 μm channels

When Figures 6.6 and 6.8 are compared, we find that the adhesion of alumina to the silicon sidewall appears to be lower than that of silica. Portions of the alumina film are peeled off from the surface of silicon channels. Therefore, the alumina preparation recipe was modified.



Figure 6.8 Alumina on 100 μm channels

Figure 6.9 shows the particles of alumina film in the microchannel. The size of particles is approximately 80 nm, which dramatically increases the surface area of

catalysts compared to sputtered catalysts. This is indeed the reason for using the sol-gel method as the method of choice for catalyst support coating in the subsequent studies.



Figure 6.9 SEM picture of alumina particles.

X-ray Photoelectron Spectroscopy (XPS) Analysis

X-Ray Photoelectron Spectroscopy (XPS) was used to identify the chemical state and atomic concentration of the elements present in the coating of the catalyst support [110]. The ratio of Si:O in the silica film prepared by the sol-gel method was determined to be 1:2 from the XPS results. As mentioned in the Chapter V, two recipes were used for silica preparation. Recipe A consists of TEOS with HNO₃, and Recipe B consists TEOS with HCl. From Table 6.2, one can see that Si:O in Recipe A is close to 1:2 than that in Recipe B. Therefore, all the silica in this study was fabricated using Recipe A.

Table 6.2 Atomic concentration table for different processes

Concentration	C1s [0.314]	N1s [0.499]	O1s [0.733]	Si2p [0.368]
Recipe A	8.72	0.47	61.15	29.66
Recipe B	6.34	0.38	63.17	30.11

Nilgun Ozer et al. have determined the binding energies of aluminum and oxygen in the alumina film, which was prepared using aluminum-sec-butoxide, isopropanol, acetylacetone, nitric acid, and water. The standard peaks are given in Table 6.3 [110].

Table 6.3 Standard binding energy peaks of the elements in alumina

Element	Binding Energies
Al with oxygen	73.6 - 74.5
Oxygen with Al ₂ O ₃	529.8 - 531.8
Carbon with oxygen	286 - 288

The peaks of each element have shifted to the left by ~ 5 eV. For example, in all of the XPS results, the C1's peak is at around 291eV because of the contamination by some carbonate species. The shift of the peaks has been explained by Bhattacharya et al., who have found that the position of the carbon C1's peak varies according to the substituent attached to the carbon atom. They have further determined that carbon becomes electronegative when it is attached to a more electropositive substituent such as metals making the carbon shift to a lower binding energy. If, however, the carbon is attached to a more electronegative substance, it would cause the peak to shift to higher

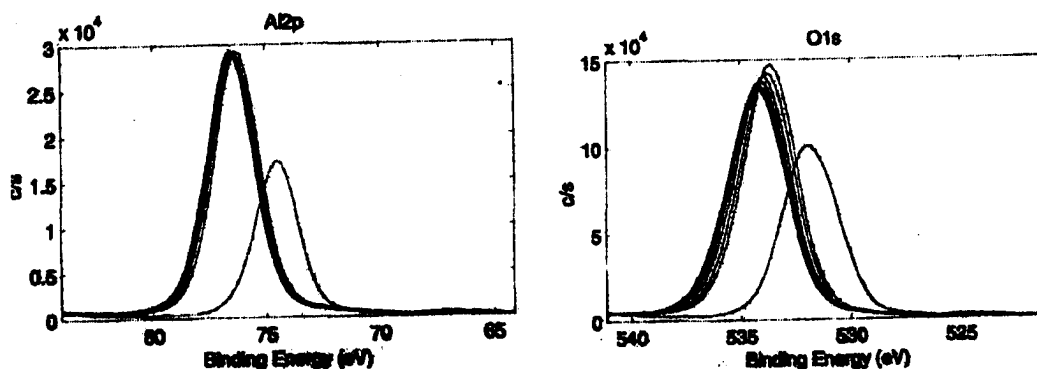


Fig 6.10 XPS peak shape of alumina during sputter depth profiling

binding energy [111]. Also, upon interaction with the environment, the chemistry of the outermost layers of solids invariably becomes different [112]. Therefore, the ratio of the aluminum to oxygen in the samples is not equal to the stoichiometric ratio of 1:1.5. In this study, we find that the Al:O of Al_2O_3 formed by the modified Yoldas method was found to be 1:1.242. Sputter etching for 10 minutes was carried out to find out the composition of the alumina film starting from the surface and going deeper into the alumina film. Usually, there is a significant drop in the percentage of oxygen and aluminum as one etches deeper into the film. Also, the peak shifts towards the lower binding energy, indicating that the aluminum we found in the lower layers is bonded with oxygen rather than hydroxides. Before sputter etching, the Al peak was obtained at around 77.5 eV, but after ion sputter etching, the peak was obtained at around 74 eV (Figure 6.10), which is in accordance with the standard values and which also, as discussed by Ozer et al., implies that the composition of aluminum and oxygen after ion sputter etching should at least approach the stoichiometric coefficient [112].

After silica and alumina were deposited inside the microchannels, platinum was impregnated into the silica or alumina gel. A 2% wt. loading of platinum was first tried on the silica film. No gains were noted in the conversion of cyclohexene. The loading was increased further. The conversion of cyclohexene was detected at a catalyst loading of 50%. For the catalyst performance study, four different samples were studied in order to determine the effect of aging and the platinum ion concentration (Table 6.4).

Table 6.4 Different sol-gel coated Pt conditions

Parameters	A	B	C	D
Sol gel solution aging time (weeks)	2	10	2	10
Pt concentration compared to SiO ₂ (%)	50	50	100	100

In Figure 6.11, the four different concentrations of platinum solution with different aging times were impregnated on the silica film. The plots show that peaks of

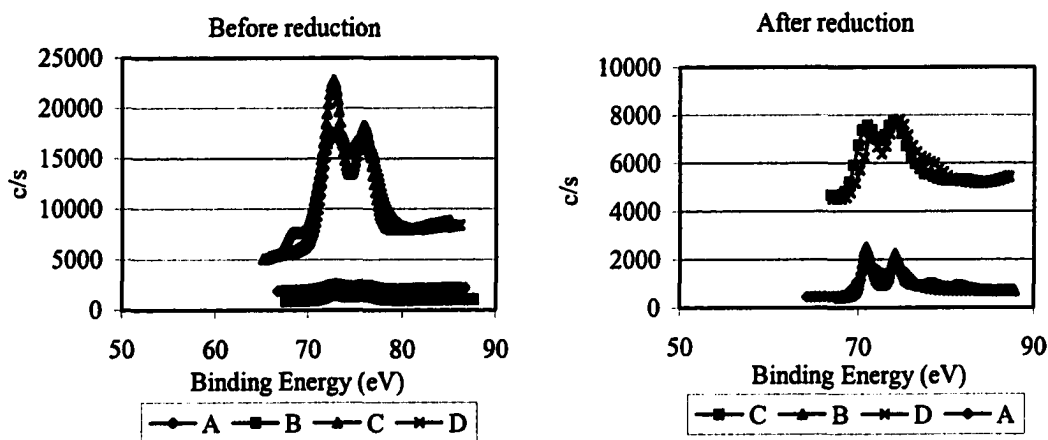


Figure 6.11 XPS plot of Different samples of impregnated platinum on sol gel support.

higher Pt concentration are more intense than those of low concentrations and peaks of shorter aging time are taller than those of longer aging time. On the basis of these results, we chose to impregnate Pt⁺² on the channels of the microreactor using the platinum solution, with 100% Pt loading without any aging. XPS studies also were done on the substrate coated with silica and impregnated with Pt⁺² before reduction (when Pt was present in the form of Pt⁺²) and after reduction (when Pt is in Pt⁰ state), to determine

whether the reduction was accomplished or not. Figure 6.13 shows that the peak profile after reduction is similar to the standard peak profile. The peaks shift from 73.125 eV before reduction to 71eV after reduction. Compared to Figure 6.12, we can see the changing of platinum's chemical state from Pt^{+2} in PtSi or Pt_2Si to Pt^0 . The distance between the two peaks is 3.3 eV, which is in agreement with that reported in literature



Figure 6.12 Binding energy shift in Pt [110]

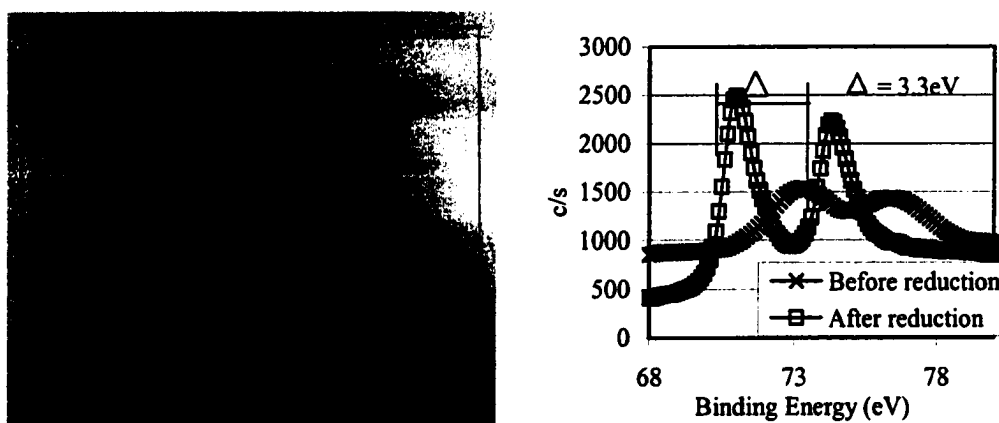


Figure 6.13 Comparison between the Pt^0 standard plot [110] and the experimental result (before and after reduction of Pt)

[110]. Figure 6.14 shows the XPS depth profile of Pt that was sputter-etched for 60 minutes in the XPS analyzer corresponding to a material removal depth of 1.2 μm . The concentration of platinum inside the silica was constant, which confirmed that silica made by the sol-gel method has the pore structure and high surface area and that catalysts can go inside the silica, bond with silicon, and adsorb on the surface of silica after reduction.

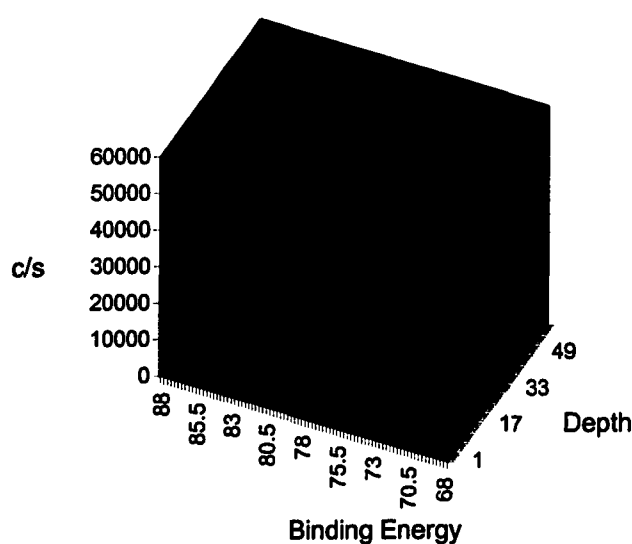


Figure 6.14 Sputtered XPS profile of Pt

BET Surface Area Measurement

Surface area measurement plays a crucial role in choosing the best method for the preparation of catalyst supports. Surface area measurements of the substrates coated with alumina or silica were performed using a Quantachrome NOVA 2000 series instrument. Nitrogen was used as adsorbate in these measurements. The Brunauer-Emmett-Teller (BET) method was used to compute the surface area.

For alumina, Table 6.5 shows the specific surface area (SSA) of alumina prepared by different methods. For example, for the modified Yoldas method, where alumina is produced from freshly prepared sols, the specific surface area is about 390 m²/g. After aging for 7 days, it was reduced to 331 m²/g. When it was calcinated at 450 °C for 3 hours, the specific surface area dropped further down, to 273 m²/g. These results mean that longer aging time and calcinations will decrease the specific surface area. Having compared these three methods, we decided that the Wang et al. method was to be selected for supporting the catalysts during the reactions because it had the highest SSA after some long aging time and high temperature calcination. One must note that dip coating was the only application method employed for the alumina coating.

Table 6.5 Specific surface area for alumina coated by different procedures

Method	Yoldas method (specific surface area in m ² /gm)	Modified Yoldas method (specific surface area in m ² /gm)	Wang et al method (specific surface area in m ² /gm)
No aging	308.88	390.35	397.84
Aged for 7days	107.74	331.34	367.95
Calcination for 3 hrs at 450 °C	205.67	273.13	279.67

For silica, dip coating, drop coating, and spin coating were used to apply the sol-gel into 5 µm and 100 µm channel microreactors with different aging times. Before silica coating, the surface area was 0.0031m² for 5 µm channel microreactors and 0.0003 m² for 100 µm channel microreactors. After sol-gel coating of the silica, the surface area increased by a factor of 1,000-10,000. Table 6.6 shows that the reactors with dip coating

Table 6.6 The surface area results of silica prepared by different coating techniques

channel	5	5	5	5	5	100	100	100	100	100
Coating methods	spin	spin	drop	dip	dip	spin	drop	drop	dip	dip
Aging time (weeks)	6	10	10	6	10	10	6	10	6	10
Bake T	200	200	200	200	200	200	200	200	200	200
Bake time	20	20	20	20	20	20	20	20	20	20
SA (before coating)	0.00 31	0.00 31	0.0 031	0.00 31	0.00 31	0.00 31	0.00 03	0.00 03	0.00 03	0.00 03
SA (after coating)	3.50	4.13	6.67	6.67	7.43	5.07	1.16	2.95	4.40	5.95

have larger surface area than those with drop coating and spin coating. Moreover, longer aging time yielded a higher surface area. Under similar conditions, the reactor with 5 μm channels has a higher surface area compared to that with 100 μm channels because there are more channels (799 channels in 5 μm reactor and 39 channels in 100 μm reactor). However, the increase of surface area from the 100 μm reactor to the 5 μm reactor is not proportional to the increase in the number of channels. One explanation is that the silica did not adequately cover the 5 μm channel microreactor, and blocked the channel from top, as shown in Figure 6.6 and 6.7. Therefore, a large difference of the surface area between the 5 μm and 100 μm microreactors is not observed. Performance of the two reactor widths was similar for the sol-gel supported catalysts.

Mixed Catalyst Analysis with EDX and VSM

Previous results about the catalyst and its support characteristics were for a single catalyst, Pt. Platinum was employed here for cyclohexene conversion and preferential oxidation of CO. For the F-T synthesis reaction, alumina was used as a catalyst support, and mixed Fe/Co was the catalyst to yield higher alkanes [42, 48]

The EDX spectrometer is equipped with a super quantum dry Si(Li) detector that has an elemental analysis capability in the wide range : from boron through uranium with better than 145 eV resolution. Figure 6.15 shows the X-ray spectrum of the sol-gel deposited micro-channel reactor surface.

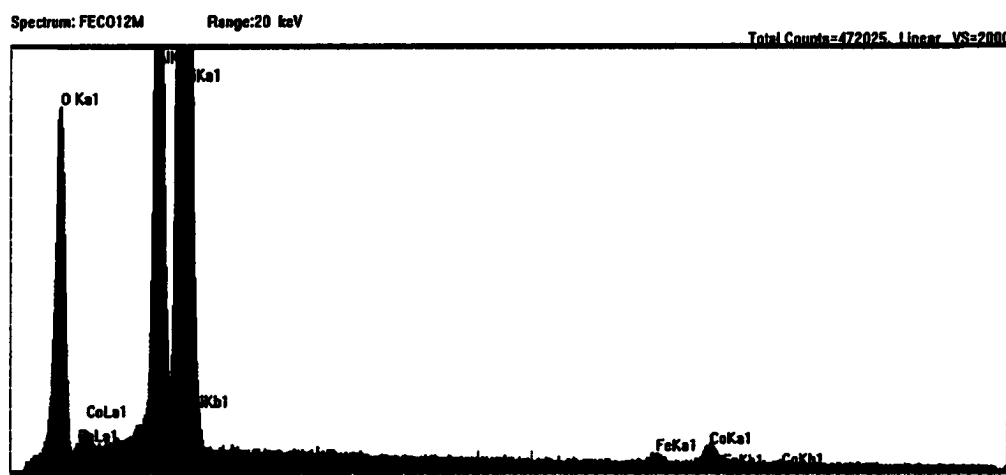


Figure 6.15 X-ray spectrum from EDX spectrometer for a sol-gel deposited micro-reactor. (S. Naidu, Grambling State University)

Table 6.7 shows the results of EDX elemental analysis for sol-gel coating. The intended composition of Fe and Co according to the solution mixture is 12% each for Fe and Co. The result shows that Fe and Co had a lower percentage of loading than expected. However, the percent composition of the catalyst was found to be uniform.

Table 6.7 EDX composition analysis result

Sample Type	O	Al	Fe	Co	%Loading of Fe	%Loading of Co	Coating quality
Sol-gel coating	91.3	4.38	1.76	2.60	2.52	3.68	Uniform

The magnetization characteristics of the Co/Fe encapsulated Al_2O_3 sol-gel micro-reactors were determined using the 880A Digital Measurement Systems Vibrating Sample Magnetometer (VSM).

Figure 6.16 shows a paramagnetic behavior mostly coming from the iron and cobalt oxides. During hydrogenation, the Fe and Co oxides are reduced to pure metals as evidenced by the ferromagnetic nature shown in Figure 6.17. Pure Fe and Co are ferromagnetic while their oxides are paramagnetic. The ferromagnetic nature disappears in the post-catalytic reaction (Figure 6.18) sample. This behavior may be attributed to the formation of species such as Fe and Co carbides during the catalytic reaction.

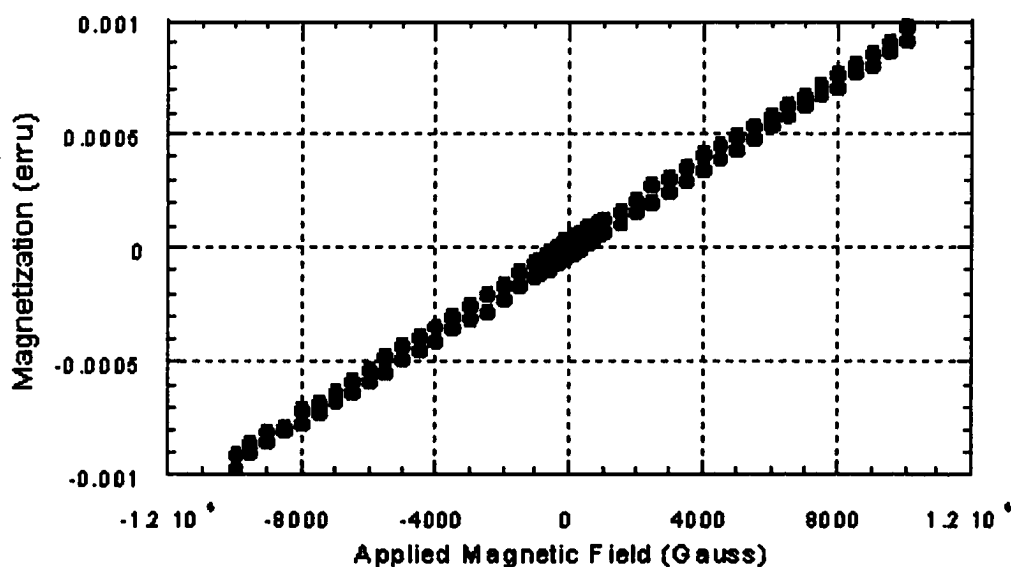


Figure 6.16 Magnetization of as-deposited sol-gel coated Fe/Co micro-reactor. (S. Naidu, Grambling State University)

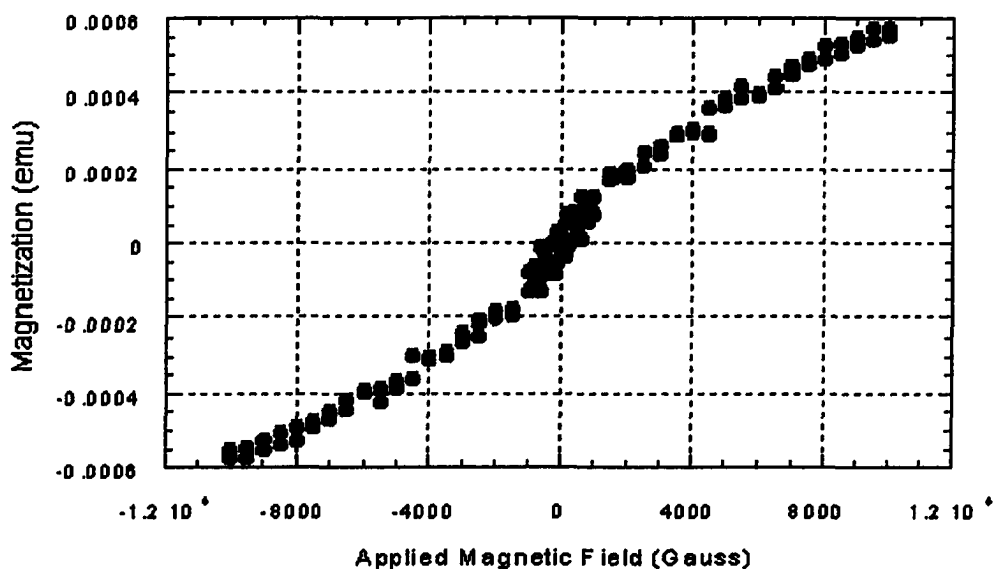


Figure 6.17: Magnetization of hydrogenated (pre-catalytic reaction) sol-gel coated Fe/Co micro-reactor. (S. Naidu, Grambling State University)

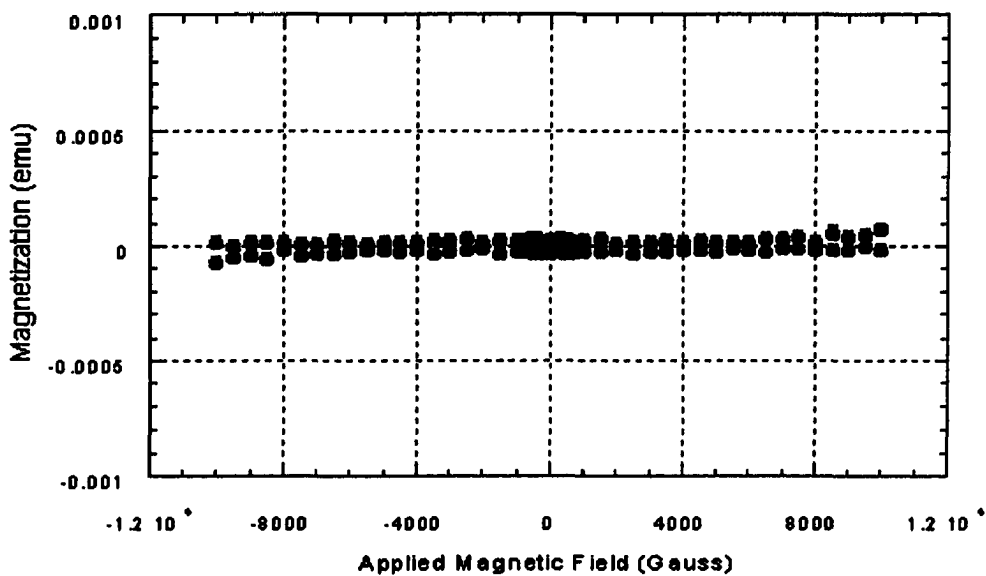


Figure 6.18 Magnetization of sol-gel coated micro-reactor after catalytic reaction is conducted. (S. Naidu, Grambling State University)

CHAPTER VII

CATALYST PERFORMANCE AND APPLICATION IN MICROREACTION

Catalyst Performance in Cyclohexene Reaction

After the characterization of catalyst/support with XPS, SEM, surface area measurement, EDX, and VSM, the microreactor was put on the reaction setup for testing catalyst activity and efficiency by cyclohexene conversion reaction. In this reaction, platinum was the catalyst, and the silica and alumina were the catalyst supports.

In preparation of the experiment, the reactor was evacuated 1 hour, followed by hydrogen treatment for 2 hours at room temperature. The reactants were H₂ and cyclohexene, with Argon as the carrier gas. Helium was used as a dilution gas at the outlet of the experimental setup and the flow rate was maintained at 5 sccm.

There are four different kinds of catalyst conditions that were tested for the conversion of cyclohexene to cyclohexane and benzene. (Table 7.1)

Table 7.1 Four different kinds of catalyst conditions

A	B	C	D
Sputtered Pt on bare silicon	Sputtered Pt on silicon oxide formed by sol gel method	Impregnated Pt on silicon oxide formed by sol gel method	Impregnated Pt on aluminum oxide formed by sol gel method

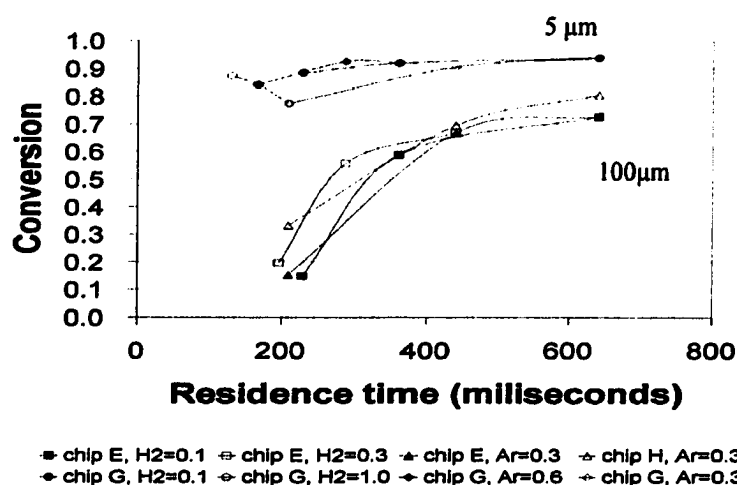


Figure 7.1 Conversion vs. residence time on sputtered Pt (R. Besser, X. Ouyang, S. Zhao)

Figure 7.1 shows the conversion changes with the residence times of reactants in the microreactor coated with sputtered Platinum (Catalyst condition A). When the residence time is increased from 200 milliseconds to 800 milliseconds, the conversion of cyclohexene increases observably in the 100 μm channel microreactor. The increased surface area available in the 5 μm channel reactor results in high conversions for all the residence times tested. The conversion of cyclohexene in the 5 μm channel reactor is always higher than that in the 100 μm channel reactor due to the increased surface area available the 5 μm channel reactor.

Figure 7.2 shows the conversion of cyclohexene with 100 μm channels using catalyst condition B, which is sol-gel coated silica with sputtered Pt. Compared to Figure 7.1, for 100 μm channels, the conversion using silica-supported sputtered Pt is higher than that with sputtered Pt alone. This is because the surface roughness of silica film increases the surface area of sputtered platinum. The fact that the silica-supported

sputtered Pt is better than sputtered Pt alone also can be confirmed from data shown in Figure 7.3. For silica-supported sputtered Pt, the conversion doesn't drop at higher partial pressure ratios of H_2/C_6H_{10} .

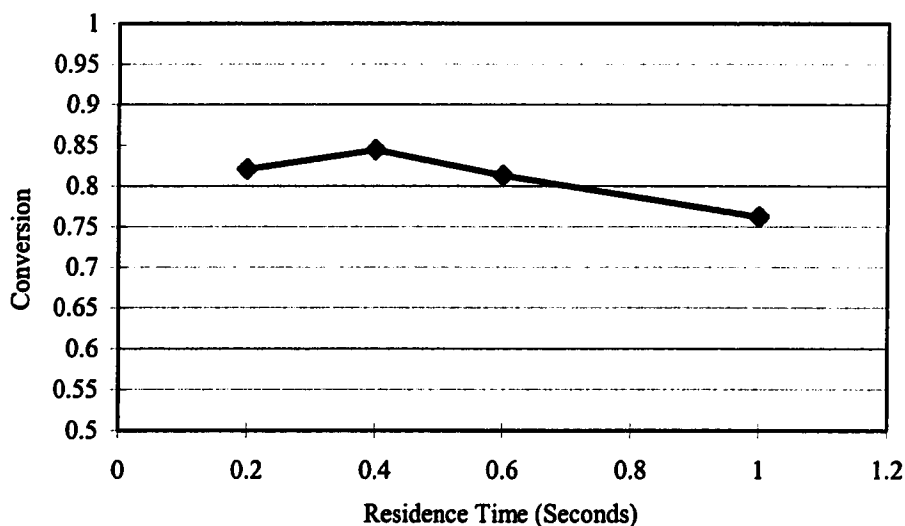
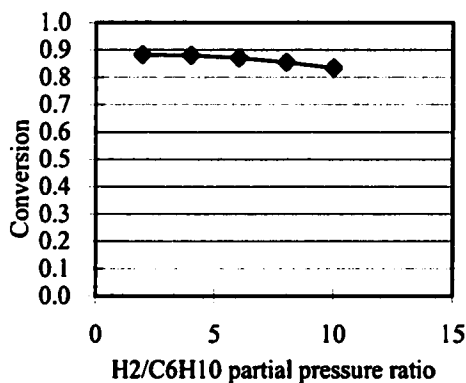
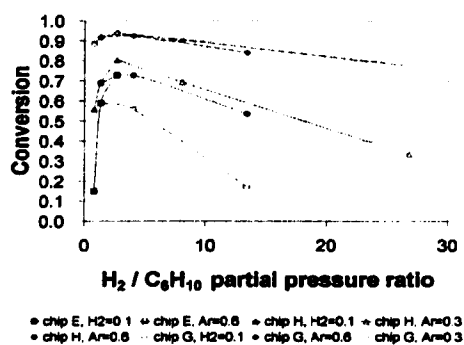


Figure 7.2 Conversion vs. residence time on silica-supported, sputtered Pt



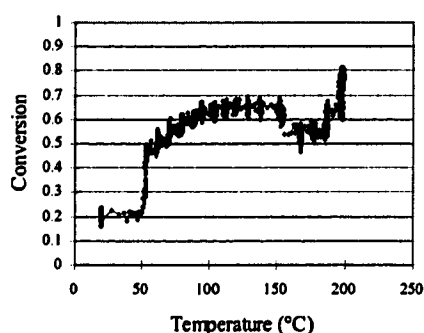
Sputtered Pt on silica sol-gel support



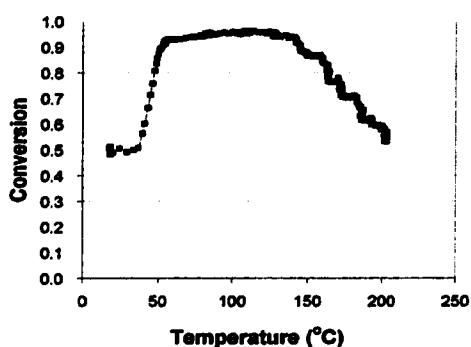
Sputtered Pt without sol-gel supports

Figure 7.3 Comparison of conversion vs. H_2/C_6H_{10} partial pressure ratio. (R. Besser, X. Ouyang, S. Zhao)

The conversion change with temperature under catalyst condition A is different from that under catalyst condition B. (Figure 7.4) At temperatures lower than 50 °C, the conversion of cyclohexene in catalyst condition A is higher than that in catalyst condition B. When the temperatures are held between 50 °C and 150 °C, the conversions under both conditions increase slightly. However, the conversion using condition A is higher than that using condition B. When the temperature is higher than 150 °C, the conversion in condition A drops, but the conversion under condition B increases. Thus, one can conclude that silica sol-gel support is suitable for reactions at higher temperatures.



Sputtered Pt on silica sol-gel support



Sputtered Pt without sol-gel supports

Figure 7.4 Comparison of conversion of cyclohexene vs. temperature.
(R. Besser, X. Ouyang, S. Zhao)

Figure 7.5 shows the selectivity for conversion of cyclohexene to cyclohexane and benzene at different temperatures for catalyst conditions A and B. For silica-supported sputtered Pt, the selectivity to cyclohexane is always higher than the selectivity to benzene both at low or high temperatures. However, for sputtered Pt without support, the selectivity to benzene is higher than the selectivity to cyclohexane when the temperature is higher than 150 °C. These interesting results suggest that, at high

temperature, silica-supported sputtered Pt prefers formation of cyclohexane, while sputtered Pt without support mainly yields benzene.

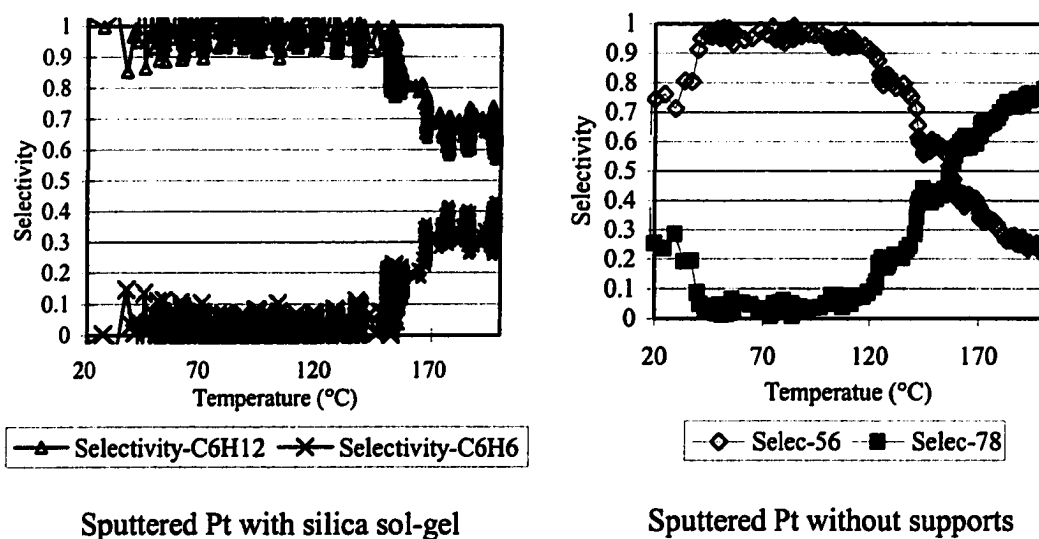


Figure 7.5 Comparison of selectivity vs. temperature

A series of experiments were designed to compare the performance of sputtered catalyst condition A with impregnated so-gel catalyst condition C. The temperature and flow rates for reactants were varied as shown in Table 7.2. The respective conversion of cyclohexene is also included in Table 7.2. Each setting for flow and temperature

Table 7.2 Experimental design for comparison of impregnated Pt with sputtered Pt

Temp (°C)	H ₂ (sccm)	Ar (sccm)	He (sccm)	Conversion using impregnated Pt
62.5	0.82	0.28	5	0.9006446
62.5	0.82	0.82	5	0.9485676
62.5	0.28	0.82	5	0.9428213
125	0.55	0.55	5	0.9346983
187.5	0.28	0.28	5	0.8789347
187.5	0.82	0.28	5	0.9166284
187.5	0.82	0.82	5	0.9102714

combination is kept for 2 hours to stabilize the data from the mass spectrometer to obtain the observed conversion.

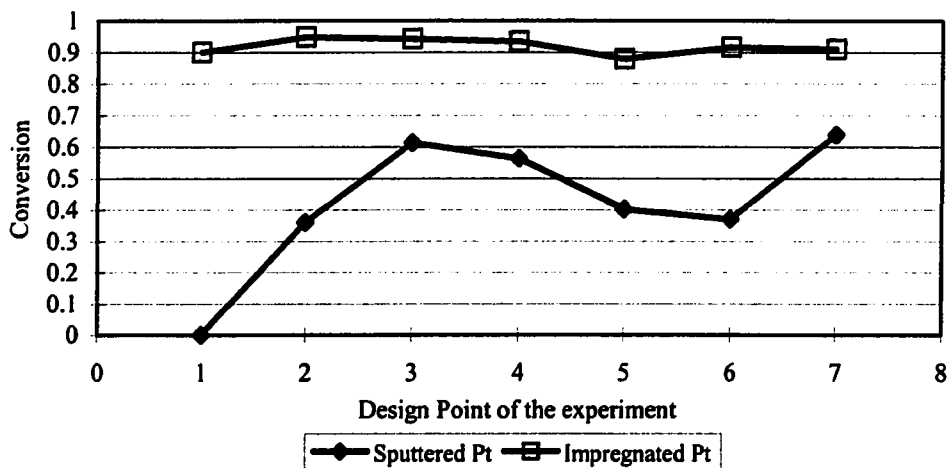


Figure 7.6 Conversion comparison for impregnated Pt and sputtered Pt

Hydrogen treatment of the catalyst was performed at the beginning of the experiment by flowing 1 sccm of pure hydrogen at room temperature. The cyclohexene was then fed into the reactor using argon as a carrier gas. The system stabilized after 4 hours. Cyclohexene conversion on impregnated Pt remained same (90%) at all flow and temperature settings (around 90%) This can be compared to that obtained using sputtered Pt (Figure 7.6). From other experiments, we have also found that the conversion of silica-supported impregnated Pt is higher than that of silica-supported sputtered Pt.

Deactivation of the catalyst was also studied. In the experiment depicted in Figure 7.8, the conversion increases at higher temperature for all but the last experiment performed on that particular microreactor. The lower conversion is an indication that catalyst deactivation need to be examined further for Pt impregnated on the sol-gel silica.

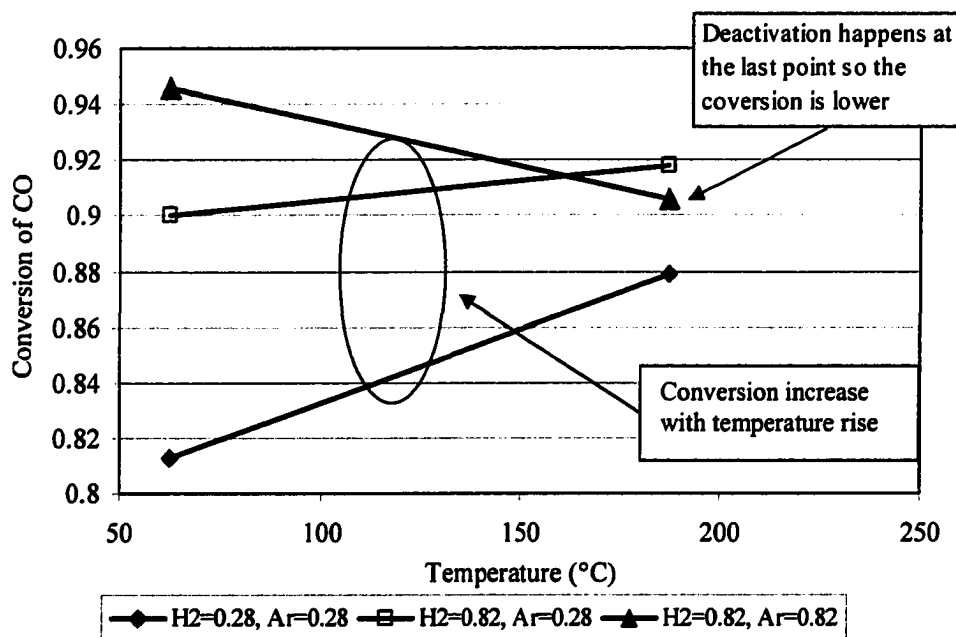


Figure 7.7 Temperature effect on conversion of cyclohexene using impregnated Pt (X. Ouyang, S. Zhao)

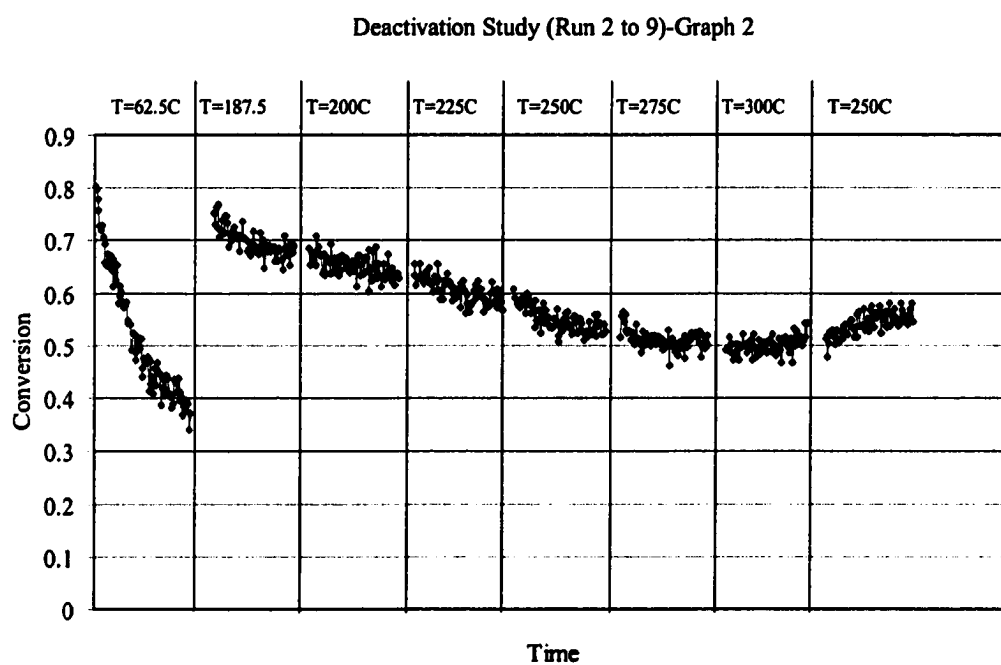
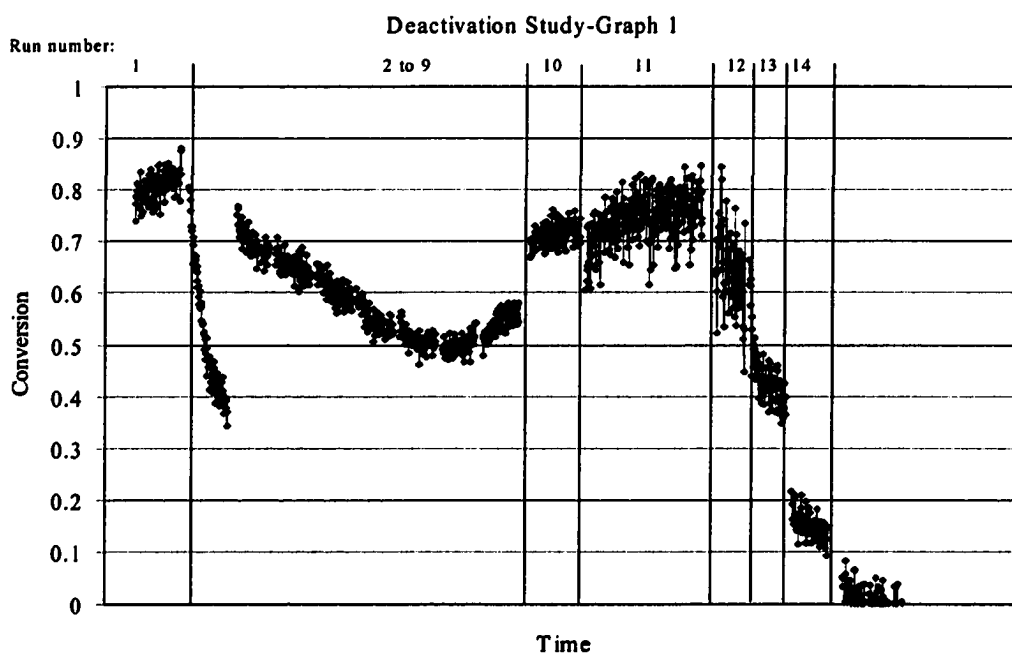
Using the same reactor at the experimental settings listed in Table 7.3, deactivation at different temperatures was studied. Before the experiment started, one-hour of vacuum and one hour of hydrogen treatment were performed to activate the catalyst. As shown in the conversion calculation in Figure 7.7, as deactivation occurred, the conversion of cyclohexene was much lower than in the previous experiments at the same flow/temperature settings. At the first setting, $T=125\text{ }^{\circ}\text{C}$, an 82% conversion was observed with no deactivation over the 2 hour period. However, in the second setting, $T=62.5\text{ }^{\circ}\text{C}$, deactivation occurred dropping the conversion from 70% to 40%.

Table 7.3 Reaction design for studying the deactivation of impregnated Pt

Run number	Time (min)	T (°C)	F ₁ (H ₂)	F ₂ (Ar)	F ₃ (He)
1	120	125	0.55	0.55	5
2	60	62.5	0.82	0.82	5
3	60	187.5	0.82	0.82	5
4	60	200	0.82	0.82	5
5	60	225	0.82	0.82	5
6	60	250	0.82	0.82	5
7	60	275	0.82	0.82	5
8	60	300	0.82	0.82	5
9	60	250	0.82	0.82	5
10	90	250	0.55	0.55	5
11	180	250	0.28	0.28	5
12	60	100	0.28	0.28	5
13	60	100	0.55	0.55	5
14	60	100	0.82	0.82	5
15	60	50	0.82	0.82	5
16	60	20	0.82	0.82	5
17	60	20	0	0.82	5

As the temperature was increased from 187.5 °C (Run number 3) to 275 °C (Run number 7), the deactivation was observed, but the deactivation rate drop was not as high as in the second setting (T=62.5 °C). Here, it is important to point out that, at the 8th setting (T=300 °C), conversion was not dropping but increasing during the experiment. Following the 8th setting, a conversion increase (Figure 7.8-graph 2) was found in the 9th setting (T=250 °C). For the rest of the experiment, as the temperature was dropped again (see in the table), deactivation reaction dominated, especially at Run number 12, when the temperature was dropped from 250 °C to 100 °C. The rapid deactivation observed at low temperature is likely due to carbon formation on the surface of the catalyst (Figure

7.8 graph 3). Moreover, we have found that the lifetime of impregnated Pt is longer than sputtered Pt for a single reaction condition, totaling 7 days versus 2 days.



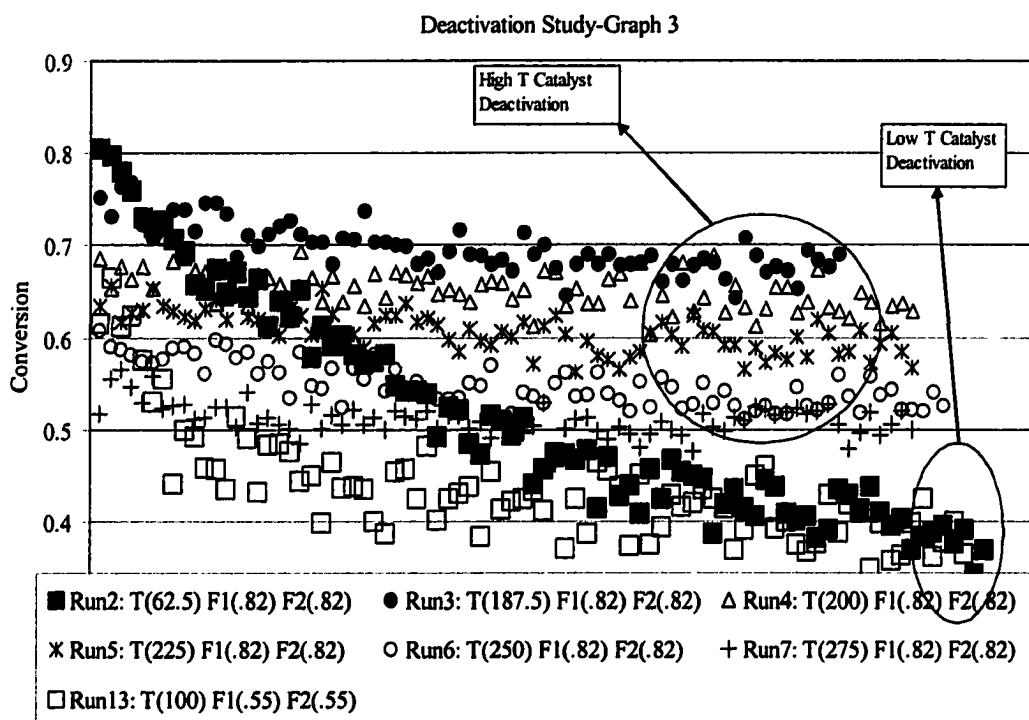


Figure 7.8 Deactivation study on impregnated Pt

In this comparison of physical deposition methods of catalysts versus supported catalysts, it is clear that the supported catalysts produce higher conversion and longer catalyst lifetime than physically deposited catalysts. In addition, the chemical methods employed to produce the supports does not require large capital equipment that sputter deposition requires.

The suitability of using alumina as a support versus silica was also examined. Impregnated Pt on alumina sol-gel prepared by Wang *et al.* method was tested for the conversion reaction of cyclohexene. The reaction was also carried out after 1 hour of H₂ treatment followed by 20 minutes of vacuum. Then the reactant gas was allowed to flow into the microreactor.

Figure 7.9 shows the conversion of cyclohexene versus temperature with the impregnated Pt with alumina support. From the plot, one can see that the conversion remains constant at a high level (above 96 %) as the temperature increases. When the temperature was reduced, however, the conversion decreased gradually. The conversion dropped rapidly at 120 °C, and became almost zero temperatures below 50 °C. Comparing this result with the result based on silica-supported, impregnated Pt, one can conclude that the conversion of impregnated Pt on aluminum oxide is higher than that of impregnated Pt on silicon oxide. However, the lifetime of impregnated Pt on aluminum oxide appears to be shorter than that of impregnated Pt on silicon oxide.

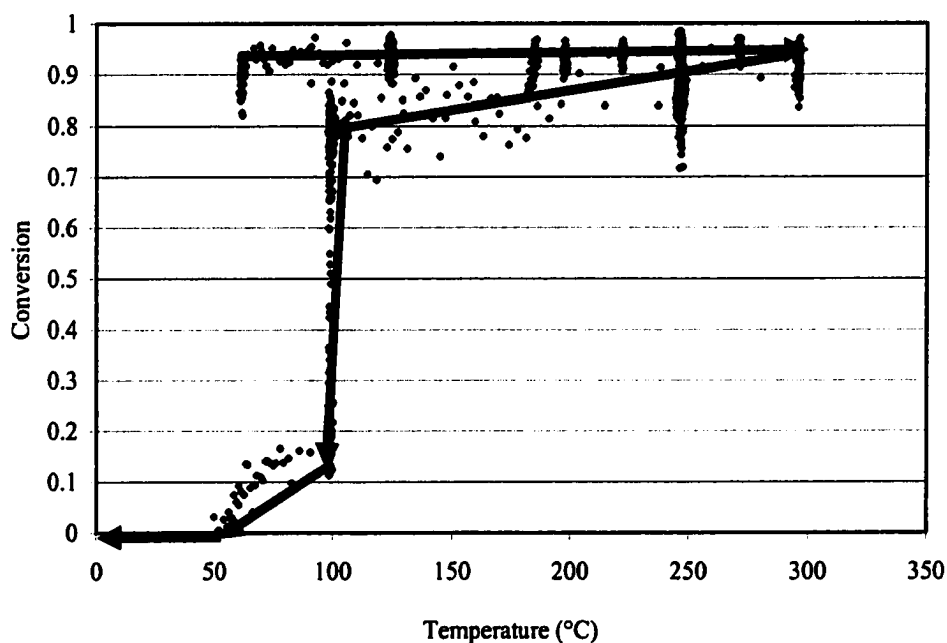


Figure 7.9 Cyclohexene conversion using impregnated Pt on alumina support.

The following conclusions can be drawn from the above work:

1. Cyclohexane product was favored by with sputtered Pt with silica sol-gel while benzene was favored by sputtered Pt without the silica sol-gel support.
2. Catalysts resulting in the highest to lowest conversion are impregnated Pt on aluminum oxide, impregnated Pt on silicon oxide, sputtered Pt on silicon oxide, and sputtered Pt without any support.
3. Catalysts lifetime in the order from longest to shortest are impregnated Pt on silicon oxide, impregnated Pt on aluminum oxide, sputtered Pt on silicon oxide, and sputtered Pt without support.
4. High conversion of cyclohexene at short residence times was realized using sputtered Pt in the 5 μm microreactor or impregnated Pt in the 100 μm microreactor, indicating high efficiency and high productivity of the microreactor.

Application of Catalyst Study

After performing catalyst characterization and conforming catalyst activity and efficiency, the work was started on two commercially significant reactions: Fischer-Tropsch (T-F) synthesis to high alkanes and preferential oxidation for CO amelioration in hydrogen fuel cell feeds. F-T synthesis is a technology for conversion of natural gas to liquid and is an attractive alternative for bringing static gas resources to market. CO amelioration is a required processing step to prevent CO poisoning in a Proton Exchange Membrane (PEM) fuel cell.

Fischer-Tropsch Synthesis

There are several groups working on F-T synthesis, such as Texas A&M University, Exxon Mobil, Shell, *etc* [42, 41]. The main catalysts used for this type of reaction are Ru, Fe, and Co. Fe and Co were selected as catalysts because iron has high activity and cobalt-based catalysts show lower water-gas shift activity, which is undesirable in this reaction. Sputtering deposition and sol-gel method were employed for the fabrication of catalysts.

Deposition of Fe and Co by Sputtering 300 μm Fe and 100 μm Co were deposited on the microreactors separately because of the sputtering deposition limitation, which means that sputter can only make a uniform thin film of pure materials layer by layer.

An initial experiment involved studying catalyst behavior over a period of time, the effect of temperature, and H_2/CO flow ratio on conversion. Reactants were fed for a period of 12 hours before any conversion could be observed. This observation illustrates the utility of our approach for characterizing activation behavior. Then $\text{H}_2:\text{CO}$ flow ratio was maintained at 3:1 (0.3 sccm to 0.1 sccm) and temperature was slowly increased, with the result that methane conversion improved with each increase of temperature. From the experiments on 2 iron and 2 cobalt based 100 μm channel reactors, iron was found to have a higher catalyst activity than cobalt. This is consistent with that reported in the literature. For iron-coated reactors, the conversion ranged from 28% to 70%, while only 5% to 18% for cobalt catalyst at 200 °C and 250 °C, respectively (Figure 7.10). No

water-gas shift reaction was detected, nor was catalyst deactivation observed during experiments for both Fe and Co reactors.

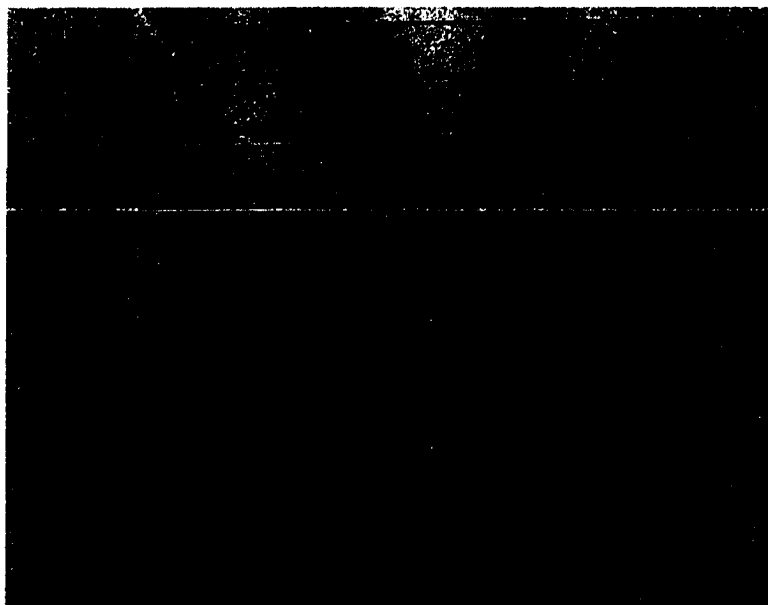


Figure 7.10 F-T synthesis study with sputtered Fe and Co
(Conversion vs. temperature) (Cooperation with Xun Ouyang)

Another experiment was carried out with a Fe coated 100 μm reactor at 250 $^{\circ}\text{C}$ while H_2/CO flow ratio was varied from 1:1 to 10:1. The results are shown in Figure 7.11. An increase in CO conversion was observed with higher H_2/CO ratios. This observation may come from the difference in chemisorption ability of H_2 and CO onto the catalyst surface.

The conversion presented above is all for methane. Methanation reaction has been chosen as a preliminary CO hydrogenation study leading to F-T synthesis. But the mechanisms of methanation and F-T synthesis are different. In F-T synthesis, the objective is to produce high molecular weight hydrocarbons. That is why the F-T synthesis is also called gas-to-liquids technology. However, with sputtered Fe or Co, only

methane was produced. Thus, the experiments were conducted using encapsulated sol-gel catalysts.

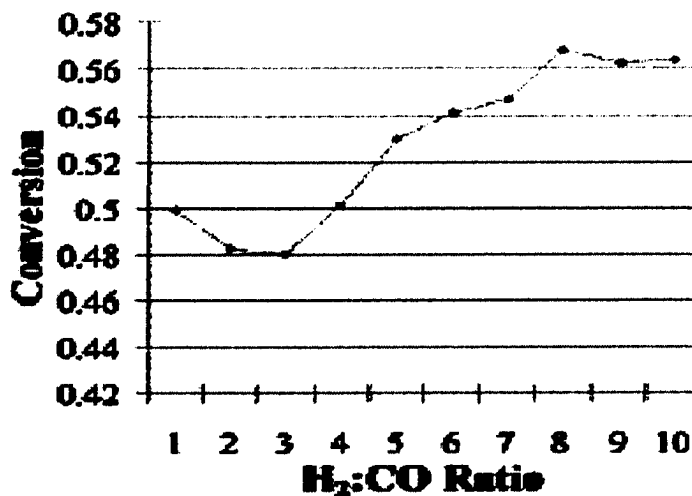


Figure 7.11 F-T synthesis study with sputtered Fe and H₂/CO ratio.
(Cooperation with Xun Ouyang)

Mixed Fe and Co by Sol-Gel Technology Having Considered Fe with higher activity and Co with no water-gas shift activity, a mixed catalyst of Fe and Co was chosen. The catalyst support is alumina because it can yield higher conversion than silica as discussed for cyclohexene conversion reactions. Initially, 6% Fe and 6% Co loading by weight were deposited using alumina sol-gel support, the same concentration used in conventional scale reactors. The catalysts was treated with H₂ of 1 sccm at 300 °C to change the chemical state of the catalyst from Fe⁺ and Co⁺ to Fe⁰ and Co⁰ since reduced metals can act as catalysts. However, no reaction was observed. When the loading of catalyst was changed to 12% Fe and 12% Co, an appreciable conversion of CO was realized.

Figure 7.12 shows that the conversion of CO varies with the H₂/CO ratio. At lower H₂/CO ratios, the conversion increases with the increase in H₂/CO ratio. But the

main trend on conversion decreases with the increase of H_2/CO ratio, and this is in agreement with that in normal scale reported in literature [48].

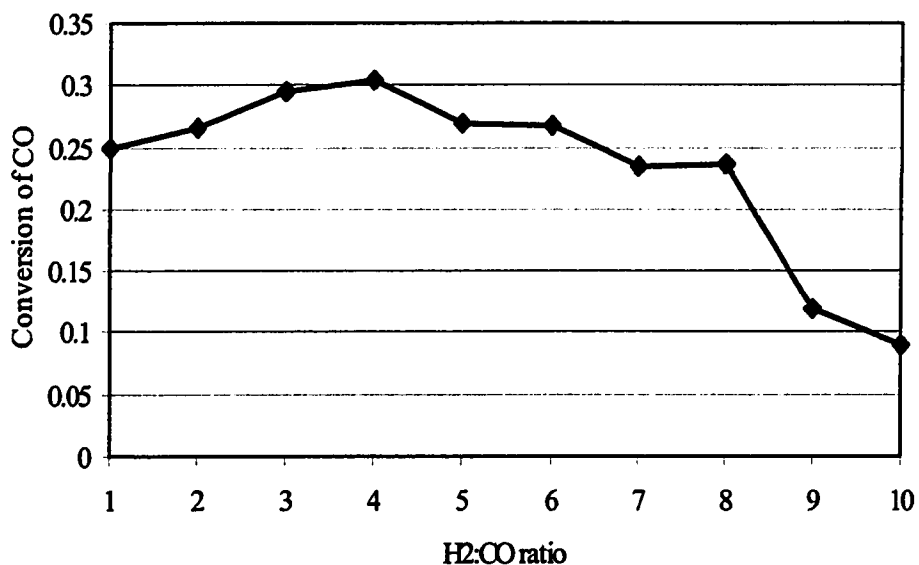


Figure 7.12 F-T study with sol-gel coated Fe/Co catalyst at 240 °C (Conversion vs. H_2/CO ratio)

Based on the conversion presented above, and that reported from other research groups, we focused on using H_2/CO ratio of 2:1 and 3:2. As shown in Figure 7.13, the conversion of CO was always higher with a H_2/CO ratio of 3:2 than a H_2/CO ratio of 2:1 at different temperatures. Figure 7.14 compares the conversion with high/low rates at different temperatures. With increasing temperatures, the conversion increased at low flow rates. This result confirms that a longer residence time yields higher conversion of CO.

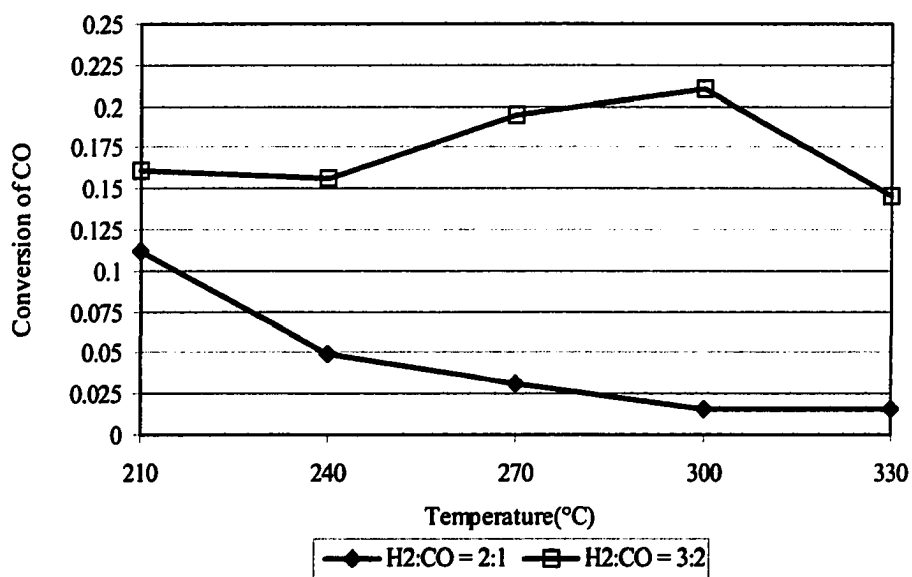


Figure 7.13 F-T synthesis study with alumina sol-gel coated Fe/Co catalyst. (conversion vs. temperature)

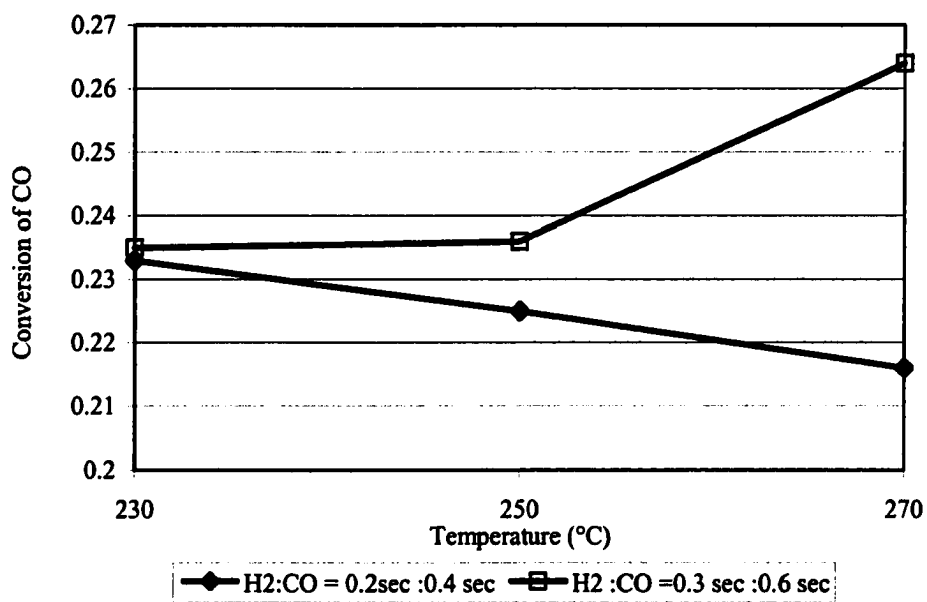


Figure 7.14 F-T synthesis study with alumina sol-gel coated Fe/Co catalyst (conversion vs. temperature with different flow rate).

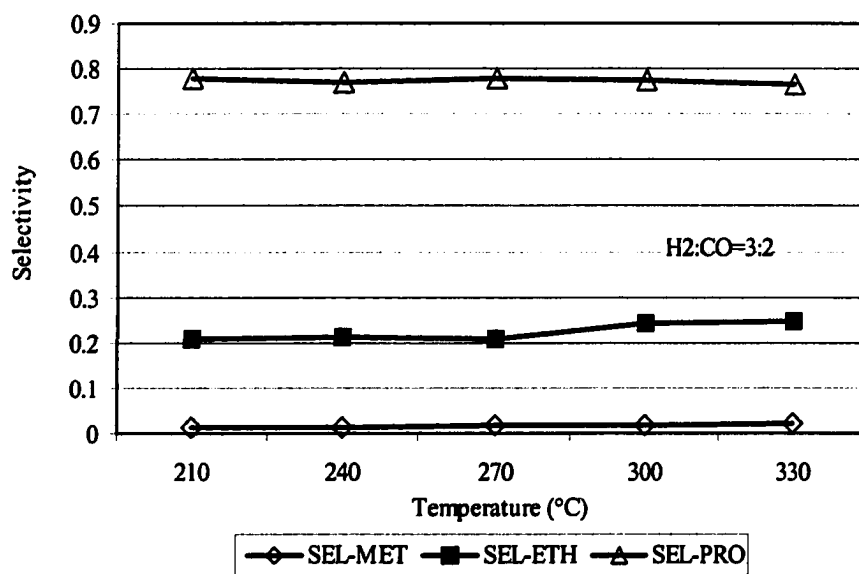


Figure 7.15 F-T synthesis study with alumina sol-gel coated Fe/Co catalyst. (selectivity vs. temperature)

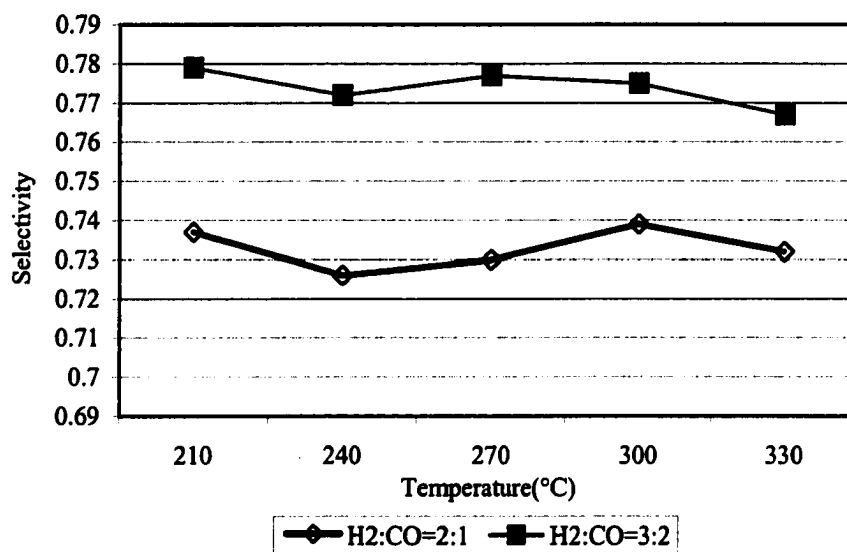


Figure 7.16 F-T synthesis study with alumina sol-gel coated Fe/Co (selectivity to propane vs. temperature with different ratios of H₂/CO)

As mentioned before, the purpose of this study is to produce higher alkanes. So, the selectivity to different products, C₁, C₂,..., C_n should be considered. From Figure

7.15, one can see almost 80% of CO produced propane, 20% CO produced ethane, and little methane was produced. That is the reason the sol-gel method was employed here.

The fact that a H₂/CO ratio of 3:2 is better than a H₂/CO ratio of 2:1 can be confirmed by the results presented in Figure 7.16. The selectivity to propane is 76% to 78% for a H₂/CO ratio of 3:2, compared with 72% to 74% for a H₂/CO ratio of 2:1.

In our initial studies, the conversion of CO using sol-gel encapsulated Fe/Co was very low, 20%-30%. This can be improved further using a higher loading of catalyst, 24% Fe and 24% Co. The conversion of CO to higher alkanes > 50% at the H₂:CO ratio of 3:1 has been achieved at 220 °C.

Comparing reactions by sputtered Fe/Co with sol-gel coated Fe/Co, the following conclusions can be drawn:

1. With sputtered Fe and Co, only methane can be produced. The activity and efficiency of Fe is higher than that of Co.
2. With sol-gel encapsulated Fe/Co catalyst, high molecular weight hydrocarbons have been produced. A higher Fe/Co loading is required to improve the conversion of CO.
3. A H₂/CO ratio of 3:2 yields a higher conversion of CO in the microreactor coated with sol-gel encapsulated Fe-Co catalyst.
4. Higher alkanes may be realized at higher pressure, which is currently limited by the current reaction setup.
5. In addition, for the preparation of catalysts, sol-gel coated Fe/Co is much cheaper than sputtered Fe and Co because of cheaper raw materials and the facilities.

Preferential Oxidation for CO Amelioration in Hydrogen Fuel Cell Feeds

Fuel cells, like batteries, convert the chemical energy directly to electrical energy without inefficient combustion. Therefore, they can compete with other energy sources (gasoline, battery, etc.), in areas such as the automotive industry and the cell phone industry. For example, fuel cells are used today for operating a very limited number of cars on the streets in Japan. Preferential oxidation of CO in hydrogen fuel cells is a new challenge as H₂ is the main source for a fuel cell and the presence of CO in it will deactivate the fuel cell. Based on the information available in the literature, cobalt and platinum can be employed as catalysts. Platinum was chosen because Co requires higher temperatures than Pt [113,15]. Pt impregnated in sol-gel support was used instead of sputtered Pt because of its higher activity and longer lifetime demonstrated in the previous studies of the conversion of cyclohexene to cyclohexane and benzene.

The mixed gas used in our experiments consists of 70% H₂, 2% CO and 28% Ar. Air or O₂ has been used as the oxidizer.

Preferential Oxidation for CO in Hydrogen Fuel by Air. The reaction was started with one hour of vacuum, followed by two hours of H₂ treatment to activate the catalyst. By changing the reaction temperature from 40 °C to 240 °C, some CO₂ was produced at 160-200 °C. For these experiments, the Pt loading was 50% by weight to silica. The ratio of O₂/CO was varied from 0.3, 0.5, 0.75, 1, 2 to 10 by keeping the mixed gas at 1scm and changing the air flow rate from 0.02 to 0.4 (Figure 7.17, 7.18). The temperature of the experiments was held constant at 200 °C. The conversion of CO decreases when the ratio of O₂/CO increases until the O₂/CO ratio is 2.5. Above the O₂/CO ratio of 2.5, there

is a steep increase in conversion. The conversion reaches a maximum at a ratio of 4. The conversion decreases as the ratio is increased further. At higher ratios, the conversion remains relatively constant. Low ratios favor the oxidation of CO. Higher oxygen ratios favor the oxidation of CO.

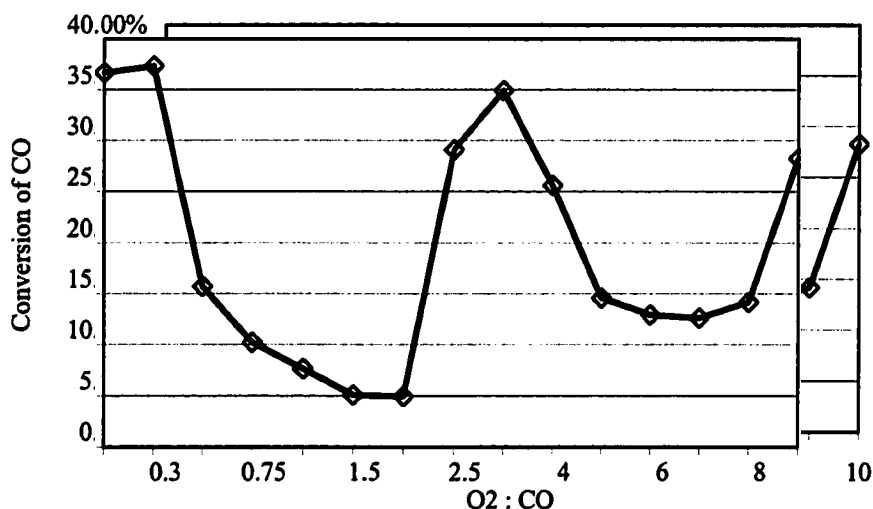
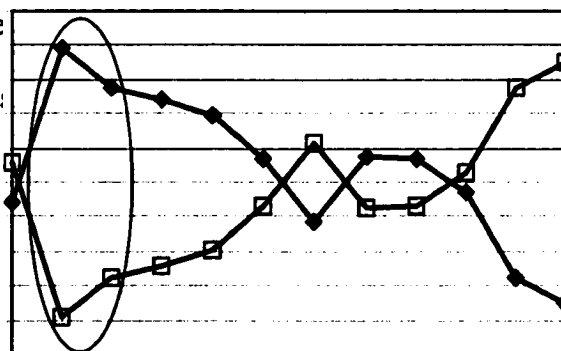


Figure 7.17 Preferential oxidation for CO at 200 °C (Conversion vs. ratio of O₂/CO)

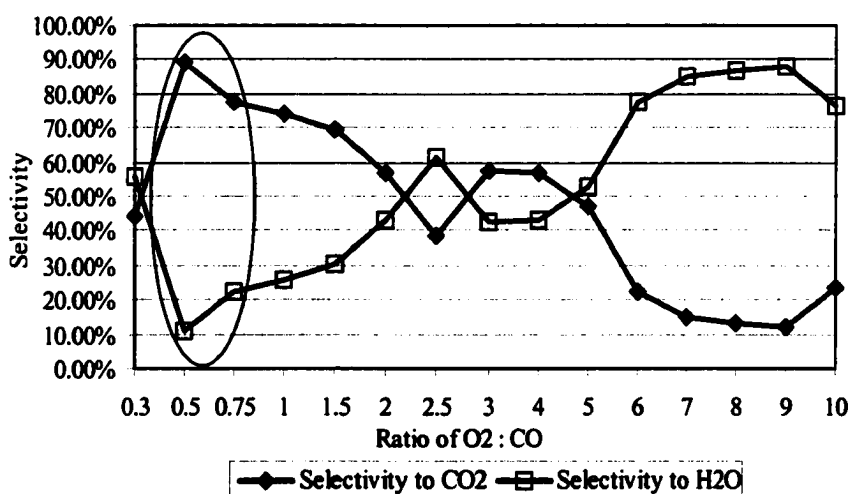


Figure 7.18 Preferential oxidation for CO (Selectivity vs. ratio of O₂/CO)

The conversion of CO over Pt obeys a single site Langmuir-Hinshelwood kinetic model [39], where O_2 and CO compete for the same sites. (See circled region in Figure 7.17). This is in agreement with that reported in the literature [15].

Based on both plots presented above, the region of low O_2/CO ratios was explored further. The Pt loading was increased from 50% to 100% to further increase the conversion of CO. The total flow rate was maintained at 1.75 sccm, and two O_2/CO ratios were studied. The conversion versus temperature with different O_2/CO ratios is shown in Figure 7.19. The conversion of CO decreases with increase in temperature. The O_2/CO ratio of 0.75 yields higher conversion than the O_2/CO ratio of 1.5. This is consistent with the trend shown in Figure 7.17 and that reported in the literature [97]. In Figure 7.20, when the temperature is increased from 120 °C to 220 °C, the selectivity to H_2O increases, compared with the decrease of selectivity to CO_2 , which is again consistent with that reported in the literature [15]. Selectivity to H_2O is always higher than to CO_2 for the temperatures and flow rates tested.

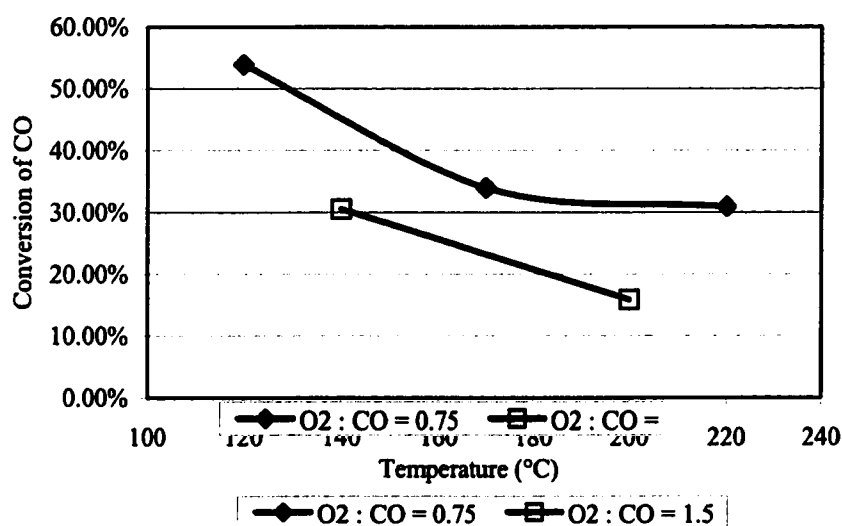


Figure 7.19 Preferential oxidation for CO (Conversion vs. temperature with different O_2/CO ratio) (Air as oxidizer)

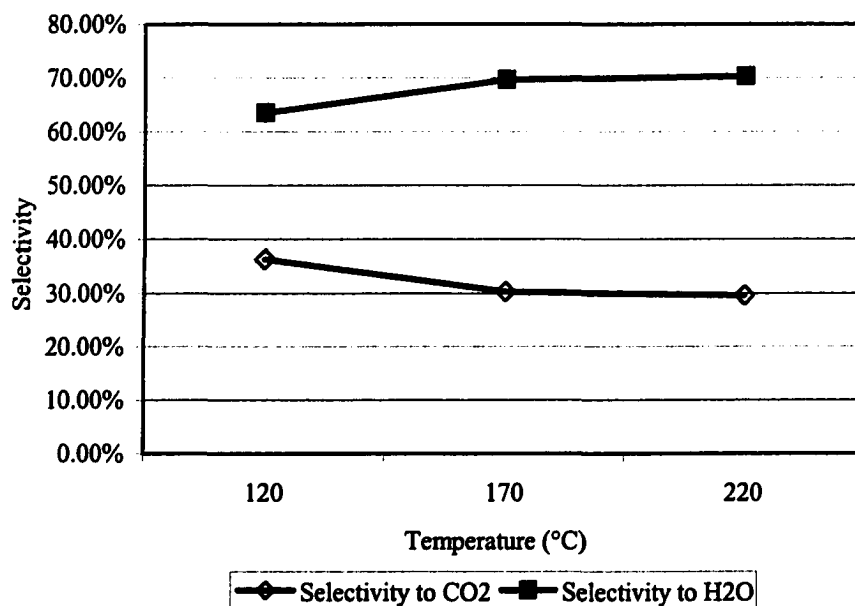


Figure 7.20 Preferential oxidation for CO (Selectivity vs. temperature with O₂/CO ratio of 0.75) (Air as oxidizer)

Preferential Oxidation for CO in Hydrogen Fuel by Pure O₂. Because air is only 21% oxygen, the reactor system had to be modified to achieve the same O₂/CO ratio using pure oxygen as was previously examined using air. The total flow rate through the reactor was varied between 0.2 and 1 sccm, which is much lower than the air flow rate between 1.5 and 2 sccm.

At first, temperature and O₂/CO ratio were varied at a total flow rate of 0.6 sccm. In Figure 7.21, the conversion and selectivity did not vary substantially as the temperature was varied. The selectivity to CO₂ was highest at 170 °C, which is consistent with that in conventional scale reported in the reference [97].

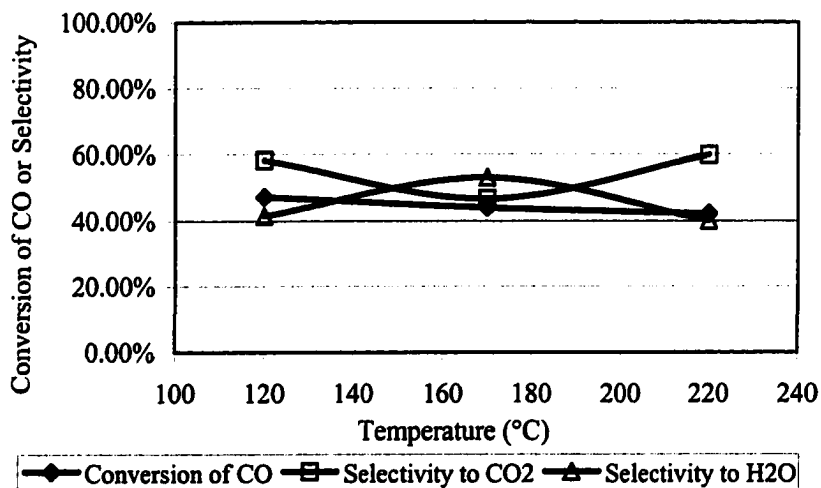


Figure 7.21 Preferential oxidation for CO (Conversion of CO or Selectivity vs. temperature with O_2/CO ratio of 0.5 and total flow rate of 0.6 sccm)

Figure 7.22 depicts the total flow rate versus conversion of CO and selectivity. The reaction has been carried out at 170 °C with an O_2/CO ratio of 0.5. The conversion decreases with a decrease in residence time. The selectivity to CO_2 is higher than to H_2O at low flow rates, and lower than to H_2O at high flow rates.

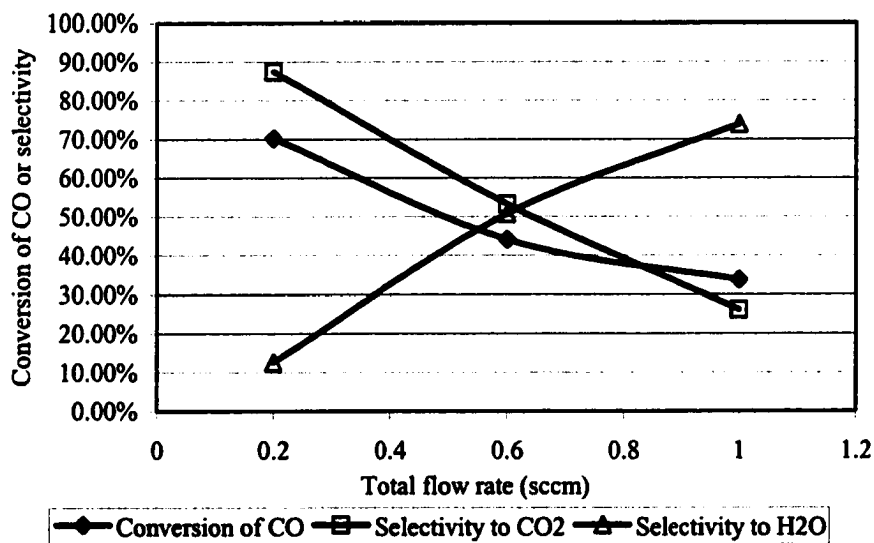


Figure 7.22 Preferential oxidation for CO (Conversion of CO or Selectivity vs. Residence time with O_2/CO ratio of 0.5)

As mentioned regarding cyclohexene conversion reactions, silica-supported, impregnated Pt has a long lifetime. Catalyst stability over long time periods is a requirement for commercialization of this technology. Stability of the Pt catalyst was tested at 170 °C, an O₂/CO ratio of 0.5 and a total flow rate of 0.6 sccm (Figure 7.23). After 40 hours of operation, the conversion of CO did not change appreciably.

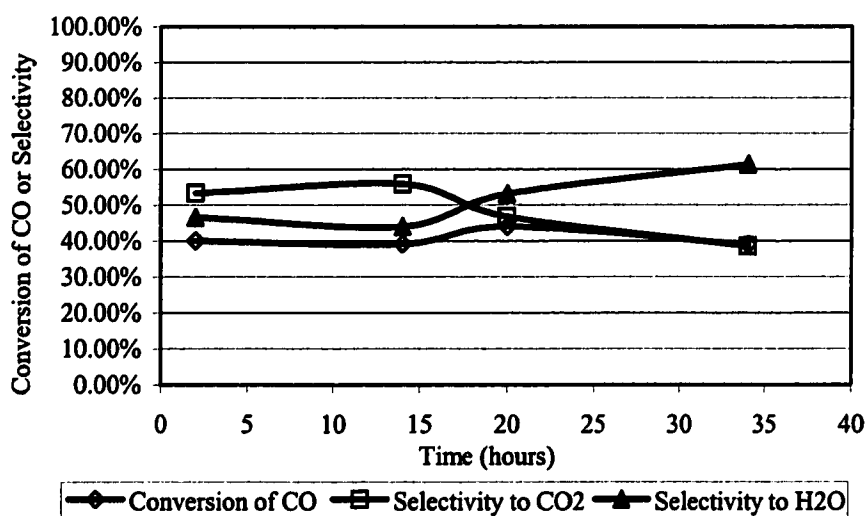


Figure 7.23 Preferential oxidation for CO (Conversion of CO or Selectivity vs. time with O₂/CO ratio of 0.5)

Based on the above discussion, it can be concluded as follows:

1. Residence time affects both the conversion of CO and the selectivity to CO₂.
Longer residence time yields high conversions of CO and selectivity toward CO₂.
2. The conversion and selectivity of this reaction is not sensitive to broad temperature changes at the residence time tested.
3. The conversion of CO and selectivity to CO₂ decreases with increasing O₂ concentration. A stoichiometric quantity of oxygen was found to produce optimum results.

4. Impregnated platinum supported by silica gel is a suitable catalyst for preferential oxidation for CO in a hydrogen fuel cell. No deactivation of the catalyst is observed after 40 hours of reaction.

CHAPTER VIII

STATISTICAL ANALYSIS

For any experiment, it is more efficient to examine all possible causes of variation simultaneously rather than one at a time. Fewer observations are usually needed, and one gains more information about the system being investigated. This simultaneous study is known as a “factorial experiment.” It can save time and cost. Response surface methodology is developed to aid the improvement of manufacturing processes in the chemical industry.

In this study, a Central Composite Design (CCD), the most popular second-order design for response surface methodology, has been used in preferential oxidation for CO amelioration in hydrogen fuel cell feeds. There are three factors that we consider important to the experiment. Temperature(x_1), CO:O₂ ratio(x_2), and the Total Flow rate(x_3) are the three independent factors. The conversion of CO and the selectivity of CO₂ are considered as the dependent variables.

According to the CCD, 18 runs have been carried out and all the design and experimental observations that were collected using the microreaction set up system are shown in Table 8.1, where Part A is the uncoded values and part B is the coded values. Y₁ is the conversion of CO, and Y₂ is the selectivity of CO₂. The software, SAS, was utilized for analyzing the experimental observation.

Table 8.1 Central Composite Design for Fuel Cell Experiment:

A					B				
Observation	Run Order	Temperature T(OC)	CO:O ₂ Ratio R	TotalFlow Rate FL(sccm)	x1	x2	x3	Conversion Y1	Selectivity of CO ₂ Y2
1	13	140.24	1.01	0.36	-1	-1	-1	0.5956	0.7265
2	18	140.24	1.01	0.84	-1	-1	1	0.3749	0.3383
3	7	140.24	3.24	0.36	-1	1	-1	0.5346	0.8569
4	2	140.24	3.24	0.84	-1	1	1	0.3712	0.5113
5	14	199.76	1.01	0.36	1	-1	-1	0.5765	0.7477
6	8	199.76	1.01	0.84	1	-1	1	0.3186	0.3272
7	5	199.76	3.24	0.36	1	1	-1	0.5068	0.6348
8	11	199.76	3.24	0.84	1	1	1	0.3667	0.4406
9	1	170.00	2.13	0.60	0	0	0	0.4010	0.5338
10	16	170.00	2.13	0.60	0	0	0	0.3901	0.3862
11	6	170.00	2.13	0.60	0	0	0	0.3923	0.5594
12	9	170.00	2.13	0.60	0	0	0	0.4410	0.4680
13	12	120.00	2.13	0.60	-1.7	0	0	0.4735	0.5843
14	3	220.00	2.125	0.6	1.7	0	0	0.4225	0.5991
15	4	170.00	0.25	0.60	0	-1.68	0	0.4226	0.5389
16	10	170.00	4.00	0.60	0	1.68	0	0.4512	0.5434
17	15	170.00	2.13	0.20	0	0	-1.7	0.7017	0.8741
18	17	170.00	2.13	1.00	0	0	1.68	0.3375	0.2610

Table 8.2 SAS output of the 2nd-order fuel cell model on CO conversion with parameter estimates for the uncoded factor levels.

The RSREG Procedure

Parameter	Design factor	Standard Estimate	Error	Parameter Estimate from Coded	t Value	Pr > t	Data
Intercept	1	1.508258	0.287724	5.24	0.0008		0.407030
x1	1	-0.004948	0.002796	-1.77	0.1148		-0.023822
x2	1	-0.103630	0.053910	-1.92	0.0908		-0.004690
x3	1	-1.330814	0.261789	-5.08	0.0009		-0.170858
x1*x1	1	0.000012568	0.000007746	1.62	0.1434		0.031421
x2*x1	1	0.000162	0.000260	0.62	0.5502		0.015191
x2*x2	1	0.005777	0.005510	1.05	0.3251		0.020311

x3*x1	1	-0.000243	0.001207	-0.20	0.8453	-0.004865
x3*x2	1	0.081712	0.032214	2.54	0.0349	0.061284
x3*x3	1	0.642821	0.120698	5.33	0.0007	0.102851

Table 8.3 SAS output of the 2nd-order fuel cell model on CO₂ selectivity with parameter estimates for the uncoded factor levels.

The RSREG Procedure

Parameter	Design factor	Standard Estimate	Error	Parameter Estimate from Coded		Data
				t Value	Pr > t	
Intercept	1	2.418602	0.754116	3.21	0.0125	0.486707
x1	1	-0.013772	0.007329	-1.88	0.0970	-0.031666
x2	1	0.072598	0.141296	0.51	0.6213	0.038333
x3	1	-1.958690	0.686142	-2.85	0.0213	-0.291537
x1*x1	1	0.000042091	0.000020303	2.07	0.0719	0.105227
x2*x1	1	-0.001140	0.000681	-1.67	0.1326	-0.106867
x2*x2	1	0.015607	0.014442	1.08	0.3113	0.054870
x3*x1	1	0.002084	0.003163	0.66	0.5285	0.041688
x3*x2	1	0.125501	0.084432	1.49	0.1755	0.094126
x3*x3	1	0.507344	0.316345	1.60	0.1474	0.081175

Table 8.4 SAS output of the Estimated Ridge of Maximum Response for the conversion of CO.

The RSREG Procedure

Estimated Ridge of Maximum Response for Variable y

Coded Radius	Estimated Response	Standard Error	Uncoded Factor Values		
			x1	x2	x3
0.0	0.407030	0.012169	170.000000	2.125000	0.600000
0.1	0.425323	0.012104	169.373894	2.114155	0.560382
0.2	0.445720	0.011924	168.856357	2.093821	0.520804
0.3	0.468263	0.011682	168.423220	2.066378	0.481322
0.4	0.492979	0.011472	168.056242	2.033532	0.441957
0.5	0.519887	0.011434	167.741721	1.996518	0.402713

0.6	0.549002	0.011742	167.469315	1.956234	0.363581
0.7	0.580333	0.012566	167.231137	1.913347	0.324554
0.8	0.613890	0.014025	167.021104	1.868359	0.285620
0.9	0.649679	0.016153	166.834464	1.821652	0.246771
1.0	0.687703	0.018926	166.667466	1.773525	0.207996

Table 8.5 SAS output of the Estimated Ridge of Maximum Response for the selectivity of CO₂.

The RSREG Procedure					
Estimated Ridge of Maximum Response for Variable y					
Coded Radius	Estimated Response	Standard Error	Uncoded Factor Values		
			x1	x2	x3
0.0	0.486707	0.031895	170.000000	2.125000	0.600000
0.1	0.517048	0.031722	169.364948	2.143983	0.560531
0.2	0.548993	0.031250	168.547733	2.153036	0.521074
0.3	0.582632	0.030615	167.574263	2.153265	0.481733
0.4	0.618042	0.030063	166.469131	2.145755	0.442575
0.5	0.655287	0.029960	165.254587	2.131508	0.403641
0.6	0.694421	0.030763	163.950167	2.111412	0.364949
0.7	0.735487	0.032922	162.572736	2.086231	0.326502
0.8	0.778521	0.036741	161.136750	2.056610	0.288296
0.9	0.823553	0.042315	159.654608	2.023087	0.250318
1.0	0.870609	0.049578	158.137025	1.986103	0.212553

Table 8.6 SAS output of the correlation between CO conversion and CO₂ selectivity.

Spearman Correlation Coefficients, N = 18			
Prob > r under H ₀ : Rho=0			
	x	y	
x	1.00000	0.90299	
	<.0001		
y	0.90299	1.00000	
	<.0001		

Conclusion from data analysis using SAS:

From Table 8.2, the 2nd-order model for CO conversion is:

$$y = 1.508258 - 0.004948x_1 - 0.10363x_2 - 1.330814x_3 + 0.000012568x_1^2 + 0.000162x_1x_2 + 0.005777x_2^2 - 0.000243x_1x_3 + 0.081712x_2x_3 + 0.642821x_3^2$$

From Table 8.3, the 2nd-order model for the selectivity of CO₂ is :

$$y = 2.418602 - 0.013772x_1 + 0.072598x_2 - 1.95869x_3 + 0.000042091x_1^2 - 0.00114x_1x_2 + 0.015607x_2^2 + 0.002084x_1x_3 + 0.125501x_2x_3 + 0.507344x_3^2$$

From Table 8.4, the 2nd-order model of CO conversion shows that the temperature, CO: O₂ ratio, and Total Flow Rate combination at the point (167 °C, 1.77, and 0.207 sccm) gives a maximum conversion of CO (68.77%). From Table 8.5, the 2nd-order model of the selectivity of CO₂ shows that the temperature, CO: O₂ ratio, and Total Flow Rate combination at the point (158 °C, 1.99, and 0.213 sccm) gives a maximum selectivity of CO₂ (87.06%).

From Table 8.6, the correlation coefficient of the conversion of CO and selectivity of CO₂ is 0.903. This indicates that the conversion of CO and the selectivity of CO₂ are highly correlated.

According to the SAS result, 158 °C, a 1.77 CO: O₂, and a 0.208 sccm flow is predicted to produce the maximum conversion of CO and selectivity of CO₂. When this combination was used in the 2nd-order model for CO conversion and 2nd-order model for CO₂ selectivity, the CO conversion was 69.31% and CO₂ selectivity was 88.1%.

Unfortunately, the highest conversion of CO and selectivity towards CO₂ was produced at the lowest flow rate the equipment would operate. Ideally, one would want to

further reduce the total flow rate, but that is not possible with the equipment that is currently available. Additional experiments are planned at 0.2 sccm to determine sensitivity of O₂:CO ratio and reactor temperature at this flow rate.

CHAPTER IX

CONCLUSIONS

In this study, catalysts of platinum, iron and cobalt have been successfully microfabricated by two types of methods: physical and chemical methods. In the case of the physical method, 50 nm Pt, 30 nm Fe, and 10 nm Co were deposited into the microreactor by sputtering deposition to yield a uniform thin film inside the microchannels of the microreactor. Chemical methods, such as sol-gel method and ion impregnation, were employed to increase the surface area of the catalysts inside the microreactors. Silica-supported or alumina-supported Pt and alumina-supported Fe/Co were fabricated by modifying the methods reported in the literature.

Characterization of catalysts with supports was performed using SEM (scanning electron microscopy), XPS (X-ray photoelectron spectroscopy), and BET surface area measurement, EDX (Energy Dispersive X-Ray), and VSM (Vibrating Sample Magnetometer) techniques. The 5 μm wide channel dimension tested did not allow uniform coverage of sol-gel on the wall of the microchannels, while the 100 μm wide channel reactor did allow uniform coverage. The size of support particles coated by a sol-gel method has a diameter of 80 nm, which dramatically increases the surface area of catalysts compared to that of sputtered catalysts. The concentration of platinum inside silica support was found to be uniform. The surface area of catalysts with supports is 7 m^2 , which is much higher than the calculated area of a microreactor without support

(0.003 m²). The adhesion of alumina to the silicon sidewall is lower than that of silica. Also dip coatings resulted in larger surface area of catalysts than drop coatings and spin coatings. The ferromagnetic nature of Fe/Co has been changed before and after the chemical reaction.

Two microreactor geometries were used for testing the activity and efficiency of catalysts. Straight line channels with 5 μm and 100 μm in width and wave line channels 5 μm in width were micromachined by lithography and ICP etching. The challenges in ICP etching were overcome by optimizing the cycle times of SF₆ gas flow, bias power, and chamber pressure.

The cyclohexene conversion reaction was utilized for comparison of catalysts fabricated by different methods. The activity and efficiency of sol-gel coated catalysts is much higher than that of sputtered catalysts. Catalysts tested for conversion of cyclohexene in descending order of activity are: impregnated Pt on aluminum oxide, impregnated Pt on silicon oxide, sputtered Pt on silicon oxide, and sputtered Pt without support. The effect of residence time on the conversion of cyclohexene is observably smaller than that of surface area. The descending order of observed catalysts' lifetime are: impregnated Pt on silicon oxide, impregnated Pt on aluminum oxide, sputtered Pt on silicon oxide, and sputtered Pt without support.

Fischer-Tropsch (F-T) synthesis and preferential oxidation of CO in a fuel cell were two applications studied in the microreactors. Over 50% conversion of CO in F-T synthesis and over 70% conversion of CO in preferential oxidation were accomplished. The selectivity to propane is 78% and the selectivity to CO₂ is over 80%, respectively.

In Fischer-Tropsch synthesis, with sputtered Fe and Co, only methane can be produced. The activity and efficiency of Fe is higher than Co. With a sol-gel encapsulated Fe/Co catalyst, higher molecular weight hydrocarbons have been produced. A higher Fe/Co loading is recommended to improve the conversion of CO. A H₂/CO ratio of 3:2 yields a higher conversion of CO in the microreactor coated with sol-gel encapsulated Fe-Co catalyst. Higher alkanes may be realized at higher pressure; however, the microreactor setup described in this dissertation was limited to atmospheric pressure studies only.

In the preferential oxidation of CO for fuel cells, long residence times are required to yield a high conversion of CO and selectivity to CO₂. Temperature variations between 120 °C and 220 °C were not significant at the residence time tested. The highest selectivity to CO₂ was observed at 170 °C. The conversion of CO and selectivity to CO₂ decreases with increase of the O₂ concentration above the stoichiometric amount for the desired reaction. An O₂/CO ratio of 0.5 is a very good ratio for CO conversion. Impregnated platinum supported by silica gel is a suitable catalyst for preferential oxidation for CO in the presence of hydrogen. No deactivation of catalyst is observed after 40 hours of reaction.

A Central Composite Design (CCD) of experiment was performed to efficiently analyze the parameters of the preferential oxidation of CO reaction. Three parameters were analyzed using experimental data from 18 runs. The model predicts an optimum combination of temperature, CO: O₂ ratio, and total flow rate of 158 °C, 1.77, and 0.207 sccm will result in 69% conversion of CO and 88% selectivity to CO₂.

APPENDIX
NOMENCLATURE

μm	micrometer
nm	nanometer
Kn	Kundsen number
λ	mean free path
d	characteristic dimension
k	Boltzmann's constant
T	temperature
d_i	gas molecule diameter
P	gas partial pressure
R_s	specific turnover rate
f	catalyst reaction turnover frequency
a	catalyst surface area
RP	reaction probability
F	flux of molecules striking the surface of unit area
R	gas constant
M	average molar weight
W	a mount of materials
k	proportionality constant
Pt	gas pressure
D	anode-cathode distance
V	working voltage
i	discharge current
W	weight of gas
P/P _o	relative pressure
C	BET constant
s	slope of BET plot
i	intercept of BET plot
W _m	weight of a monolayer
S _t	total surface area
S	specific surface area
w	sample weight
KE	kinetic energy of the emitted electron
h	energy of the photon
BE	binding energy
ϕ_s	work function of the spectrometer
d	analysis depth of XPS
θ	take-off angle of the analyzed electrons
ϵ_x	a random error variable
β_i	measure of the local <i>linear effect</i> of the <i>i</i> th factor
η_x	mean response

REFERENCES

1. Regis, Ed. "Nano the emerging science of nanotechnology: remaking the world-molecule by molecule." *Boston: Little, Brown and Company*, 1995. 74.
2. Surangalika H. and Besser R.S., "Study of Cyclohexene Hydrogenation and Dehydrogenation in a Microreactor", *Proceedings of the 6th International Conference on Microreaction Technology (IMRET VI)*, New Orleans, LA, ed. I. Renard, AIChE, 2002.
3. Stefan Johansson, Erik Fridell, Bengt Kasemo, "Microreactor for studies of low surface area model catalysts made by electron-beam lithography", *Journal of Vacuum Science and Technology, Part A: Vacuum, Surfaces and Films* 46~ *National Symposium of the American Vacuum Society*, Oct25-Oct 29 1999, v18 n4 I Jul 2000.
4. Atwater James E, Akse James R, Mcinnis Jeffrey A, Thompson John O, "Aqueous phase heterogeneous catalytic oxidation of trichloroethylene", *Applied Catalysis B:Environmental* vii ni Dec27 1996.
5. Finnerty Caine, Tompsett Geoff A, Kendall Kevin, Ormerod R Mark, "SOFC system with integrated catalytic fuel processing", *Journal of Power Source*, 86 1 Sep 13-Sep 16 1999 2000.
6. Hamid Derouane-Abd, Sharifah Bee, Lambert Denis, Derouane Eric G., "Dehydroisomerization of n-butane over (Pt,Cu)/H-TON catalysts", *Catalysis Today* 63 2-4 Dec 2000.

7. Norberg, P., Petersson, L.G., and Lundstorm, I., 1993. "Characterization of Gas Transport Through Micromachined Submicron Channels in Silicon", *Vacuum*, Vol. 45, No.1, pp. 139-144.
8. Srinivason, R. *et al.*, 1997. "Micromachined Reactors for Catalytic Partial Oxidation Reactions", *AIChE Journal*, Vol. 43, No. 11, pp. 3059-3068.
9. Oyama S.T., Somorjai G.A., *J.Chem. Educ.*, 65,765(1986)
10. Ravi Srinivasan, 1-Ming Hsing, Peter E.Berger, Klavs F.Jensen, "Micromachined reactors for catalytic partial oxidation reactions. *AIChE Journal*, v43, no.11, November 1997, pp.3059.
11. Francis J., Besser R., Deng Q., Fang J., Elmore B., Cui T., "Experimental system for the study of gas-solid heterogeneous catalysis in microreactors", *Proceedings of SPIE-the International Society for Optical Engineering Microfluidic Devices and Systems III* Sep 18-Sep 19 2000 v4177 2000.
12. Johansson Stefan, Fridell Erik, Kasemo Bengt, "Microreactor for studies of low surface area model catalysts made by electron-beam lithography", *Journal of Vacuum Science and Technology, Part A: Vacuum, Surfaces and Films* 46~ National Symposium of the American Vacuum Society, Oct25-Oct 29 1999, v18 n4 I Jul 2000.
13. Atwater James E, Akse James R, Mcinnis Jeffrey A, Thompson John O, "Aqueous phase heterogeneous catalytic oxidation of trichloroethylene", *Applied Catalysis B:Environmental* vii ni Dec27 1996.
14. Caine Finnerty, Geoff A Tompsett, Kevin Kendall, R Mark Ormerod, "SOFC system with integrated catalytic fuel processing", *Journal of Power Source*, 86 1 Sep 13-Sep

- 16 1999 2000.
15. Korotkikh Olga, Farrauto Robert, "Selective catalytic oxidation of CO in H₂: fuel cell applications", *Catalysis Today* 62(2000) 249254.
16. Sadykov, V.A.; Pavlova, S.N., Saputina, N.F., Zolotarskii, I.A., Pakhomov, N.A., Moroz, E.M., Kuzmin, V.A., Kalinkin, A.V., *Catalysis Today* 611 Aug 2000 Elsevier Science Publishers B.V. p 93-99.
17. Corma, Avelino, Martinez, Agustin, "Zeolites and zeotypes as catalysts", *Advanced Materials*, v7 n2 Feb 1995.
18. Dalai, Ajay K., Sethuraman, R., Katikaneni, Sai P.R., Idem, R.O., "Synthesis and characterization of sulfated titania solid acid catalysts", *Industrial & Engineering Chemistry Research*, v 37 n 10 Oct 1998.
19. Chui, Zh.J., Wang, L., Wang, K.Y., Song, Q.H.; Wang, J.T., Lu, K., "Catalytic properties of Fe₇₈Si₁₂B₁₀ alloys prepared by ball milling", *Materials Science & Engineering A: Structural Materials: Properties, Microstructure and Processing* *Structural Materials: Properties, Microstructure and Processing Proceedings of the Seventh International Conference on Rapidly Quenched Materials* Aug 13-17 1990 v A134 Mar 25 1991.
20. Segal, E., Madon, R.J., and Boudart, M., *J. Catal.* 52, 45-49 (1978).
21. Davis, S.M. and Somorjai, G.A., *J. Catal.* 65, 78-83 (1980).
22. Xu, C. and Koel, B.E., "Adsorption and desorption behavior of n-butane and isobutane on Pt(111) and Sn/Pt(111) surface alloys", *Surf. Sci.* 304, 249-266 (1994).

23. Chen, J.G. and Fruhberger, B., "Reactivities of carbon- and nitrogen-modified Mo(110): a comparison of modification effects by surface and interstitial adatoms", *Surf. Sci.* 367, L102-L110 (1996).
24. Su, K., Kung, K.Y., Lahtinen, J., Shen, Y.R., and Somorjai, G.A., *J. Molec. Catal. A: Chem.* 141, 9-19 (1999).
25. Rase, H.F. "Handbook of Commercial Catalysts: Heterogeneous Catalysts," *CRC Press*, Boca Raton, 2000), pp. 105-204.
26. Gary, J.H. and Handwerk, G.E., "Petroleum Refining, Technology and Economics," *Marcel-Dekker*, New York, 2001, pp. 175-214.
27. Weissermel, K. and Arpe, H.-J., "Industrial Organic Chemistry," *Wiley VCH, Weinheim*, 1997, pp. 314-17.
28. Sandestede, G. in "Catalysis from A to Z, A Concise Encyclopedia," (B. Cornils, W.A. Herrmann, R. Schlogl, and C.-H. Wong, Eds.). *Wiley VCH, Weinheim*, 2000, pp. 228-29.
29. Burstein, G.T.:(Univ of Cambridge, Cambridge, Engl), "Fuel cells on the road to success" Source: *Materials World*, v 6, n 7, Jul, 1998, p 412-413 Publisher: Inst of Materials, London, Engl ISSN: 0967-8638 CODEN: MORLEE In English
30. Dicks, Andrew L.(British Gas plc, UK), "Hydrogen generation from natural gas for the fuel cells systems of tomorrow" Source: *Journal of Power Sources*, v 61, n 1-2, Jul-Aug, 1996, *Proceedings of the 1995 4th Grove Fuel Cell Symposium Opportunities, Progress and Challenges*, Sep 19-22 1995, London, UK, p 113-124

Publisher: Elsevier Science S.A., Lausanne, Switzerland ISSN: 0378-7753 CODEN: JPSODZ In English

31. Manasilp, Akkarat, Gulari, Erdogan, "Selective CO oxidation over Pt/alumina catalysts for fuel cell applications" Source: *Applied Catalysis B: Environmental*, v 37, n 1, Apr 8, 2002, p 17-25 ISSN: 0926-3373 CODEN: ACBEE3 In English
32. Ito, Takashi, "Technologies and catalysts of hydrogen generation for fuel cells" Source: *Nihon Enerugi Gakkaishi/Journal of the Japan Institute of Energy*, v78, n11, 1999, p 911-920 Publisher: Maruzen Co Ltd, Tokyo, Japan ISSN: 0916-8753 CODEN: NENGEM In Japanese
33. Mitchell, Philip C.H., Wolohan, Peter;Thompsett, David;Cooper, Susan J.; Source: *Journal of Molecular Catalysis, A: Chemical*, v119, n1-3, May 23, 1997, *Proceedings of the 1996 6th International Conference on Theoretical Aspects of Heterogeneous Catalysis*, Jun 2-7 1996, Tarragona, Spain, p 223-233 ISSN: 1381-1169 CODEN: JMCCF2 InEnglish
34. Dudfield, C.D., Chen, R.;Adcock, P.L., "Evaluation and modelling of a CO selective oxidation reactor for solid polymer fuel cell automotive applications" Source: *Journal of Power Sources*, v85, n2, 2000, p 237-244 Publisher: Elsevier Sequoia SA, Lausanne, Switzerland ISSN: 0378-7753 CODEN: JPSODZ In English
35. Dudfield, C.D., Chen, R.;Adcock, P.L., "A carbon monoxide PROX reactor for PEM fuel cell automotive application" Source: *International Journal of Hydrogen Energy*, v 26, n 7, July, 2001, p 763-775 ISSN: 0360-3199 CODEN: IJHEDX In English

36. Denis, M.C., Lalande, G.;Guay, D.;Dodelet, J.P.;Schulz, R., "High energy ball-milled Pt and Pt-Ru catalysts for polymer electrolyte fuel cells and their tolerance to CO"
Source: *Journal of Applied Electrochemistry*, v 29, n 8, 1999, p 951-960 Publisher:
Kluwer Academic Publishers, Dordrecht, Netherlands ISSN: 0021-891X CODEN:
JAELBJ In English
37. Storch H.H., Golumbic N., Anderson R.B., "The Fischer-Tropsch and Related Syntheses", *Wiley & Sons*: New York, 1951.
38. Zhipan Liu, P. Hu, "A New Insight into Fischer-Tropsch Synthesis", *J.Am. Chem.Soc.* 2002, 124, 11568-11589.
39. Farrauto R.J., Bautholomew C.H., " Fundamentals of Industrial Catalytic Process",
Blackie Academic and Professional 1997, UK, 1997 (Chapter 1, 38-39)
40. Gerold Parkinson, "Fischer-Tropsch Finds New Life", *Chemical Engineering*, 104 4,
39 (1997).
41. Benjamin Eisenberg, Rocco A. Fiato, "The evolution of advanced gas-to-liquids technology", *CHEMTECH* October 1999, pp32-37.
42. Bukur, D.B., Lang, X., "Development of Iron Fischer-Tropsch Catalysts", for *DOE Contract*.
43. Liu Ning, Chen Jingguang G., "Synergistic effect in the dehydrogenation of cyclohexene on C/W (111) surfaces modified b submonolayer coverage Pt", *Catalysis Letters (2001)*, 77(1-3), 35-40. ISSN: 1011-372X.

44. Liu Ning, Chen Jingguang G., "A comparative surface science study of carbide and oxycarbide. The effect of oxygen modification of the surface reactivity of C/W(111)", *Surface Science* (2001), 487(1-3), 107-117. ISSN: 0039-6028.
45. Roberts Jeffrey T., Madix Robert J., "Reactions of weak organic acids with oxygen atoms on silver (110): facile and selective conversion of cyclohexene to benzene", *Surface Science* (1990), 226(3), L71-L78, ISSN: 0039-6028.
46. Hunka Deborah E., Land D.P., "Dehydrogenation of cyclohexene to benzene on Pd (111)", *Book of Abstracts, 214th ACS National Meeting*, Las Vegas, NV, September 7-11 (1997).
47. Hassan Salah A., Sadek Salwa A., "Various characteristics of supported CoPc on Al₂O₃, SiO₂ and SiO₂- Al₂O₃ as selective catalysts in the oxidative dehydrogenation of cyclohexene", *Studies in Surface Science and Catalysis* (1996), 100(Catalysts in Petroleum Refining and Petrochemical Industries 1995), 407-18, ISSN: 0167-2991.
48. Bruce Linda A., Hoang Manh, "Ruthenium promotion of Fischer-Tropsch synthesis over coprecipitated cobalt/ceria catalysts", *Applied Catalysis A: General*, 100 (1993) 51-67.
49. Joshi, A. 1998, "Fabrication of A Miniaturized Chemical Process", *Master's Thesis*, Louisiana Tech University, Ruston, LA.
50. Liu, J. Q. Tai, Y. C., *et al.*, 1993. "Micromachined Channel Pressure Sensor System for Micro Flow Studies", *The 7th International Conference on Solid-State Sensors and Actuators, Transducers '93*, pp. 995-998.

51. Arkilic, E.B., Breuer, K.S., 1994. "Gaseous Flow in Microchannels", *ASME Application of Microfabrication to Fluid Mechanics Proceedings, Chicago, IL, FED-VD. 197*, pp 57-66.
52. Somarjai, G. Al, 1994. Introduction to Surface Chemistry and Catalysis, *John Wiley and sons, New York*.
53. Zheng A., 2000, "Fabrication of A Miniaturized Chemical Process", *Master's Thesis*, Louisiana Tech University, Ruston, LA.
54. Marc Madou, "Fundamentals of Microfabrication". *CRC Press*, ISBN 0-8493-9451-1.
55. SZE S.M., " *VLSI Technology*", Second Edition, ISBN 0-07-062735-5.
56. Pandhumsoporn T., Feldbaum M., Gadgil P., Puech M., and Maquin P., " High Etch Rate, Anisotropic Deep Silicon Plasma Etching for the Fabrication of Microsensors", *SPIE Vol. 2879*, 1994, pp 94-102.
57. Bhardwaj J. K., Ashraf H., *SPIE* 2639 (1995) 224.
58. Hill R., *J. Vac. Sci. Technol. B* 14 (1996) 547.
59. Marxer C., Gretillat M. A., de Rooij N. F., Battig R., Anthamatten O., Valk B., Vogel P., *Proceedings of the Tenth annual International Workshop on Micro Electro Mechanical Systems*, Nagoya, Japan, IEEE, New York, 1997 p. 49.
60. Shin W.C., McDonald J.A., Zhao S., and Besser R.S., "Etching Characteristics of a Micromachined Chemical Reactor Using Inductively Coupled Plasma", *Proceedings of the 6th International Conference on Microreaction Technology (IMRET VI)*, New Orleans, LA, ed. I. Renard, AIChE, 2002.

61. Grill A 1994 *Cold Plasma in Material Fabrication, From Fundamental to Applications* (New York: IEEE Press)
62. Rosnagel S M, Cuomo J J and Westwood W D (eds) 1990 *Handbook of Plasma Processing Technology* (Park Ridge: Noyes)
63. Rutscher A and Deutsch H (eds) 1983 *Wissenspeicher Plasmatechnik* (Leipzig: Fachbuchverlag)
64. Brinker C.J., Scherer G.W., *Sol-gel Science*, Academic Press, San Diego, CA, 1990.
65. Katayama S., Sekine M., Fudouzi H., Kuwabara M., *J.Appl.Phys.* 71 (1992) 2795.
66. Sanchez C., Livage J., Henry M., Babonneau F., *J. Non-Cryst. Sol.* 100 (1988) 65.
67. Brinker C.J., Hurd A.J, Frye G.C., Ward K.J., Ashley C.S., *J. Non-Cryst. Sol.* 121 (1990) 294.
68. Devreux F, Boilot J-P, Chaput Fand Lecomte A 1990 *Phys. Rev. A* 41 6901.
69. Boillot J-P, Biteaut J, Chaput F, Gacoint T, Brunt A, Darracq B, Georget P and Levy Y, "Organic-inorganic solids by sol-gel processing: optical applications", *Pure Appl. Opt.* 7 (1998) 169-177. Printed in the UK.
70. Clemens Bechinger, Hans Muffler, Claudia Schafle, Otle Sundberg, Paul Leiderer, "Submicron metal oxide structures by a sol-gel process on patterned substrates", *Thin Solid Films* 366 (2000) 135-138.
71. Fung C D, Cheung P W, Ko W H and Fleming D G 1985 *Micromachining and Micropackaging of Transducers* (Amsterdam: Elsevier Science) p 41
72. Ju B K 1995 *Study on the direct bonding of silicon wafers for microelectromechanical systems* *Dr Thesis* The University of Korea, Seoul, p 8

73. Holloway P H, Sbastain J. Trottier T, Swartand H and Petersen R O 1995 *Solid State Technol.* August 47
74. Ljibisa Ristic 1994 *Sensors Technol. Devices* 207.
75. Choi W, Ju B., Lee Y., Jeong J., Haskard M R, Lee N, Sung M. and Oh M., "Experimental Analysis on the Anodic Bonding With an Evaporated Glass Layer," *J. Micromech. Microeng.* 7 (1997) 316-322. Printed in the UK
76. Ju B. K. and Oh M. H. 1994 Fabrication of silicon membrane using fusion bonding and two-step electrochemical etch-stopping *J. Mater. Sci.* 29 664-8
77. Roberds B. E. and Farrens S. N. 1993 Low temperature silicon direct bonding *Electrochem. Soc. Proc.* 93 240-4
78. Wallis G and Pomerantz D I 1969 *J. Appl. Phys.* 40 3946
79. Brooks A A and Donovan R P 1972 Low-temperature electrostatic silicon-to-silicon seals using sputtered borosilicate glass *J. Electrochem. Soc.* 119 545-6
80. Yozo Kanda et al 1990 *Sensor Actuators A* 21/23 939.
81. "Micromachined Transducers Sourcebook",
82. Postek, Michael T, Robert D. Larrabee, William J. Keety and Egon Marx. " The Application of Transmission Detection to X-ray Mask Calibration and Inspection," *Proceedings of the SPIE conference Integrated circuit Metrology, Inspection, and Process Control V.* Vol 1464.37.
83. Postek, Michael T, and David C. Joy, "Submicrometer Microelectronics Dimensional Metrolgy: Scanning Electron Microscope," *Journal of Research of the National Bureau of Standards.* Vol 92. No.3 1987. 207.

84. Moulder, John F., William F. Stickle, Peter E. Sobol, and Kenneth D. Bomben. "Handbook of X-Ray Photoelectron Spectroscopy." Edited by Jill Chastain and Roger C. King, Jr. Physical Electronics, Inc Eden Prairie, Minnesota. 28.
85. Teng Y., Sakurai H., "Oxidative removal of CO contained in hydrogen by using metal oxide catalysts", *International Journal of Hydrogen Energy*, 24 (1999) 355-358.
86. Birks, L.S. "McGraw-Hill Encyclopedia of Science and Technology." 8th edition. Vol 19.644.
87. Feldman, Leonard C. and James W. Mayer. "Fundamentals of Surface and Thin Film Analysis" New York: North-Holland, 1986, 47.
88. Moulder, John F., William F. Stickle, Peter E. Sobol, and Kenneth D. Bomben. "Handbook of X-Ray Photoelectron Spectroscopy." Edited by Jill Chastain and Roger C. King, Jr. Physical Electronics, Inc Eden Prairie, Minnesota. 28.
89. <http://www.quantachrome.com/GasSorption/index.htm>
90. Brunauer S., Emmett P., *J. Amer. Chem. Soc.*, 60, 309 (1938).
91. *Quantachrome Instruments NOVA MANUAL version 6.11* for high speed gas sorption analyzer.
92. <http://www.swt.edu/~wg06/manuals/vsm/vsm.htm>
93. Angela Dean, Daniel Voss, "Design and Analysis of Experiments", ISBN: 0-387-98561-1
94. http://www.microresist.de/shipleypod_en.htm
95. <http://grover.mirc.gatech.edu/data/msds/index.phtml?type=photoresist>.

96. *Sputtering system operational procedures & software help screens*
97. Akkarat Manasilp, Erdogan Gulari, "Selective CO oxidation over Pt/alumina catalysts for fuel cell application", *Applied Catalysis B: Environmental* 37 (2002) 17-25.
98. *Principles of Scanning Electron Microscopy*.
99. *AMRAY User's Manual*.
100. <http://www.quantachrome.com/GasSorption/NOVA-Series-Specs.htm>
101. <http://www.dms-magnetics.com/880.shtml>
102. User's Manual & Technical References for QMS 100/200/300 Gas Analyzer
103. Okuzaki S., Okude K. and Ohishi T., "Photoluminescence behavior of SiO₂ prepared by sol-gel processing", *Journal of Non-crystalline Solids*, vol. 265, pg 61-67.
104. Lopez T., Bosch P., Moran M. and Gomez R., "Pore-Size Controlled Pt/SiO₂ catalysts," *React.Kinet.Catal.Lett.*, 52 (1), 65-71, 1994.
105. Yoldas B.E., "Alumina Sol Preparation from Alkoxides", *American Ceramic Society bulletin*, Vol. 54, Issue 3, 1975, pg 289-290.
106. Kurokawa Y., Suga T, "Transparent alumina films derived from two sources of AlCl₃.6H₂O and aluminum iso propoxide by sol-gel method"
107. Wang Z. and Lin Y.S., "Sol-gel synthesis of pure and copper oxide coated mesoporous Alumina granular particles", *Journal of Catalysis*, Vol. 174, pg 43-51, 1998.

108. Pecchi G., Morales M. and Reyes P., "Pt/SiO₂ Catalysts Obtained by the Sol-Gel Method. Influence of the PH of Gelation on the Surface and Catalytic Properties," *React. Kinet. Catal. Lett.*, 61 (2), 237-244, 1997.
109. Prokopenko V. B., Gurin V. S., "Surface segregation of transition metals in sol-gel silica films", *J.Phys.D: Appl. Phys.* 33(2000) 3152-3155.
110. John F. Moulder, William F. stickle, Peter E.Sobol, Kenneth D.Bomben, Handbook of X-ray photoelectron spectroscopy, a reference book of standard spectra for identification and interpretation of XPS data, by published by *Physical Electronics, Inc.*
111. Bhattacharya A.K., Pyke D.R., Walker G.S., Werrett C.R., *The surface reactivity of different aluminas* as revealed by their XPS C1s spectra.
112. Paparazzo E., "XPS, AES and EELS studies of Al surfaces" vol.62, May 2001, pg 47 - 60.